3D PRINTING-BASED MANUFACTURING METHOD FOR BIOMASS-FUNGI COMPOSITES

A Dissertation

by

ABHINAV BHARDWAJ

Submitted to the Graduate and Professional School of
Texas A&M University
in partial fulfillment of the requirements for the degree of

DOCTOR OF PHILOSOPHY

Chair of Committee,	Zhijian Pei
Co-Chair of Committee,	Na Zou
Committee Members,	Brian Shaw
	Sarah Wolff
Head of Department,	Lewis Ntaimo

December 2021

Major Subject: Industrial Engineering

ABSTRACT

Biomass-fungi composites represent a sustainable material with applications in the construction and packaging industries. Currently, molding is used to manufacture biomass-fungi composite products. 3D printing of these composites would facilitate greater design flexibility for various construction and packaging applications.

This dissertation presents a novel 3D printing process for the manufacturing of products using these composites. It includes the mechanical processing and employing a printability aiding additive to facilitate 3D printing. Mechanical mixing was used to convert the loose, biomass-fungi material into a liquid slurry. Psyllium husk powder was used as a printability aiding additive that prevented phase segregation during the printing process thereby avoiding problems such as nozzle blocking. The appropriate amount of printability aiding additive was also determined by analyzing the print quality of mixtures varying in the content of this additive. The rheological properties of these mixtures have also been discussed. The effect of mixing process parameters (such as mixing time and mixing type) on fungal growth has been studied. Furthermore, this dissertation also presents the effects of printing process parameters (such as print speed and air pressure) on fungal growth. Lastly, the tensile and compressive strength data of these composites has been presented.

DEDICATION

To my supportive parents: Dr. Tilak Raj Bhardwaj and Mrs. Kavita Bhardwaj, my caring wife Julie and my loving daughter, Alisha.

ACKNOWLEDGEMENTS

I express my sincere gratitude to my adviser Dr. Zhijian Pei for his academic and professional mentorship through my doctorate study. I could not have completed this journey without his patience, strategic leadership, and insightful supervision. I could not have picked a better mentor for my Ph.D. study.

I would also like to thank my committee co-chair, Dr. Na Zou, and my committee members, Dr. Shaw, Dr. Wolff for their guidance, support, advice, and suggestions that helped me accomplish my research objectives. I am grateful to Dr. Scott Jones at the National Institute of Standards and Technology (NIST), Mr. Lucht at Ecovative Design, and Dr. Peiran Wei at the Soft Matter Facility at Texas A&M University for their enriching research collaborations during the course of my study.

I am thankful to work with some excellent colleagues: Xingjian (Ken) Wei, Joseph G. Vasselli, Al Mazedur Rahman, Ketan Thakare, and several other graduate and undergraduate students. The camaraderie I shared with these colleagues helped me overcome the research challenges that every experimental investigator must overcome.

Life as a researcher presents certain personal challenges. I am grateful to my wife, Julie, and our loving daughter Alisha for keeping me motivated through those times.

Last but not the least, I thank my parents, my brother and his family, and my mother-in-law for their continuous support and encouragement.

CONTRIBUTORS AND FUNDING SOURCES

Contributors

This work was supervised by a dissertation committee consisting of committee chair, Professor Zhijian Pei of the Department of Industrial and Systems Engineering (ISEN). Committee co-chair Professor Na Zou of the Department of Engineering Technology & Industrial Distribution (ETID), and committee members Professor Brian Shaw of the Department of Plant Pathology and Microbiology and Professor Sarah Wolff of the Department of Industrial and Systems Engineering.

Since all the chapters in this dissertation are papers published by the student, detailed information about contributors for specific chapters is provided in those papers.

Funding Sources

Major portion of the research contained in this dissertation was financially supported by the startup funds of Professor Pei. A portion of this dissertation was funded through the T3: Texas A&M Triads for Transformation project titled: "*3D Printing of Biomass-Based Materials for Construction*". Financial support in the form of graduate teaching assistantship was provided by the ISEN and ETID departments. The author is grateful for the financial support.

The contents of this dissertation are solely the responsibility of the authors and do not necessarily represent the official views of Texas A&M University.

TABLE OF CONTENTS

Page

LIST OF FIGURES

Page

LIST OF TABLES

Page

1. INTRODUCTION

Additive manufacturing (AM) is defined as "*a process of joining materials to make objects from 3D model data, usually layer upon layer, as opposed to subtractive manufacturing methodologies*" [1]. Metals and polymers represent the two major categories of materials used in AM [2]. Additionally, materials such as ceramics and composites are also used in AM. As per the ISO/ASTM standard, there are seven types of AM processes [1]. These are: Binder Jetting, Directed Energy Deposition, Material Extrusion, Material Jetting, Powder Bed Fusion, Sheet Lamination, Vat Photopolymerization. Details about these AM processes will be discussed in subsequent chapters. In industry, AM processes are mostly used to produce functional parts and to ascertain fit and assembly of parts as shown in Figure 1 [2].

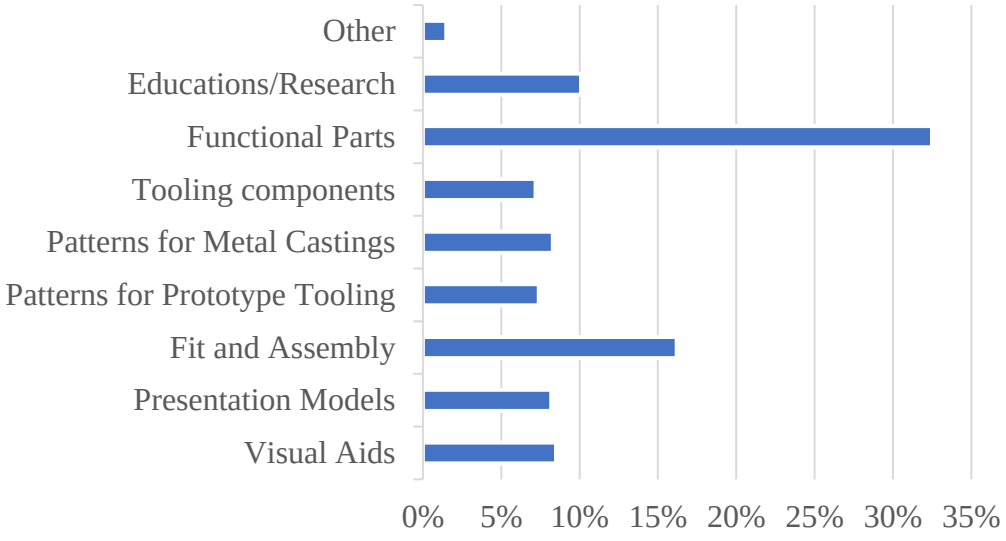

Figure 1: Company tasks using AM processes [2]

The AM sector is a $5.165 billion industry [2]. AM is used in industries such as: industrial businesses and machines, aerospace, motor vehicles, consumer products/electronics, medical/dental, and academic institutions (see Figure 2) [2]. However, the architecture and construction industry accounts for only 3.1% of the total AM applications [2].

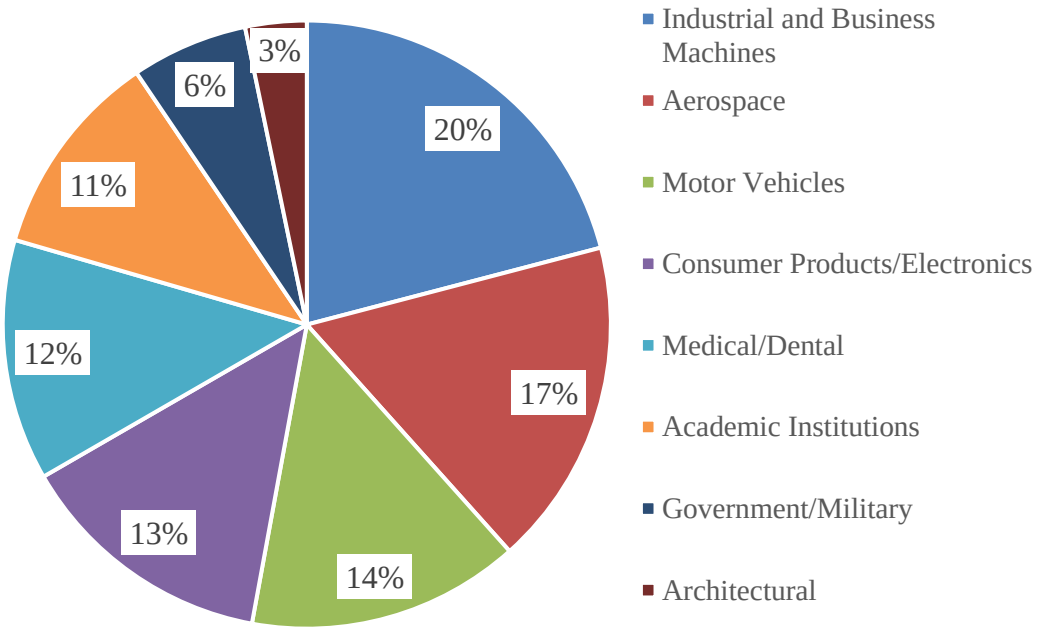

Figure 2: Applications of AM in different industries [2]

The global construction industry has an annual output of $8.5 trillion [3]. It employs up to 10% of the workforce in industrialized countries [4]. It is also a major source of employment in the US. In 2016, the construction industry employed 4.3% of the total US workforce [5,6]. However, safety and productivity represent two key challenges for this

industry. As per International Labor Organization's estimates, 25% to 40% of work-related deaths occur at construction sites [4]. Productivity in the construction industry is also perceived to be declining or stagnant [7,8].

AM can help address these challenges. AM machines can boost productivity by working all day. Automated construction systems can perform dangerous tasks thereby improving safety. Furthermore, AM processes can present significant cost savings through printing of stay-in-place formworks during construction of buildings [9]. Accordingly, application of AM processes for construction has gathered interest in Switzerland [10], Germany [11] and Singapore [12]. New companies are bringing AM technology to the construction industry [13–16].

While many groups are reporting studies in 3D printing of cementitious materials, environmental sustainability remains an important concern. Cement and concrete (a mixture of cement, sand, water, and gravel) are not sustainable materials. Every ton of cement production results in the release of 0.9 tons (846.5 kg) of CO_2 into the atmosphere [17]. As per the Economist, "*Cement-making alone produces 6% of the world's carbon emissions. Steel, half of which goes into buildings, accounts for another 8%*" [18]. Researchers have highlighted the need for bio-based, sustainable materials for the construction industry [19].

Environmental sustainability also represents a major challenge for the packaging industry. Plastic pollution has reached a dangerous level. Plastic waste has been found at the Mount Everest [20] as well as in the Marianas Trench [21]. Researchers estimate that 60% of the plastic produced since 1950 has been discarded into our environment, 10% has

been incinerated, and only 7% has been recycled [22]. Moreover, these plastics may take decades and centuries to decompose [23]. AM can be very useful in the packaging industry to develop custom solutions for consumers. However, there is a need for sustainable materials alternative to plastics.

Currently, there is no significant research in the area of additive manufacturing of sustainable materials (such as biomass-fungi composites) that also harness biofabrication. Biofabrication refers to "*the production of complex products from raw materials such as living cells, molecules, extracellular matrices, and biomaterials*" [24]. These advantages in sustainability are facilitated through the use of renewable raw materials and limited energy use (since the process utilizes biological systems for production) [25,26].

This dissertation addresses this knowledge gap. It is structured as follows: Chapter 2 presents a state-of-the-art review of the AM processes used in the construction industry along with knowledge gaps and challenges for each process. Chapter 3 presents an experimental study to identify feasible process parameter regions for the material extrusion process used in this research. Chapter 4 presents the results of a new AM-based manufacturing method using a sustainable biomass-fungi composite material. Chapters 5 establishes the relationship between material rheology and material composition. Chapter 6 studies the relationship between mechanical properties of the oriented parts and process parameters. Chapters 7 presents the contributions of this dissertation to the literature and discusses future research opportunities.

References

[1] ISO/ASTM52900-15, A., 2015, Standard Terminology for Additive Manufacturing – General Principles – Terminology.

[2] Caffrey, T., Wohlers, T., and Campbell, R. I., 2016, Wohlers Report 2016, Wohlers Associates, Inc.

[3] Construction Intelligence Center, 2015, Global Construction Outlook 2020.

[4] International Labour Organization, 2005, "Facts on Safety at Work," Int. Labor Off. Tech. Rep.

[5] Bureau of Labor Statistics, 2017, "2016 U.S. Employment by Major Industry Sector" [Online]. Available: https://www.bls.gov/emp/ep_table_201.htm. [Accessed: 18-Dec-2017].

[6] Bureau of Economic Analysis, 2016, "Gross Domestic Product by Industry: First Quarter 2016" [Online]. Available: https://www.bea.gov/newsreleases/industry/gdpindustry/2016/gdpind116.htm. [Accessed: 18-Dec-2017].

[7] NIST, 2011, "Metrics and Tools for Construction Productivity Project" [Online]. Available: https://www.nist.gov/programs-projects/metrics-and-tools-construction-productivity-project. [Accessed: 03-Dec-2018].

[8] Nasir, H., Ahmed, H., Haas, C., and Goodrum, P. M., 2014, "An Analysis of Construction Productivity Differences between Canada and the United States," Constr. Manag. Econ., 32(6), pp. 595–607.

[9] Wangler, T., Lloret, E., Reiter, L., Hack, N., Gramazio, F., and Kohler, M., 2016,

"Digital Concrete : Opportunities and Challenges," pp. 67–75.

[10] Swiss National Science Foundation, 2014, "National Center for Competence in Research-Digital Fabrication" [Online]. Available: http://www.snf.ch/en/researchinFocus/nccr/digital-fabrication/Pages/default.aspx.

[11] University of Stuttgart, 2018, "New Cluster of Excellence: Integrative Computational Design and Construction for Architecture," Dtsch. Forschungsgemeinschaft [Online]. Available: http://icd.uni-stuttgart.de/?p=24111.

[12] Singapore Centre for 3D Printing, 2016, "Singapore Centre for 3D Printing" [Online]. Available: www.sc3dp,.ntu.edu.sg.

[13] Contour Crafting, 2017, "Contour Crafting Corporation" [Online]. Available: http://contourcrafting.com/.

[14] XtreE, 2015, "XtreE" [Online]. Available: https://www.xtreee.eu/.

[15] Apis Cor, 2016, "Apis Cor" [Online]. Available: http://apis-cor.com/en/faq/texnicheskie-xarakteristiki-3d-printera/. [Accessed: 12-Oct-2017].

[16] Technology, B., 2015, "Branch Technology" [Online]. Available: https://www.branch.technology. [Accessed: 01-Oct-2017].

[17] Habert, G., 2013, "Environmental Impact of Portland Cement Production," Eco-efficient Concr. F. Pacheco-Torgal, S. Jalali, J. Labrincha, VM John (ed.), Woodhead Publ. Cambridge, pp. 3–25.

[18] 2019, "Why More Buildings Should Be Made of Wood," Econ. [Online]. Available: https://www.economist.com/leaders/2019/01/05/why-more-buildings-should-be-made-of-wood.

[19] Biernacki, J. J., Bullard, J. W., Sant, G., Brown, K., Glasser, F. P., Jones, S., Ley, T., Livingston, R., Nicoleau, L., Olek, J., Sanchez, F., Shahsavari, R., Stutzman, P. E., Sobolev, K., and Prater, T., 2017, "Cements in the 21 St Century: Challenges, Perspectives, and Opportunities," J. Am. Ceram. Soc., pp. 1–28.

[20] Napper, I. E., Davies, B. F. R., Clifford, H., Elvin, S., Koldewey, H. J., Mayewski, P. A., Miner, K. R., Potocki, M., Elmore, A. C., Gajurel, A. P., and Thompson, R. C., 2020, "Reaching New Heights in Plastic Pollution—Preliminary Findings of Microplastics on Mount Everest," One Earth, 3(5), pp. 621–630.

[21] Chiba, S., Saito, H., Fletcher, R., Yogi, T., Kayo, M., Miyagi, S., Ogido, M., and Fujikura, K., 2018, "Human Footprint in the Abyss: 30 Year Records of Deep-Sea Plastic Debris," Mar. Policy, 96, pp. 204–212.

[22] Geyer, R., Jambeck, J. R., and Law, K. L., 2017, "Production, Use, and Fate of All Plastics Ever Made," Sci. Adv., 3(July), pp. 25–29.

[23] Jones, M., Mautner, A., Luenco, S., Bismarck, A., and John, S., 2020, "Engineered Mycelium Composite Construction Materials from Fungal Biorefineries: A Critical Review," Mater. Des., 187, p. 108397.

[24] Mironov, V., Trusk, T., Kasyanov, V., Little, S., Swaja, R., and Markwald, R., 2009, "Biofabrication: A 21st Century Manufacturing Paradigm," Biofabrication, 1(2), p. 22001.

[25] Holt, G., McIntyre, G., Flagg, D., Bayer, E., Wanjura, J., and Pelletier, M., 2012, "Fungal Mycelium and Cotton Plant Materials in the Manufacture of Biodegradable Molded Packaging Material: Evaluation Study of Select Blends of Cotton

Byproducts," J. Biobased Mater. Bioenergy, 6(4), pp. 431–439.

[26] Jiang, L., Walczyk, D., Mcintyre, G., and Kin, W., 2016, "Cost Modeling and Optimization of a Manufacturing System for Mycelium-Based Biocomposite Parts," 41, pp. 8–20.

2. ADDITIVE MANUFACTURING PROCESSES FOR INFRASTRUCTURE CONSTRUCTION: A REVIEW [1]

2.1. Introduction

AM has found increasing applications in aerospace [27,28], industrial/business machines [28], motor vehicles [29], consumer products/electronics [30,31], medical [32,33], and architectural industries [2]. However, the architectural and the construction industry account for only 3.1 % of the total AM applications [2].

The global annual output of the construction industry is $8.5 trillion [3]. In industrialized countries, the construction industry employs 6 % to 10 % of the workforce [4]. However, the construction industry also faces major challenges in safety and productivity. Estimated by the International Labor Organization, one fatal accident occurs every ten minutes on construction sites around the world [4]. Productivity in the construction industry is also perceived to be declining or stagnant [7,8].

In the U.S., the construction industry is one of the leading contributors to the economy, and accounted for 4.3 % of the total national employment in 2016 [5,6]. However, in 2016, the American Society of Civil Engineers assigned a grade of D+ to the U.S. infrastructure [34]. Restoration and improvement of urban infrastructure has been identified as a grand challenge for engineering in the 21st century by the National Academy of Engineering [35]. With respect to building better infrastructure, the Academy professed the importance

[1] Reprinted with permission from "Additive Manufacturing Processes for Infrastructure Construction: A Review" by Bhardwaj et al., 2019. Journal of Manufacturing Science and Engineering, 141(9), p. 091010, Copyright 2019 by ASME.

of new construction methods. It stated, "*Novel construction materials may help address some of these challenges. But dramatic progress may be possible only by developing entirely new construction methods"* [35].

AM processes can make a significant contribution to the construction industry. First, human safety would improve due to development of automated construction systems that can carry out dangerous jobs that were previously performed by humans. Additionally, AM machines could work 24 hours a day and 7 days a week, thereby providing a momentous boost to productivity. In concrete construction, more than 50 % of the total cost is spent on formwork and labor [36]. AM processes can present significant cost savings through printing of stay-in-place formworks [9].

Application of AM processes for construction has gathered interest in several countries. In the U.S., the National Science Foundation (NSF) supported a workshop on AM for Civil Infrastructure Design and Construction to review the present state of and examine future prospects of AM processes in infrastructure construction [37]. Germany [11], Singapore [12], and Switzerland [10] have setup research centers focused on researching AM processes for construction applications. Several companies have emerged globally in the field of AM for construction applications [13–15,38–40].

Several review papers in the field exist. They focused on particular materials such as concrete [41,42], discussed trends in the field [43], and presented specific technologies prevalent at the time of publication [44–46]. Rapid and significant developments in this field merit an up-to-date review. The primary goal of this state-of-the-art paper is to review AM processes in infrastructure construction.

Table 1: AM processes and their principle, material, and potential applications

Process	***Process Principle***	***Material***	***Highlight***	***Application***
Contour Crafting	Material Extrusion	Concrete, ceramics	• Layer thickness: 13 mm • Uses horizontal and vertical trowels • Printed wall dimensions:1.5 m (L) X 0.15 m (W) X 0.6 m (H)	Large-scale structures
Concrete Printing	Material Extrusion	Concrete	• Layer thickness: 4 mm-6 mm • Nozzle size: 9 mm • Prototype printer build envelope: 5.4 m (L) X 4.4 m (W) X 5.4 m (H)	Formwork, structure
Digital Construction Platform	Material Extrusion	Polymer foam	• Layer thickness: 35 mm • Material: polyurethane foam (Dow chemical's Froth-Pak insulation) • Hydraulic-arm, Electric-arm and track system for motion • Print example: hemispherical dome; height of 3.7 m, diameter of 14.6 m	Formwork
Flow-based fabrication	Material Extrusion	Hydrogel	• Pneumatic extrusion using six 300 cc plastic syringe barrels with rubber plungers and High Density Polyethylene (HDPE) nozzles • Material viscosity range: 500 cP to 50,000 cP at room temperature	Structures
Big Area Additive Manufacturing (BAAM)	Material Extrusion	Polymer	• Material: Polymer pellets • Platform build volume: 6 m (L) X 2.4 m (W) X 1.8 m (H)	Large -scale tools, structures
C-FAB™	Material Extrusion	Polymer	• Extruder attached to a 12.5 ft. robotic arm installed on a 35 ft. rail • 3D printed cell-like matrix/mesh of size 58 ft (L) X 25 ft. (W)	Prefab composite walls, structures, furniture
D-Shape	Binder Jetting	Sandstone	• Layer thickness: 5 mm-10 mm • Nozzle: 300 nozzles placed 20 mm apart • Prototype print area: 6 m X 6 m	Structure
Selective Separation Shaping (SSS)	Other	Ceramics	• Uses two types of powder: B-powder and S-powder • B-powder: constitutes the final part • S-powder: used as a separator • Sintering temperature of S-powder is higher than that of B-powder	Structures

*Table **1*** presents various AM processes presented in this paper. Following this introduction, Sections 2.2 to 2.5 discuss additive manufacturing processes that have been used in civil infrastructure construction. Each section presents process principle, application examples, and gaps. The last section contains concluding remarks

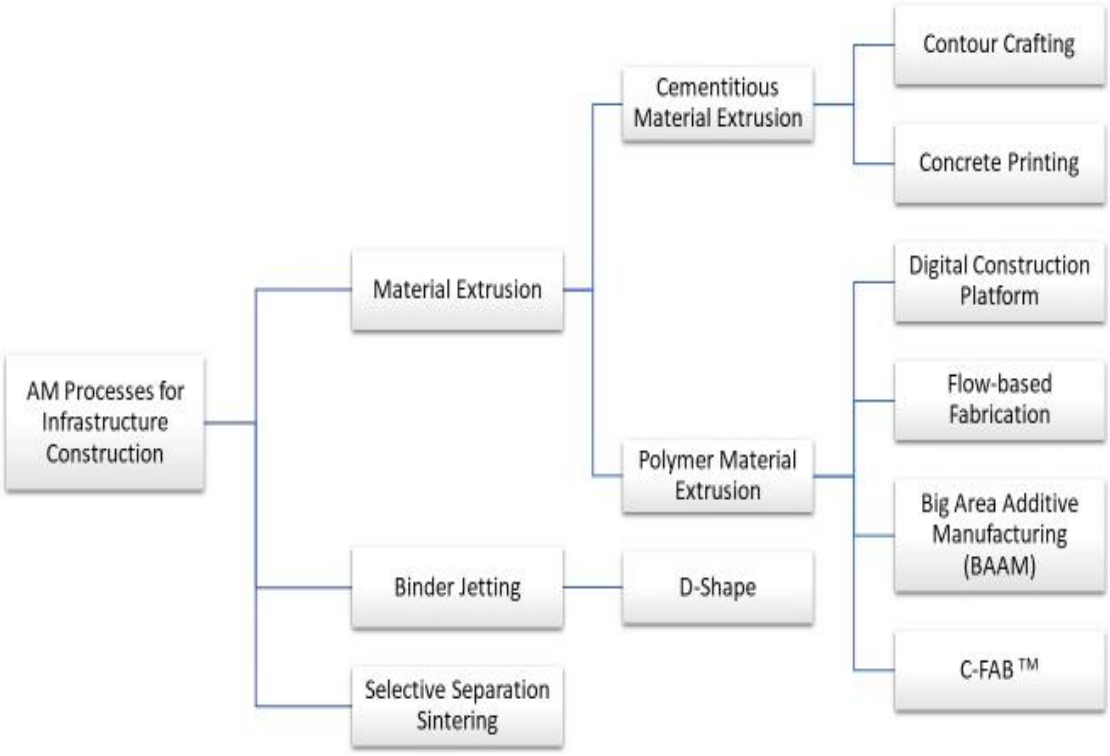

Figure 3: Classification of AM processes for infrastructure construction

2.2. Material extrusion

In material extrusion, material (either cementitious or polymer) is selectively dispensed through a nozzle or orifice [1].

2.2.1. Cementitious material Extrusion

2.2.1.1. Contour Crafting

Contour crafting[2] and concrete printing are both extrusion-based processes for AM of cementitious materials. Contour Crafting was developed by researchers at the University of Southern California [47]. This AM process is based on an extrusion and filling procedure to construct large-scale structures [48,49].

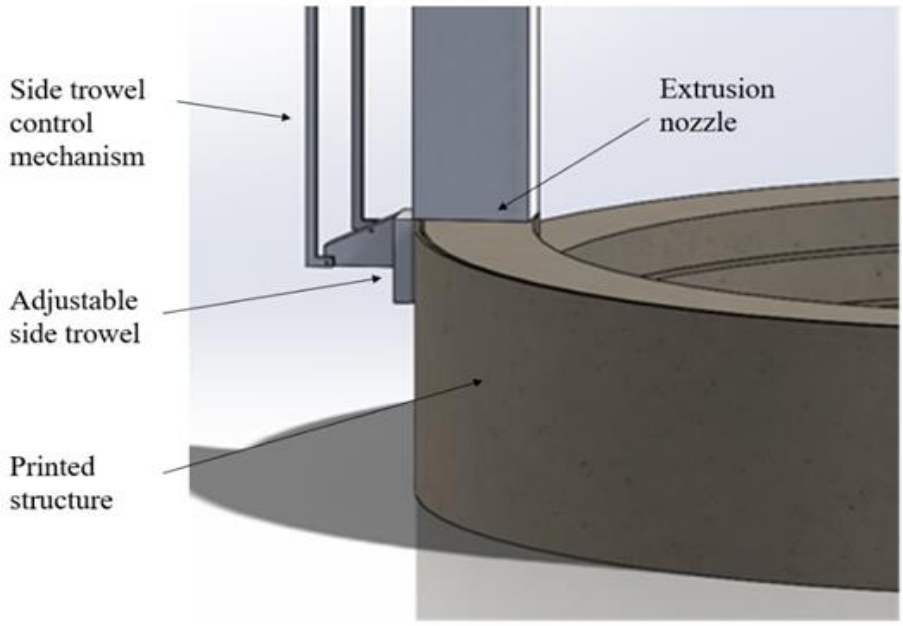

Figure 4: Illustration of contour crafting

[2] Certain commercial products are identified in this paper to specify the materials used and the procedures employed. In no case does such identification imply endorsement or recommendation by the National Institute of Standards and Technology, nor does it indicate that the products are necessarily the best available for the purpose.

As illustrated in Figure 4, in contour crafting, mortar mixture is deposited using a nozzle capable of motion along three axes. Mortar cement is defined as "*a hydraulic cement, primarily used in masonry construction, consisting of a mixture of portland or blended hydraulic cement and plasticizing materials (such as limestone or hydrated or hydraulic lime), together with other materials introduced to enhance one or more properties such as setting time, workability, water retention, and durability*" [50]. Top and side trowels (attached to the deposition system) are used to guide/direct material flow as they pass over the extruded mortar mixture. The top trowel (not shown in Figure 4) smooths the top surface layer, thereby aiding adhesion with the next layer to be deposited [51]. The orientation of the side trowel can be changed to produce a smooth exterior surface. The thickness of the deposited layer is limited by the height of the trowel. Layer thickness, the print resolution for contour crafting, is approximately 13 mm [52]. The large diameter of the nozzle in contour crafting also facilitates faster build times as compared to other cementitious AM processes such as concrete printing and D-shape [53]. On printing one layer, the nozzle is raised by an amount equal to the thickness of the deposited layer. This extrusion process is repeated until the structure is obtained. In most cases, this structure (called "contour") can serve as the formwork that can, subsequently, be filled with a concrete mixture. The filling process can be performed in a batch manner.

Early demonstration of contour crafting process consisted of a concrete wall structure printed using commercially available materials [49]. A new mortar mixture was developed for this process using Type II hydraulic plastic portland cement. Extruded layers 19 mm wide and 13 mm thick were used to print the structure (formwork in this case) [51]. It

measured 1.5 m (L) X 0.6 m (H) X 0.15 m (W) [51]. A batch of prepared mortar mixture was expended in 10 minutes during the printing process [51]. Thereafter, the process was paused until the new batch was loaded in the system. [51]. The filling process was also performed in a batch manner during which the concrete mixture was poured in manually (in incremental depths of 13 cm) and allowed to cure before proceeding with the contour crafting process [49].

A focus on improving process performance led to optimizing the nozzle design [54] and the cement mixture [49,51,54–58]. Square orifices produced better bonding and material flow during printing than elliptical orifices [54]. The initial cement mixture formulated for this process (comprising Type II hydraulic plastic portland cement, sand, plasticizer, and water) showed a compressive strength of 2741 psi (18.9 MPa) [49]. The effect of aggregate size on strength of structures has also been analyzed [48]. Cast cylindrical specimens were tested for compressive strength. Mixtures with smaller maximum aggregate size displayed higher compressive strengths. The improvement was 104 % for the 3/32 in (2.4 mm) aggregate mixture at 28 days as compared to the 1/2 in (12.7 mm) aggregate mixture [48]. Improvements in compressive strength for smaller maximum aggregate size were also observed during early age strength tests performed at 42 minutes. This observation was mostly attributed to the decrease in aggregate volume with respect to the total composite volume [48]. Due to their compatibility with the extrusion system and good compressive strength, concrete mixtures with maximum aggregate size of 3/32 in (2.4 mm) and 3/16 in (4. 76 mm) were used for further experimentation. Cubic samples were cast using three different layering processes to

mimic the contour crafting process and to analyze the effect of layer thickness and time lapse between layers on bond strength [48].

Certain properties of concrete mixtures are well defined in the conventional construction industry. For example, workability is defined as the property of freshly mixed concrete that affects the ease with which it can be mixed, placed, consolidated, and struck off [59]. However, new property definitions are needed for concrete mixtures used in AM processes. A framework was proposed for laboratory testing of cementitious materials used in contour crafting [60]. This framework was used to analyze the effects of nano-clay, silica fume, and polypropylene fiber inclusion on workability of a printing mixture [60]. The materials were evaluated in terms of print quality, shape stability, and printability window. Print quality referred to the surface quality, squared edges, and dimensional conformity of the printed layer [60]. Shape stability was defined as the ability to resist deformations during layer-wise concrete construction [60]. Printability window was defined as the timespan during which the mixture could be extruded from the nozzle with acceptable quality [60]. While inclusion of silica fume and nano-clay significantly increased the shape stability of the mixture, the addition of polypropylene fiber resulted in minor improvement.

The ability to construct reinforcements during extrusion was investigated by Kwon who extruded fresh layers of concrete mixture over a metallic coil reinforcement [61]. Cross-sections of these layers exhibited reasonable adhesion between layers [62]. Alternately, Khoshnevis [63] proposed the use of robotic placement of modular steel mesh for reinforcement during printing of structures.

Optimization of tool-paths was also performed for single and multiple machines using different numbers of nozzles [64–66]. Additionally, geometric conformity of surfaces constructed using contour crafting was analyzed [67]. Research was carried out on the effect of topological interlocking of layers on interface bond strength [68]. Cube samples of 4 in (101.6 mm) were cast in a batch manner (to simulate the contour crafting process) with interlocking rectangular teeth at the interface [68]. While these interlocking teeth had constant width, their depth varied from 0.25 in (6.35 mm) to 0.75 in (19.05 mm). Samples with a depth of 0.5 in (12.7 mm) showed an increase in bond strength of 17 % on average [68].

Construction of large structures using contour crafting usually requires big gantries which may be difficult to assemble at a construction site. In contrast, a cable-based system would be easy to transport and deploy. Researchers conducted a theoretical analysis of a cable-based system for contour crafting [69,70]. This contour crafting cable robot concept was designated as Cable-Suspended Contour Crafting Construction (C^4) [69,70].

Contour crafting can have extraterrestrial applications. High energy cost associated with escaping earth's gravity has proved to be a major impediment to space flight. A promising solution is to minimize the payload mass [71]. Contour crafting could be employed to construct long-term habitats suitable for humans on Mars and lunar surfaces using locally available materials [55,61,72–77]. This concept of using locally available materials is referred to as In-situ Resource Utilization (ISRU). It implies "*the ability to extract and process resources at the site of exploration into useful products such as propellants, life support and power system consumables, and radiation and rocket exhaust*

plume debris shielding" [78,79]. For example, given their abundance on Mars, sulfur-based materials could be used for construction [55]. Moreover, sulfur concrete is a good candidate for construction applications on Mars because it does not require a significant amount of water [55]. Sulfur concrete has been printed using contour crafting [55] using a mixture comprising elemental sulfur, sulfur modifier, coarse aggregate, and fine aggregate. This mixture was pre-melted and mixed at 150 ℃ and fed into a reservoir. The elemental sulfur reached its desirable state in 1 hour and was extruded using a KUKA robotic arm having 6 degrees of freedom (DOF) [55]. Researchers identified workability as a critical property for contour crafting of sulfur cement as it affected transportation and extrusion of print material and, thereby, part quality in terms of strength and surface finish [55]. The mixture temperature and sulfur proportion were identified as important variables affecting extrusion [55]. While high temperature during extrusion led to less porosity, reduced sulfur proportion led to improved surface and shape quality. However, reduced sulfur content also led to an increase in porosity.

Since contour crafting and concrete printing are both extrusion-based processes using cementitious materials, the gaps in these processes will be presented collectively at the end of this section.

2.2.1.2. Concrete Printing

Concrete printing was developed by researchers at Loughborough University. In this process, printing time can be reduced by minimizing the non-printing movements of the nozzle [80]. The layer thickness varied from 4 mm to 6 mm [53]. The prototype printer had a build envelope of 5.4 m (L) X 4.4 m (W) X 5.4 m (H). Cement and gypsum-based

materials were printed using a single 9 mm nozzle capable of moving along three directions. Concrete printing had longer built times than contour crafting because of this small layer thickness. The surface finish resulting from this process was ribbed due to the absence of smoothening trowels [53]. For illustration of this process, please refer to Figure 4. Unlike contour crafting, trowels are absent in concrete printing.

Researchers printed a bench-like structure called the "Wonder bench" using this process. The dimensions of this 1000 kg structure were 2 m (L) X 0.9 m (W) X 0.8 m (H) [80]. The structure comprised 128 layers (layer thickness of 6 mm) with an average printing time of 20 minutes per layer [80]. The structure had 12 through holes or "voids" of varying shapes that could provide routes for building services. Additionally, 23 through holes were incorporated into the design to facilitate structural reinforcement. Reinforcement bars of 8 mm diameter were inserted, post-tensioned and grouted to put the part in predetermined compression [53].

Research in concrete printing led to the definition of properties for wet materials to obtain a stable extruded layer. These properties were: extrudability, workability, open time, and buildability, pumpability, and layer cycle-time [81,82]. Extrudability was defined as the capacity of the material to pass through small pipes and nozzles at the printing head [81]. This property was influenced by the workability of the material [81]. Buildability referred to the capacity to print a certain number of layers or height [81]. Open time was defined as the time during which the material consistency was good enough to maintain extrudability. Extrudability and buildability were identified as the most critical properties in fresh concrete [81]. Fresh concrete was referred to as the "*concrete that*

possesses enough workability so that it can be placed and consolidated by the intended methods" [83]. Pumpability denoted the ease with which fresh concrete mixture is transported from pump to extrusion nozzle [81]. Layer cycle-time was defined as *"the time delay between fresh mortar being placed in the same location on top of the previous layer*" [82]

Different cementitious materials have been studied for concrete printing. Rushing et al. [84] analyzed various conventional and non-conventional concrete mixtures suitable for AM processes using a modified clay extruder. The conventional materials were not suitable for the AM process because of material flow related problems. The researchers recommended a larger proportion of fine aggregates (such as sand) in the mixture to address these flow complications. While fly ash provided the best improvement in flow, bentonite aided shape stability. In addition, the use of polycarboxylate based superplasticizer increased the fluidity/workability of the mixture without compromising on concrete strength. Rushing et al. [84] also recommended an applied vibration during extrusion for materials that flowed poorly during extrusion but performed better during the drop table test for flow. Lim et al. [81] found that the optimum mixture for their process had a 3:2 sand-binder ratio. The binder consisted of 70 % cement, 20 % fly-ash and 10 % silica fume (by weight of dry mixture) and 1.2 kg/m^3 of 12/0.18 mm (length/diameter) polypropylene fibers [81]. The water to binder ratio was 0.26. Using a 9 mm nozzle, 61 layers could be printed without noticeable deformation and with an open time of 100 minutes. The 28-day compressive strength of the sample was 110 MPa. Malaeb et al. [85] analyzed various mixtures. The optimal mixture developed was a mortar with fine

aggregate to cement ratio of 1.28 and a fine aggregate to sand ratio of 2. They also added superplasticizer, accelerator and retarder to the mixture. A buildability of 4 layers was achieved [85]. Hambach and Volkmer [86] used a mortar mixture enhanced with reinforcing fibers (carbon, glass, and basalt) for printing. The mortar mixture had a weight percentage of 61.5 % Portland cement (type 1 52.5 R), 21 % silica fume, 15 % water, and 2.5 % water reducing agent. The water to cement mass ratio was 0.3, and 0.3 % (by mass) of hydration inhibitor was also used to avoid thickening of the paste. Geopolymers consisting of fly ash, slag, silica fume, sand, potassium silicate, water, and additives were also printed using extrusion-based AM processes [87,88].

Researchers at TU Eindhoven used a gantry-based approach to concrete printing with 4 DOF. The build envelope for their printer was 9 m X 4.5 m X 2.8 m with a linear print speed of 0.1 m/s [42]. Layer stacking problems due to the round filaments obtained from the circular nozzle led the researchers to use a 40 mm X 10 mm rectangular nozzle [42]. The speed and frequency of the pump were reduced around corners of the structure. The nozzle standoff distance [87] (height of the print head above the print surface or distance between the nozzle and the print surface) was identified as an important parameter to control the shape and properties of the printed structures [89]. Reducing the nozzle standoff distance to slightly less than the nozzle opening may facilitate compaction and interface adhesion [42]. Moreover, parameters such as print speed also have a significant effect on load bearing capacity of printed structures [42]. The no-slump mortar developed for this process comprised portland cement, siliceous aggregate, limestone filler, rheology modifiers, and polypropylene fibers. According to the researchers, the no-slump mortar

facilitated geometric accuracy and stacking of layers [42]. The 28-day compressive strength and flexural tensile strength were 30 N/mm^2 and 5 N/mm^2, respectively. However, the no-slump mortar suffered from low stiffness, low strength, and, consequently, low buildability since it was printed in a pre-setting state. Cavities in the extruded filament were an additional problem.

Researchers at the Singapore Center for 3D Printing analyzed the suitability of geopolymer mortar, lightweight mortar, and fiber-reinforced mortar for concrete printing using gantry and robotic-arm based systems [43,90]. For fly ash based geopolymers, extrudability, shape retention, buildability, and thixotropic open time (TOT) were identified as critical early-age properties to characterize the printed materials [90]. TOT was defined as "*the time interval beyond which a material loses its extrudability property*" [90]. The authors used a dimensionless number called the shape retention factor (SRF) to quantify the shape retention. It was expressed as the ratio of cross sectional areas of sample before and after demolding [90]. The researchers cautioned that the suitability of definitions and characterization were strongly dependent on chemical composition of the material and testing equipment. They postulated that fresh properties of the mixture, print direction, and print time may have a significant effect on mechanical properties of the samples [91]. Printing direction had significant effect on compressive and flexural strength of printed samples [91]. In comparison to cast samples, a 15 % increase in compressive strength at 28 days was observed for printed samples with a built direction perpendicular to the loading direction [91]. These samples were printed using components such as traditional cement, fly ash, silica fume, glass fiber, plasticizer, sand, and water. These

results were consistent with results obtained by other researchers [92,93]. For geopolymers, tensile bond strength was found to increase with reduced printing speed and nozzle standoff distance [87]. However, increase in time gap between deposition of successive had the opposite effect [87].

Gosselin et al. [94] used a 6-axis robotic arm (ABB 6620) for large-scale concrete printing. Using the tangential continuity method (TCM) the researchers were able to print non-planar layers with locally varying thickness. This method facilitated a constant contact surface between successive layers. This was a different approach from conventional printing processes in which layer thickness was constant. The printhead was fed with the mixture material and an accelerating agent. The mixture consisted of original portland cement (30 % to 40 %), crystalline silica (40 % to 50 %), silica flume (10 %), and limestone filler (10 %) by weight. The ratio of water to cement and sand was 0.1 by weight. The material also had polymer-based resin, an accelerator, and a thresholding agent. While the resin enhanced the quality of interfaces between layers, the accelerator and thresholding agent ensured setting time and rheology properties for the AM process. Demonstration examples consisted of a multifunctional wall and an acoustic damping wall element. The wall had dimensions of 1360 mm X 1500 mm X 170 mm and was printed over 12 hours. It comprised 139 layers and weighed 150 kg [94]. The acoustic element measured 650 mm X 650 mm X 300 mm and consisted of 26 layers. It was printed over a 2-hour duration.

Delta printers [95] have also been used for concrete printing. The motion of the extruder is controlled by three arms. Each of these arms is capable of motion in the vertical

direction. An example of this configuration is the DeltaWASP 2040 3D printer equipped with a clay extruder kit. Researchers used this printer to build fiber reinforced (carbon, glass, and basalt) portland cement samples [86,96]. In their study, the nozzle size was 2 mm and the layer thickness and print speed were 1.5 mm and 30 mm/s, respectively. The printing process would enforce the alignment of the fibers in the mixture. The highest flexural strength obtained was 30 MPa using 1 %, by volume of carbon fiber [86].

Xu et al. [97] used a concrete printing process for the reproduction of a historical building ornamental component in from the Huazhong University of Science and Technology (HUST) in China. A cup-shaped plinth was 3D scanned, re-modelled, and printed. The 3D printed plinth demonstrated compressive strengths of 19.8 MPa and 15.6 MPa along its vertical and lateral directions, respectively.

Optimization of building rates for these layer-by-layer printing processes have also been studied. Perrot et al. [98] developed a theoretical framework based on the comparison between the vertical stress acting on the first deposited layer and the critical stress related to plastic deformation. Hence, the framework ensured that the vertical stress did not exceed the critical stress. Although experiments were carried out to validate the simulation results, these samples were not 3D printed. The mortar comprised cement, kaolin, and limestone filler. The composition consisted of 50 % cement and equal amounts of kaolin and limestone filler, by mass. While the water/cement mass ratio was 0.41, polycarboxylate-type superplasticizer/cement ratio was 0.3 % by mass [98].

Suiker [99] provided a mechanistic model for analyzing and optimizing the mechanical performance of straight wall structures during a 3D printing process. Failure

due to elastic buckling and plastic collapse were considered in the model. The model incorporated process parameters such as printing speed, curing characteristics of the material, and geometrical features of the printed object. It presented good agreement with the experimentally observed buckling response of a 3D printed concrete wall [99]. Wolfs et al. [100] developed a numerical model to analyze the early age (0 to 90 minutes after deposition) mechanical behavior of 3D printed concrete. This model, based on time-dependent Mohr-Coulomb failure criterion and linear stress-strain behavior up to failure, was experimentally validated [100]. The experiments were conducted using the material composition discussed in [42]. The numerical results depicted the failure deformation mode to be a combination of cylindrical buckling and material yielding. This cylindrical buckling deformation was also observed during experimentation. This model was found suitable for qualitatively predicting the failure deformation mode of the printed samples. The authors concluded that geotechnical (soil) tests were appropriate to evaluate the properties of early age printed concrete.

Rheological requirements for printability (of single layers and complete objects) were studied by Roussel [101]. These requirements were evaluated in terms of yield stress, viscosity, elastic modulus, critical strain, and structuration rate [101]. Structuration or thixotropy referred to the time evolution of yield stress for a fresh concrete at rest [102]. The author stated that these rheological requirements for printability would also depend on the type of AM process and the intended shape. The transition height (H_T) [101] above which buckling was expected to dominate the failure as opposed to strength-based failure was expressed as:

$$H_T = 2\delta\sqrt{\frac{1+\upsilon}{3\sqrt{3}\gamma_c}} \quad (1)$$

Where, υ is the Poisson's ratio of the material, δ is the width of the printed wall, and γ_c is the critical shear strain at onset of flow.

Admixtures can be defined as "*ingredients that are added to a concrete batch immediately before or during mixing*" [103]. The use of additives can provide benefits such as improved workability and gain in strength. Marchon et al. [104] provided an overview of the of potential admixtures for hydration and rheology control of concrete from a physico-chemical perspective. In their analysis of admixtures for controlling setting of concrete mixtures, Reiter et al. [102] concluded that activators should be added close to the delivery point. To avoid buckling failure, it was vital that yield stress of the extruded material evolves exponentially [102].

Concrete possesses low-tensile strength. Hence, concrete structures are reinforced using steel bars in conventional construction. Currently, researchers are developing strategies for incorporating reinforcement into additively manufactured concrete structures. Researchers have used magnetic field to control the orientation of steel fibers in self compacting concrete [105]. Bos et al. [106] developed a "*reinforcement entraining device (RED)*" to introduce reinforcement medium into the concrete filament during printing. This device used a stepper motor to feed the reinforcement cable from a spool directly into the filament. High strength steel cables were used for the process due to their

high tensile strength and lateral flexibility. The ultimate tensile loads of the three types of cables used were 420 N, 1190 N, and 1925 N. These cables were identified as cables A, B, and C, with diameters of 0.63 mm, 0.97 mm, and 1.20 mm, respectively [106]. The bond strength of cables in the printed concrete was considerably lower than that in cast concrete [106]. During four-point bending tests, cables B and C failed due to cable slip. Cable A beams failed due to cable breakage. Mechtcherine et al. [107] provided an overview of implementing reinforcements for 3D printed concrete structures. The researchers also presented a fully automatic, adaptive gas-metal arc welding process for constructing reinforcements [107]. The 3D printed steel bars exhibited 20 % lower values of yield stress and tensile strength. Asprone et al. [108] classified reinforcement strategies for concrete printing based on structural principle and the stage at which they can be incorporated into the manufacturing process. Based on structural principle, reinforcement in AM structures could be integrated by printing ductile materials (such as fiber reinforced materials) that possess the required strength, printing/assembly of reinforcements, printing of compression loaded structures, or a combination of these strategies. These reinforcements could be added before, during or after the AM process [108]. Asprone et al. [109] also presented a design approach for incorporating reinforcements. This approach divided reinforced concrete members into segments into 3D printed concrete segments and steel reinforcement systems [109]. This structurally optimized approach was demonstrated by performing a full-scale three-point bending test on a 3 m long reinforced concrete beam. These AM processes could also reduce the amount of reinforcement required for concrete structures [110]. The researchers reported that weak interfaces could

be used as crack initiators thereby reducing the minimum amount of reinforcement required for concrete structures [110].

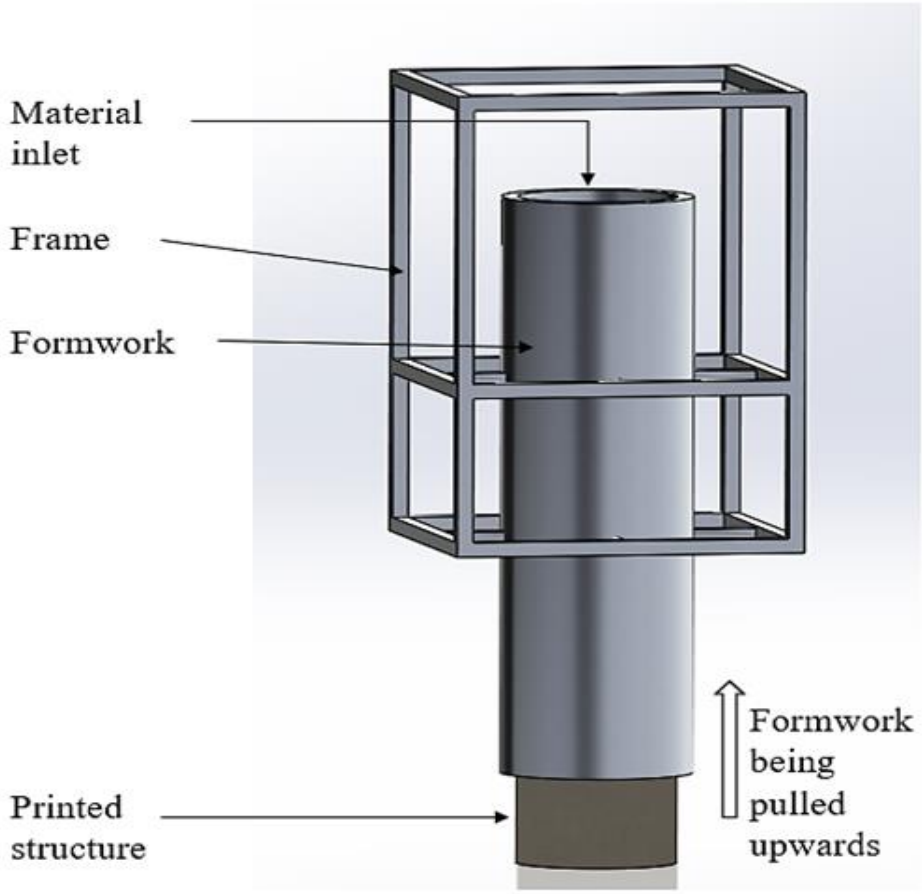

Figure 5: Illustration of smart dynamic casting (SDC)

Researchers at ETH Zurich developed a construction process called Smart Dynamic Casting (SDC). This process was used to construct complex concrete structures. The researchers wrote that, "*SDC is a robotic slipforming process which exploits the formability of concrete in the delicate period when it changes from a soft to a hard*

material." [111]. Slipforming refers to a construction process in which concrete mixture is poured into a formwork that moves in the vertical direction [111]. The velocity of the vertical motion is determined by the hydration rate of the mixture. This is to ensure that the released structure is capable of supporting its own weight. A feedback system was used to monitor the material properties. The system consisted of a significantly smaller formwork attached to a robotic arm with six degrees of freedom. The construction material was fed into the formwork. Thereafter, the formwork was lifted at a specific rate to reveal the set structure. The robotic arm facilitated precision of velocity and movement of the formwork. Additionally, a feedback system that monitored the physical properties of the concrete mixture was used to guide the robotic arm and ensure that the material was in the perfect stage for slipforming. Recently, the researchers also developed flexible formwork systems that were capable of slipforming carbon fiber reinforced concrete mixtures [112]. The flexibility of formworks was achieved by mounting flexible membranes on the formwork. Oil was injected into the membrane layers to avoid friction.

This process was demonstrated by printing an elliptical column 1800 mm in height with a rotation of 180 degrees along its height. An elliptical formwork of dimensions 125 mm (L) X 80 mm (W) X 60 mm (H) was used for this demonstration. The feedback system was used to guide the slipping velocity of the formwork. Additionally, a 4 m long canoe having a wall thickness of 1.8 cm was constructed using this process [112]. In this process, the effect of friction is magnified due to the increase in surface to volume ratio [113]. Szabo et al. [113] analyzed mortar mixture designs and acceleration strategies to address this limitation. Reinforcements have also been integrated into structures constructed using

SDC [114]. A critical aspect of the process was that small variations in concrete composition and room temperature could have a significant effect on the outcome of the process.

Researchers at Purdue University have developed direct-ink writing process [115]. Their research was guided by biologically inspired natural composite materials (such as those found in exoskeletons of arthropods, bones, and seashells) that achieve higher toughness without sacrificing stiffness and strength [115,116]. The printing setup comprised a combination of a 3D printer (Ultimaker 2 Extended+, nozzle diameter: 1.36 mm) and a 75 mL capacity material extrusion system (Structur3d Discov3ry Paste Extruder) [117]. Moini et al. [117] provided an analysis of microstructural features of printed cementitious samples. The printing mixture consisted of Type 1 cement, high-range-water-reducing-admixtures, viscosity modifying admixtures, and deionized water [117]. Cubes (25 mm) of lamellar architecture were printed with a layer thickness of 1 mm and a print speed of 25 mm/minute. Unlike the cast samples, the printed samples exhibited features such as: macropores, micropores at interfacial regions of filaments, self-rearrangement of filaments from their designed toolpath, and high accumulation of anhydrous cement particles near large pores. The researchers also analyzed bioinspired Bouligand structures for harnessing heterogeneous interfaces in cement-based materials [118].

Despite the recent surge of research in AM processes for construction applications, important challenges remain in the areas of material development, improving process knowledge, developing new technology, computational modeling, and reinforcement

strategy. Currently, cement production is not a sustainable process. Every ton of cement production results in the release of 0.9 tons (846.5 kg) of CO_2 into the atmosphere [17]. Additionally, most of the prevalent AM processes for construction applications use cementitious materials. Hence, there is need to develop new, sustainable construction materials that are compatible with emerging AM process technology.

In concrete extrusion, each layer is in a different stage of curing [42]. While the material must be fluid to exhibit good extrudability, it must also have short curing times and stiffness to support the printed layers above. Insufficient strength of the base layers can lead to distortion and affect vertical alignment of layers, eventually leading to failure [42]. Furthermore, high structuration rates could result in weak interface between layers leading to the formation of cold joints [48,101]. Hence, these conflicting requirements on material properties need to be optimally met. Significant research is required to develop an understanding of material characteristics such as chemical composition, rheology, setting, drying shrinkage and hydration to avoid clogging, segregation and aid material flow [101,102,104,119–121]. It is critical to establish the relationship between these material characteristics and mechanical properties such as compressive and flexural strength [99,100,105]. Furthering the understanding of the process will also include analyzing the effects of process parameters such as ambient environmental conditions, print speed, and curing time. This approach will require measurement science research [122] and can be bolstered by machine learning and big data analysis techniques.

Accurate computational models are required to reduce time intensive experimentation and increase the understanding of materials at several time and length scales [123]. Current

software tools are unable to capture details such as multiple material designs, hierarchical complexity between components and embedded reinforcements [19]. Development of new software tools can help to take advantage of capabilities of AM processes.

Reinforcement remains a challenge for 3D printed concrete structures. While various reinforcement strategies are under development [106–109], mechanical performance of these reinforcement strategies needs to be characterized [108]. The bond strength between the reinforcement and concrete mixtures needs to be studied further [107]. The effect of varying environmental conditions on these reinforcement strategies must be investigated [109]. On the technological front, capability to print two different materials in parallel would enable the synchronized printing of the structure and the reinforcement matrix. Alternately, development of stronger, sustainable materials would eliminate the need for reinforcement altogether.

2.2.2. Polymer Material Extrusion

2.2.2.1. Digital Construction Platform

MIT researchers developed Digital Construction Platform to construct architecture-scale structures on-site [124]. It is an automated, mobile construction system that utilizes real-time environment data for process control [124]. This system consists of a compound hydraulic arm and a smaller electric arm with four and six DOF, respectively. Motion of the system is enabled using a tracked mobile base. These tracks can be expanded or contracted laterally to facilitate stability and motion through restricted spaces. Hydraulic outriggers are also used to enhance stability during printing. According to the researchers, this system can print while moving. A real-time sensor feedback system was used to

stabilize the end-point in order to compensate for the lift system and variable environmental conditions [124]. A nozzle is used to deposit a fast curing foam to print formwork structures.

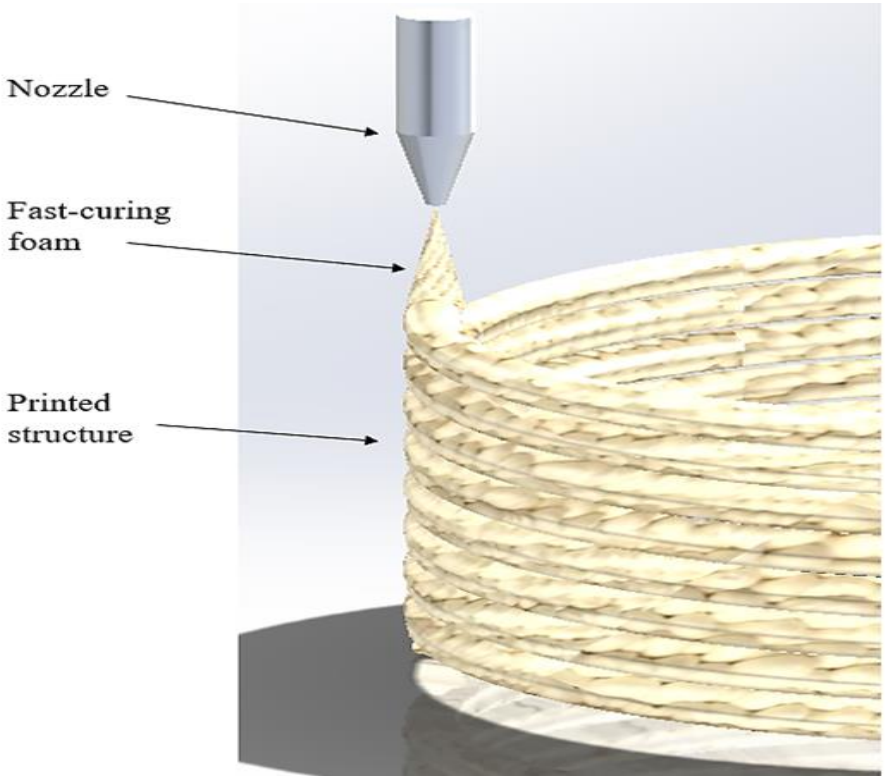

Figure 6: Illustration of the digital construction platform

Preliminary demonstration of this process consisted of a 3.7 m tall hemispherical dome with a diameter of 14.6 m printed over 13.5 hours [124]. The material used for printing this formwork structure was a polyurethane foam (Dow chemical's Froth-Pak insulation) that expanded to nearly 80 times its initial volume and started to cure in 30 seconds [124]. The density of this material was 28 kg/m^3 with compressive and tensile strengths of 161 kPa and 248 kPa, respectively [124].

Using a print speed of 0.15 m/s, layers were printed with a width of 80 mm and a thickness of 35 mm. The fabrication rate for this process was 1.728 m^3/hour [124]. The curing rate of the foam enabled the printing of horizontal overhangs without the use of sacrificial supports. The structure also demonstrated sufficient adhesion strength between layers to be used as formwork for constructing cast concrete structures. The addition of rebar ties was also successfully demonstrated. The structures printed using this process demonstrated a rough, layered texture [124].

Process parameters (such as isocyanate/polyol mixture, the distance between the spray nozzle and print surface, spray pressure, and spray flow rate) affected print roughness [124]. The researchers suggested that surface roughness could be improved using one of two methods. The rough surface could be smoothed using traditional finishing techniques such as plastering, or the foam structures could be milled and cut using subtractive fabrication processes. It is also important to note that environmental conditions played a critical role in the success of this on-site AM construction process. Even though the open hemispherical dome had a print time of 13.5 hours, the printing was done over two days. Environmental conditions such as dew were one of the causes for the delay.

Recently, a similar approach was applied to the construction of a house in France. In April 2018, researchers at the University of Nantes printed a 95 m^2 (1000 sq. ft.), five room house on-site using polymer materials and a robot (BatiPrint3D) [125]. The hollow polymer formwork was printed by the robot and was subsequently filled with concrete mixture. The printing process was completed in 18 days.

2.2.2.2. Flow-based Fabrication

Functionally graded materials (FGM) exhibit a variety of composition and structure over the volume of the material, resulting in a change of material properties [126]. Gradients in local properties can be harnessed to change the global properties of the material. Researchers at MIT developed an AM process for the construction of functionally graded materials using viscous water-based materials [127]. The pneumatic extrusion system was attached to a KUKA robotic arm. The pneumatic extrusion system consisted of six 300 mL plastic syringe barrels with rubber plungers and HDPE nozzles. These syringes were filled with print material. An air compressor and a vacuum pump were employed to provide positive and negative pressures respectively to aid material flow. The pneumatic extrusion tool was capable of handling materials ranging in viscosity from 500 cP to 50,000 cP at room temperature.

Small-scale demonstration of the process was carried out using chitosan and sodium alginate with organic aggregates [128]. The process was also demonstrated using polysaccharide hydrogels in 1 % to 12 % concentrations in w/v of 1 % acetic acid aqueous solutions. These different concentrations were used to generate gradients in opacity, viscosity, and stiffness [127]. Composites were obtained by mixing these gels with cellulose microfiber material. These materials/prints were cured at room temperature. The demonstration structure printed was a large (approximately 10 feet) self-supporting cantilever structure inspired by an insect wing or leaf venation structure [127]. The curvature of the structure was controlled by using geometrical patterning and multi-material deposition.

For this process, it would be interesting to see more large-scale examples using a variety of materials that exhibit faster curing times.

2.2.2.3. Big Area Additive Manufacturing (BAAM)

Researchers at Oak Ridge National Laboratory (ORNL) have developed Big Area Additive Manufacturing (BAAM). This process was used for large-scale AM of thermoplastic and composite materials [129]. Polymer pellets were melted and deposited on a heated build platform. The BAAM platform could accommodate structures of the size 6 m (L) X 2.4 m (W) X 1.8 m (H). The use of pellets (instead of polymer filaments) as feedstock facilitated a deposition rate 200 times faster (~ 50 kg/h) than conventional polymer systems [129]. Additionally, it also enabled a 20 times reduction in materials cost [129]. The screw design of the extruder promoted faster deposition rates using polymer pellets. The nozzle of the extruder ranged from 2.5 mm to 7.6 mm in diameter [130]. The deposition head performed the roles of melting and extruding the polymer material at a controlled rate. The deposition head can be mounted on a gantry or a robotic-arm.

In 2016, Boeing, in collaboration with ORNL, printed an airplane wing manufacturing tool, using BAAM. This tool was certified by Guinness World Records as the largest solid 3D printed item [131]. Researchers also used BAAM process to showcase a single room building module with integrated energy systems [132].

Many AM processes rely on ovens to reduce thermal gradients and distortion. In case of BAAM, there is no oven; reinforced thermoplastic materials are used to reduce printing distortions [130]. Carbon fibers are used to increase strength, stiffness, and the thermal conductivity; and to reduce the coefficient of thermal expansion, thereby reducing

distortion and warping [133]. The strength of carbon fiber reinforced polymers was close to aerospace grade aluminum [133]. The addition of reinforcement materials resulted in a significant increase in strength and stiffness in the primary deposition direction, but also resulted in significant mechanical anisotropy [129]. Hence, research is required to address mechanical anisotropy in BAAM samples to facilitate real-world applications [129].

To analyze the effects of material composition and deposition parameters on mechanical performance, researchers examined Acrylonitrile butadiene styrene (ABS), polyphenyl sulfide, and polyetherimide samples reinforced with carbon fiber and glass fiber [129]. A 7.6 mm nozzle was used to deposit an oval bead that was 8.4 mm wide and 4 mm thick [129]. The shape of the bead and the quality of the structure were dependent on process parameters such as extrusion temperature, flow rate, head speed, and material viscosity. Deposition of oval cross-sections resulted in a triangular void between adjacent beads [129]. A tamping mechanism was developed by researchers to reduce the porosity/voids between beads and improve layer consolidation. The researchers noted that these process parameters could be optimized to improve consolidation [129].

2.2.2.4. C-FAB™

Branch Technology [28,125] is an architectural fabricator in the U.S. specializing in large-scale 3D printing. Their AM process is referred to as C-FABTM. This AM process creates cell-like matrix/mesh geometry using fused deposition of polymers. The polymers used are ABS with carbon fiber or glass fiber reinforcement. An algorithm is used to create the mesh geometry and control the robotic motion without using support materials.

Thereafter, the mesh is filled with desired conventional materials to achieve the desired structure.

Examples of printed samples include prefabricated wall sections filled with conventional construction materials [28]. These modular wall sections were 3 to 4 times stronger than wood framing [125]. A demonstration pavilion using composites was printed by Branch Technology in collaboration with Oak Ridge National Laboratory (ORNL) for Design Miami [125,126].

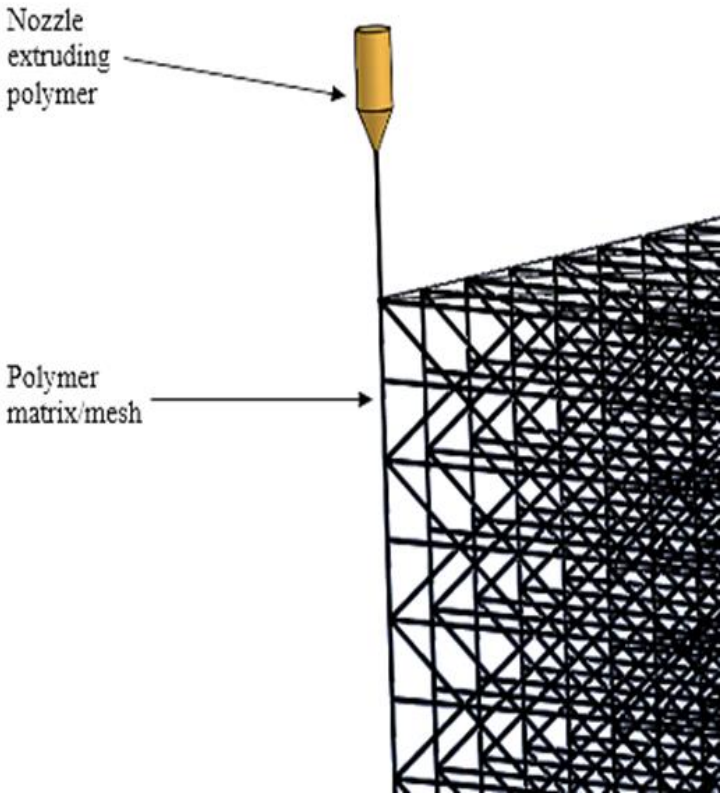

Figure 7: Illustration of C-FABTM

Researchers at ETH Zurich developed a Mesh Mold Metal process to construct stay-in-place formwork [9]. This process used a mobile, industrial robot, also referred to as "*In situ Fabricator"* for on-site construction [134]. Earlier versions of this process relied on polymer materials for constructing meshes that were later filled with cement mixtures [135,136]

2.3. Binder Jetting

Binder Jetting AM process is defined as a process in which a liquid bonding agent is selectively deposited to join powder materials [1]. Figure 8 shows an illustration of the process.

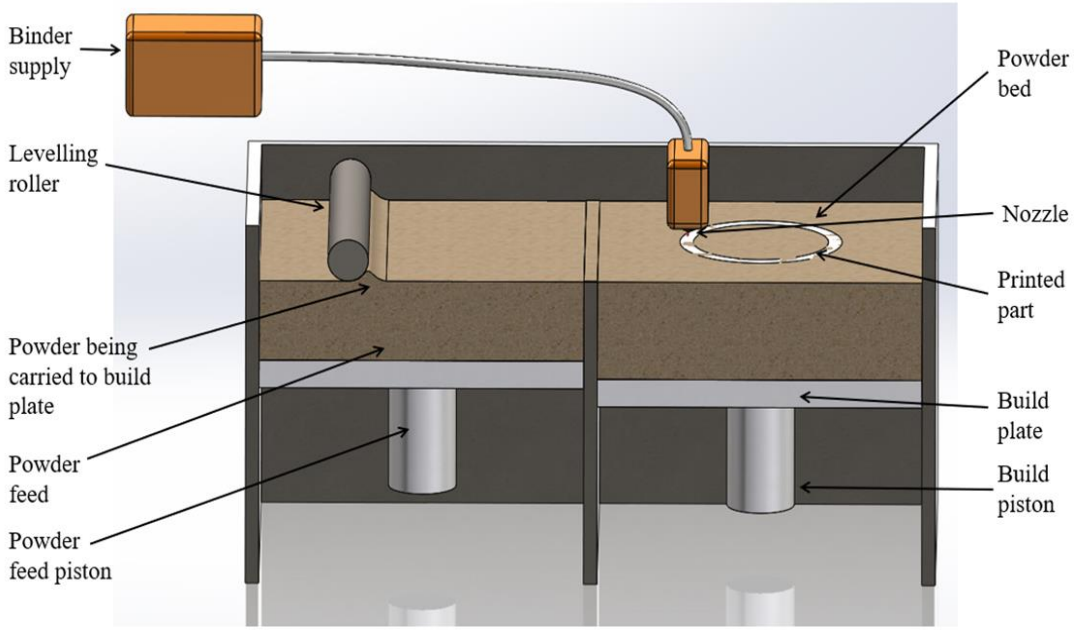

Figure 8: Illustration of binder jetting process

The D-shape is a binder jetting AM process invented by Enrico Dini [137]. This process relies on multiple nozzles that selectively deposit an inorganic binder on a sand substrate to construct sandstone structures. These nozzles are suspended by a gantry. The level of the nozzles is raised by 5 mm to 10 mm after the structural ink is deposited for a particular layer [137]. This process is repeated until the final structure is attained. On completion, the structure is removed from the powder bed.

The prototype printer had a print area of 6 m X 6 m and had 300 nozzles placed 20 mm apart [137]. The D-shape process was demonstrated by printing a gazebo. The design was based on a small microorganism called 'Radiolaria'. It was a 2 m tall sandstone structure consisting of 200 layers, each having a thickness of 10 mm [137].

Research was also carried out to analyze the feasibility of this process for constructing lunar outposts for human habitation [138]. While for terrestrial applications, an outer shell was also printed to hold the unbound material in place, for lunar applications the researchers proposed the use of two closed continuous skins to obtain the desired performance [138]. Preliminary experimental and analytical research was demonstrated using regolith simulant material under vacuum conditions [138].

The D-shape process faces some challenges in print speed and finish of the final structure. The deposited powder must be pushed over the build area and compressed before the structural ink can be deposited for each layer [53]. Furthermore, the unused powder material needs to be removed after the printing is completed. Hence, the D-shape process is slower than contour crafting and the final structure has a textured finish [53]. This may be the result of bleeding of the structural ink through the build layers.

Binder jetting systems have also been researched for cementitious materials. Currently, the sample size is limited to smaller scale objects. Feng et al [132] used a binder jetting printer (Spectrum ZP150 3D printer) capable of printing samples of dimension 356 mm (L) X 254 mm (W) X 203 mm (H). The material was a mixture of plaster powder ZP150 (comprising of plaster, vinyl polymer, and carbohydrate) and a binder material (ZB60) consisting of humectant and water [132]. The load bearing capacity of the samples was found to be dependent on build direction. Xia and Sanjayan [133] analyzed the printability of geopolymer-based material using parameters such as particle size distribution, powder density, and powder bed porosity. The prepared material consisted of a blend of slag, anhydrous sodium metasilicate, and fine sand. The printed samples exhibited anisotropic mechanical properties and geometric accuracy. Researchers also developed a material for binder jetting using a mixture of calcium aluminate cement that passed through 150 μm sieve and portland cement [134]. A water-based binder was used for printing. The porosity of samples was dependent on particle size distribution and layer thickness. More research is required to develop binder jetting systems for large scale AM of concrete structures.

Weger et al. [139] analyzed the contour precision and compressive strength of printed samples. In their process, "*selective paste intrusion*," the particle bed consisted of aggregates onto which cement paste was deposited using a nozzle. The cement paste had a water/cement ratio of 0.4 and the diameter of the aggregates was less than 3.2 mm [139]. The horizontal precision increased with decreasing permeability of the bed and yield stress of the cement paste. An increase in paste intrusion height resulted in increased strength of

samples. The samples had a compressive strength of 22.1 MPa [139]. In a recent the bed and yield stress of the cement paste. An increase in paste intrusion height resulted in increased strength of samples. The samples had a compressive strength of 22.1 MPa [139]. In a recent study, the compressive strength of samples was 70.8 MPa when the load was applied perpendicular to the printed layers [140]. The strength decreased to 64.2 MPa when the load was applied in the direction parallel to the printed layers [140].

Better control of process parameters and improving reliability represent challenges for these processes [46]. While the D-shape process can print meter-scale structures, other binder jetting processes are limited to millimeter-scale samples. Further research is required to scale-up these processes.

2.4. Selective Separation Sintering

This AM process uses two types of powders, a base powder (B-powder) that constitutes the final part and a separator powder (S-powder) that is used as a separator [141]. Like binder jetting process, this process uses a powder bed system as shown in Figure 8. As the name suggests, the role of the S-powder is to separate the part from the surrounding B-powder. Successful implementation of this process is dependent on these powders having significantly (several hundred degrees) different sintering temperatures. The printing process starts with a uniform layer of B-powder on the bed. S-powder is selectively deposited on top of the B-powder using motion actuators and a piezo vibrator. This process is repeated until all the layers are complete. The green part is moved to the sintering furnace where the sintering is carried out at a temperature that is higher than the sintering temperature of the B-powder, but lower than the sintering temperature of S-

powder. The part comprising of the B-powder is sintered and the loose S-powder is removed from the sintered part.

Preliminary experiments were carried out to demonstrate this process for space applications using ceramics and metals [141,142]. Bronze components were fabricated using alumina powder and tungsten powder as separators [141]. Lunar regolith simulant JSC-1A (sintering temperature 1100 ℃ to 1150 ℃) and Bronze (sintering temperature 780 ℃) were used as B-powder while alumina powder (sintering temperature 1500 ℃) was used as S-powder [142]. In both cases, the sintered parts were separated easily.

Since Selective Separation Sintering is a new process, significant research is required to develop process knowledge and improve control of powder deposition to improve print quality [141].

2.5. Additional Gaps

In addition to the process specific gaps discussed earlier, there are additional challenges in the application of AM processes in infrastructure construction. These challenges range from creating new materials, improving process knowledge, developing new standards to system-level integration, and design for AM processes in the construction industry.

Material development for AM processes is a significant challenge. Life-cycle assessment study conducted by Agustí-Juan and Habert [143] specified that building material production was a major factor in the relative sustainability of construction projects. Even though new AM processes have been developed, the conventional cementitious materials they use are not sustainable. These AM processes have the

potential to reduce the use of these unsustainable materials through computational structural optimization [121,143]. New, sustainable materials need to be developed for construction applications in the 21st century. These new materials must exhibit high performance especially when exposed to harsh environmental conditions. Materials able to respond to external stimuli are desirable. Such capabilities could enable the construction of self-healing structures. Computational models will be vital in developing these novel materials.

Considerable research is required to increase the process knowledge. Material characteristics, such as extrudability, buildability, rheology, drying, and shrinkage need to be studied for emerging AM processes to be successful. Currently, no formal reference tests exist for evaluating extrudability [144]. These material characteristics could be controlled through admixtures [104]. Mechanical properties of the printed parts also need to be examined. There is a need to further understand the relation between process parameters (such as print speed, layer thickness, and environmental conditions) and the final part quality. These processes must be robust and capable of performing in diverse environmental conditions. Process repeatability needs to be established. While many AM processes can print structures of a few meters in dimensions, they need to be scaled-up to print buildings covering several square meters. Also, capability of AM processes to repair infrastructure remains to be determined.

Systems technology tools such as Building Information Modeling (BIM) are emerging. BIM models facilitate digital representation of a building for project communication over its entire life-cycle [145]. Synchrony of such tools with AM

processes would enable construction professionals to make better, informed decisions. For example, these systems-technology tools could recommend construction materials, AM processes and machine parameters to achieve desired printing performance and design. These tools could also recommend on-site vs. off-site construction strategies. Such recommendations would account for environmental conditions, material and structural support requirements, budget, safety, and other factors. While some exploration has been carried out for concrete structures in this case [146], significant progress is yet to be made.

The fast pace of experimental research in this field warrants the timely development of building codes and standards. Development of performance-based metrics for concrete formulation as opposed to the current prescriptive standards could accelerate innovation [37]. An example of such a performance-based metric would be, say, material 'A' should have property 'P' that exceeds a value 'V'. This is different from prescriptive standards such as, 'material A should be mixed with materials B and C in a, b and c proportions [37]. Emerging research areas such as data informatics and tools such as Materials Genome Initiative could be vital resources in this field [147,148]. Performance-based metrics coupled with a measurement science perspective should facilitate innovation in the field of material development. Additional examples of developing standards would include the designing custom test artifacts. These artifacts would enable engineers and architects to determine the suitability of materials and AM processes to achieve intended designs.

The emergence of AM processes for construction applications would also require a rethinking of the way buildings are designed. New AM processes can facilitate complex,

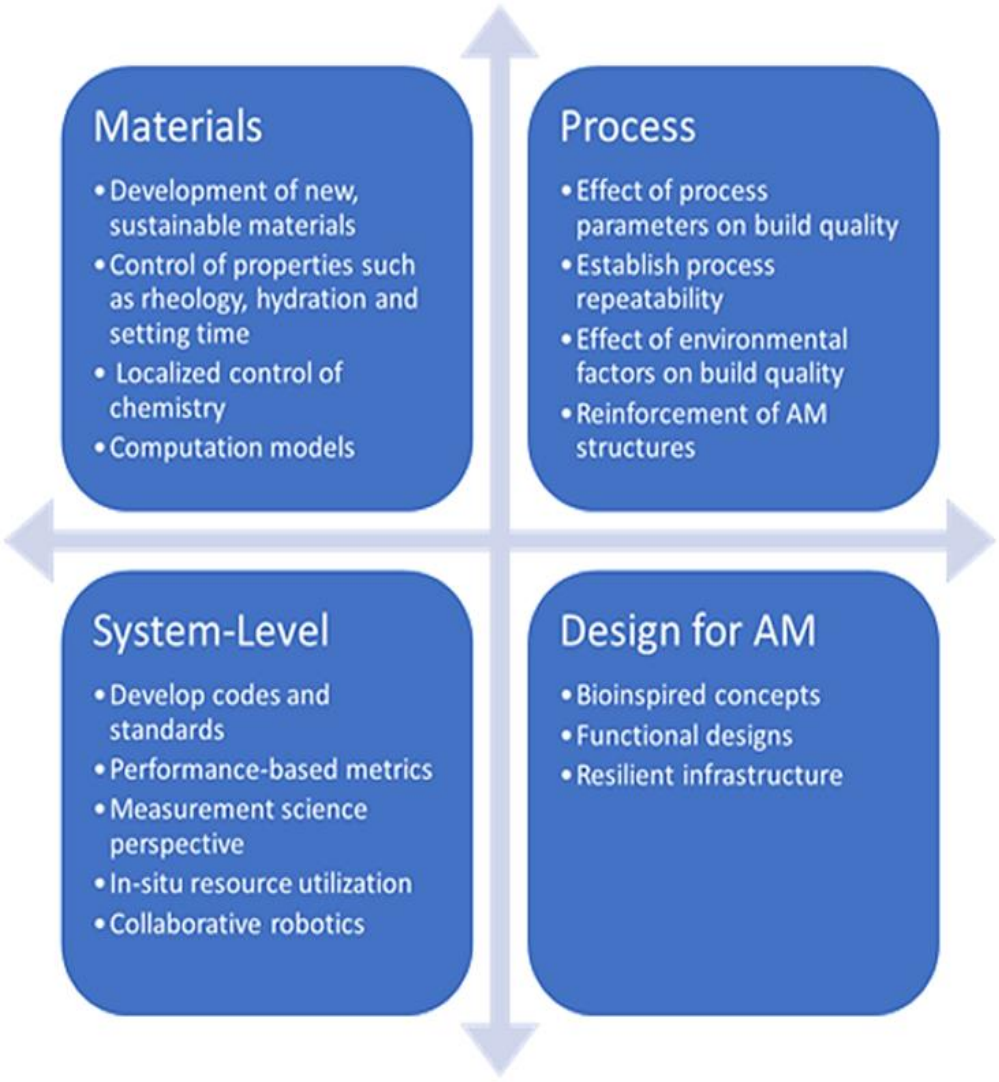

Figure 9: AM processes for construction of infrastructure: future research directions

stronger designs that use biomimicry to incorporate functionality and performance into the structural design of buildings. Currently, reinforcement remains a challenge for AM of cementitious structures. Bio-inspired designs could help address this challenge.

Large research consortia/national centers are fundamental to address the wide spectrum of challenges in this emerging field. Countries such as Germany [11], Singapore

[12], and Switzerland [10] have already setup research consortia/national centers to accelerate research in this field. However, there are no such research consortia/national centers in the U.S.

The economic and environmental impact of these AM processes also needs to be evaluated. Capability of an AM process to print building 24 hours a day, 7 days a week would also require a new approach to logistics for construction industry.

References

[1] ISO/ASTM52900-15, 2015, Standard Terminology for Additive Manufacturing – General Principles –Terminology, West Conshohocken, PA.

[2] Caffrey, T., Wohlers, T., and Campbell, R. I., 2016, Wohlers Report 2016, Wohlers Associates, Inc.

[3] Construction Intelligence Center, 2015, Global Construction Outlook 2020.

[4] International Labour Organization, 2005, "Facts on Safety at Work," Int. Labor Off. Tech. Rep.

[5] Bureau of Labor Statistics, 2017, "2016 U.S. Employment by Major Industry Sector" [Online]. Available: https://www.bls.gov/emp/ep_table_201.htm. [Accessed: 18-Dec-2017].

[6] Bureau of Economic Analysis, 2016, "Gross Domestic Product by Industry: First Quarter 2016" [Online]. Available: https://www.bea.gov/newsreleases/industry/gdpindustry/2016/gdpind116.htm. [Accessed: 18-Dec-2017].

[7] NIST, 2011, “Metrics and Tools for Construction Productivity Project” [Online]. Available: https://www.nist.gov/programs-projects/metrics-and-tools-construction-productivity-project. [Accessed: 03-Dec-2018].

[8] Nasir, H., Ahmed, H., Haas, C., and Goodrum, P. M., 2014, “An Analysis of Construction Productivity Differences between Canada and the United States,” Constr. Manag. Econ., 32(6), pp. 595–607.

[9] Wangler, T., Lloret, E., Reiter, L., Hack, N., Gramazio, F., and Kohler, M., 2016, “Digital Concrete : Opportunities and Challenges,” pp. 67–75.

[10] Swiss National Science Foundation, 2014, “National Center for Competence in Research-Digital Fabrication” [Online]. Available: http://www.snf.ch/en/researchinFocus/nccr/digital-fabrication/Pages/default.aspx.

[11] University of Stuttgart, 2018, “New Cluster of Excellence: Integrative Computational Design and Construction for Architecture,” Dtsch. Forschungsgemeinschaft [Online]. Available: http://icd.uni-stuttgart.de/?p=24111.

[12] Singapore Centre for 3D Printing, 2016, “Singapore Centre for 3D Printing” [Online]. Available: www.sc3dp,.ntu.edu.sg.

[13] Contour Crafting, 2017, “Contour Crafting Corporation” [Online]. Available: http://contourcrafting.com/.

[14] XtreE, 2015, “XtreE” [Online]. Available: https://www.xtreee.eu/.

[15] Apis Cor, 2016, “Apis Cor” [Online]. Available: http://apis-cor.com/en/faq/texnicheskie-xarakteristiki-3d-printera/. [Accessed: 12-Oct-2017].

[16] Technology, B., 2015, “Branch Technology” [Online]. Available:

https://www.branch.technology. [Accessed: 01-Oct-2017].

[17] Habert, G., 2013, “Environmental Impact of Portland Cement Production,” Eco-efficient Concr. F. Pacheco-Torgal, S. Jalali, J. Labrincha, VM John (ed.), Woodhead Publ. Cambridge, pp. 3–25.

[18] 2019, “Why More Buildings Should Be Made of Wood,” Econ. [Online]. Available: https://www.economist.com/leaders/2019/01/05/why-more-buildings-should-be-made-of-wood.

[19] Biernacki, J. J., Bullard, J. W., Sant, G., Brown, K., Glasser, F. P., Jones, S., Ley, T., Livingston, R., Nicoleau, L., Olek, J., Sanchez, F., Shahsavari, R., Stutzman, P. E., Sobolev, K., and Prater, T., 2017, “Cements in the 21 St Century: Challenges, Perspectives, and Opportunities,” J. Am. Ceram. Soc., pp. 1–28.

[20] Napper, I. E., Davies, B. F. R., Clifford, H., Elvin, S., Koldewey, H. J., Mayewski, P. A., Miner, K. R., Potocki, M., Elmore, A. C., Gajurel, A. P., and Thompson, R. C., 2020, “Reaching New Heights in Plastic Pollution—Preliminary Findings of Microplastics on Mount Everest,” One Earth, 3(5), pp. 621–630.

[21] Chiba, S., Saito, H., Fletcher, R., Yogi, T., Kayo, M., Miyagi, S., Ogido, M., and Fujikura, K., 2018, “Human Footprint in the Abyss: 30 Year Records of Deep-Sea Plastic Debris,” Mar. Policy, 96, pp. 204–212.

[22] Geyer, R., Jambeck, J. R., and Law, K. L., 2017, “Production, Use, and Fate of All Plastics Ever Made,” Sci. Adv., 3(July), pp. 25–29.

[23] Jones, M., Mautner, A., Luenco, S., Bismarck, A., and John, S., 2020, “Engineered Mycelium Composite Construction Materials from Fungal Biorefineries: A Critical

Review," Mater. Des., 187, p. 108397.

[24] Mironov, V., Trusk, T., Kasyanov, V., Little, S., Swaja, R., and Markwald, R., 2009, "Biofabrication: A 21st Century Manufacturing Paradigm," Biofabrication, 1(2), p. 22001.

[25] Holt, G., McIntyre, G., Flagg, D., Bayer, E., Wanjura, J., and Pelletier, M., 2012, "Fungal Mycelium and Cotton Plant Materials in the Manufacture of Biodegradable Molded Packaging Material: Evaluation Study of Select Blends of Cotton Byproducts," J. Biobased Mater. Bioenergy, 6(4), pp. 431–439.

[26] Jiang, L., Walczyk, D., Mcintyre, G., and Kin, W., 2016, "Cost Modeling and Optimization of a Manufacturing System for Mycelium-Based Biocomposite Parts," 41, pp. 8–20.

[27] Conner, B. P., Manogharan, G. P., Martof, A. N., Rodomsky, L. M., Rodomsky, C. M., Jordan, D. C., and Limperos, J. W., 2014, "Making Sense of 3-D Printing: Creating a Map of Additive Manufacturing Products and Services," Addit. Manuf., 1, pp. 64–76.

[28] Berman, B., 2012, "3-D Printing: The New Industrial Revolution," Bus. Horiz., 55(2), pp. 155–162.

[29] Birtchnell, T., Urry, J., Cook, C., and Curry, A., 2013, Freight Miles: The Impact of 3D Printing on Transport and Society, Lancaster University.

[30] Espalin, D., Muse, D. W., MacDonald, E., and Wicker, R. B., 2014, "3D Printing Multifunctionality: Structures with Electronics," Int. J. Adv. Manuf. Technol., 72(5–8), pp. 963–978.

[31] Macdonald, E., Salas, R., Espalin, D., Perez, M., Aguilera, E., Muse, D., and Wicker, R. B., 2014, "3D Printing for the Rapid Prototyping of Structural Electronics," IEEE Access, 2, pp. 234–242.

[32] Parthasarathy, J., Starly, B., and Raman, S., 2011, "A Design for the Additive Manufacture of Functionally Graded Porous Structures with Tailored Mechanical Properties for Biomedical Applications," J. Manuf. Process., 13(2), pp. 160–170.

[33] Heinl, P., Müller, L., Körner, C., Singer, R. F., and Müller, F. A., 2008, "Cellular Ti--6Al--4V Structures with Interconnected Macro Porosity for Bone Implants Fabricated by Selective Electron Beam Melting," Acta Biomater., 4(5), pp. 1536–1544.

[34] Economic Development Research Group Inc., 2016, Failure to Act: Closing the Infrastructure Investment Gap for America's Economic Future, American Society of Civil Engineers, Reston, Virginia.

[35] National Academy of Engineering (NAE), 2008, "NAE Grand Challenges for Engineering" [Online]. Available: http://engineeringchallenges.org/9136.aspx. [Accessed: 20-Apr-2018].

[36] Lab, R., 2007, "Think Formwork - Reduce Costs," Struct. Mag., (April), pp. 14–16.

[37] Bukkapatnam, S., Mander, J., Paal, S., Pei, Z., and Zeng, L., 2017, Workshop Report - NSF Workshop on Additive Manufacturing (3D Printing) for Civil Infrastructure Design and Construction, National Science Foundation (NSF).

[38] CyBe, 2013, "CyBe" [Online]. Available: https://cybe.eu/#section4.

[39] Winsun, 2016, “The Future of Construction-WinSun” [Online]. Available: https://futureofconstruction.org/case/winsun/.

[40] Branch Technology, 2015, “Branch Technology” [Online]. Available: https://www.branch.technology/.

[41] Perkins, I., and Skitmore, M., 2015, “Three-Dimensional Printing in the Construction Industry: A Review,” Int. J. Constr. Manag., 15(1), pp. 1–9.

[42] Bos, F., Wolfs, R., Ahmed, Z., and Salet, T., 2016, “Additive Manufacturing of Concrete in Construction: Potentials and Challenges of 3D Concrete Printing,” Virtual Phys. Prototyp., 11(3), pp. 209–225.

[43] Tay, Y. W. D., Panda, B., Paul, S. C., Noor Mohamed, N. A., Tan, M. J., and Leong, K. F., 2017, “3D Printing Trends in Building and Construction Industry: A Review,” Virtual Phys. Prototyp., 12(3), pp. 261–276.

[44] Wu, P., Wang, J., and Wang, X., 2016, “A Critical Review of the Use of 3-D Printing in the Construction Industry,” Autom. Constr., 68, pp. 21–31.

[45] Labonnote, N., Rønnquist, A., Manum, B., and Rüther, P., 2016, “Additive Construction: State-of-the-Art, Challenges and Opportunities,” Autom. Constr., 72, pp. 347–366.

[46] Lowke, D., Dini, E., Perrot, A., Weger, D., Gehlen, C., and Dillenburger, B., 2018, “Cement and Concrete Research Particle-Bed 3D Printing in Concrete Construction – Possibilities and Challenges,” Cem. Concr. Res., 112, pp. 50–65.

[47] Khoshnevis, B., and Dutton, R., 1998, “Innovative Rapid Prototyping Process Makes Large Sized, Smooth Surfaced Complex Shapes in a Wide Variety of

Materials," Mater. Technol., 13(2), pp. 53–56.

[48] Zareiyan, B., and Khoshnevis, B., 2017, "Interlayer Adhesion and Strength of Structures in Contour Crafting - Effects of Aggregate Size, Extrusion Rate, and Layer Thickness," Autom. Constr., 81, pp. 112–121.

[49] Hwang, D., and Khoshnevis, B., 2005, "An Innovative Construction Process-Contour Crafting," 22nd Int. Symp. Autom. Robot. Constr. ISARC.

[50] ASTM, 2016, "Standard Specification for Mortar Cement BT - Standard Specification for Mortar Cement."

[51] Hwang, D., and Khoshnevis, B., 2004, "Concrete Wall Fabrication by Contour Crafting," ISAR 2004 21st Int. Symp. Autom. Robot. Constr.

[52] Lim, S., Buswell, R. A., Le, T. T., Austin, S. A., Gibb, A. G. F., and Thorpe, T., 2012, "Developments in Construction-Scale Additive Manufacturing Processes," Autom. Constr., 21, pp. 262–268.

[53] Lim, S., Buswell, R. A., Le, T. T., Austin, S. A., Gibb, A. G. F., and Thorpe, T., 2012, "Developments in Construction-Scale Additive Manufacturing Processes," Autom. Constr., 21(1), pp. 262–268.

[54] Kwon, H., Bukkapatnam, S., Khoshnevis, B., and Saito, J., 2002, "Effects of Orifice Shape in Contour Crafting of Ceramic Materials," Rapid Prototyp. J., 8(3), pp. 147–160.

[55] Khoshnevis, B., Yuan, X., Zahiri, B., Zhang, J., and Xia, B., 2016, "Construction by Contour Crafting Using Sulfur Concrete with Planetary Applications," Rapid Prototyp. J., 22(5), pp. 848–856.

[56] Bukkapatnam, S., and Clark, B., 2007, “Dynamic Modeling and Monitoring of Contour Crafting—An Extrusion-Based Layered Manufacturing Process,” J. Manuf. Sci. Eng., 129(1), p. 135.

[57] Di Carlo, T., 2012, “Experimental and Numerical Techniques To Characterize Structural Properties of Fresh Concrete Relevant To Contour Crafting,” University of Southern California.

[58] Bukkapatnam, S., Khoshnevis, B., Kwon, H., and Saito, J., 2001, “Experimental Investigation of Contour Crafting Using Ceramics Materials,” Rapid Prototyp. J., 7(1), pp. 32–42.

[59] ASTM, 2018, “Standard Terminology Relating to Concrete and Concrete Aggregates 1,” pp. 1–8.

[60] Kazemian, A., Yuan, X., Cochran, E., and Khoshnevis, B., 2017, “Cementitious Materials for Construction-Scale 3D Printing: Laboratory Testing of Fresh Printing Mixture,” Constr. Build. Mater., 145, pp. 639–647.

[61] Khoshnevis, B., 2004, “Automated Construction by Contour Crafting - Related Robotics and Information Technologies,” Autom. Constr., 13(1), pp. 5–19.

[62] Kwon, H., 2002, “Experimentation and Analysis of Contour Crafting (CC) Process Using Uncured Ceramic Materials,” University of Southern California.

[63] Khoshnevis, B., 2004, “Automated Construction by Contour Crafting - Related Robotics and Information Technologies,” Autom. Constr., 13(1), pp. 5–19.

[64] Zhang, J., and Khoshnevis, B., 2013, “Optimal Machine Operation Planning for Construction by Contour Crafting,” Autom. Constr., 29, pp. 50–67.

[65] Zhang, J., and Khoshnevis, B., 2010, “Contour Crafting Process Plan Optimization Part I : Single-Nozzle Case,” J. Ind. Syst. Eng., 4(1), pp. 33–46.

[66] Zhang, J., 2009, “Contour Crafting Process Planning and Optimization,” University of Southern California.

[67] Yeh, Z., and Khoshnevis, B., 2009, “Geometric Conformity Analysis for Automated Fabrication Processes Generating Ruled Surfaces: Demonstration for Contour Crafting,” Rapid Prototyp. J., 15(5), pp. 361–369.

[68] Zareiyan, B., and Khoshnevis, B., 2017, “Effects of Interlocking on Interlayer Adhesion and Strength of Structures in 3D Printing of Concrete,” Autom. Constr., 83, pp. 212–221.

[69] Bosscher, P., Williams, R. L., Bryson, L. S., and Castro-Lacouture, D., 2007, “Cable-Suspended Robotic Contour Crafting System,” Autom. Constr., 17(1), pp. 45–55.

[70] Williams II, R. L., Xin, M., and Bosscher, P., 2008, “Contour-Crafting-Cartesian-Cable Robot System Concepts: Workspace and Stiffness Comparisons (DETC2008-49478),” *In ASME 2008 International Design Engineering Technical Conferences and Computers and Information in Engineering Conference*, American Society of Mechanical Engineers, ed., American Society of Mechanical Engineers, pp. 31–38.

[71] Good, J., Gilley, S., McLemore, C., Fikes, J., and Darby, C., 2008, “Fabrication Capabilities Utilizing In Situ Materials,” *AIAA SPACE 2008 Conference & Exposition*, p. 7854.

[72] Khoshnevis, B., Bodiford, M. P., Burks, K. H., Ethridge, E., Tucker, D., Kim, W., Toutanji, H., and Fiske, M. R., 2005, "Lunar Contour Crafting - A Novel Technique for ISRU-Based Habitat Development," 43rd AIAA Aerosp. Sci. Meet. Exhib. - Meet. Pap., p. 538.

[73] Khoshnevis, B., Carlson, A., Leach, N., and Thangavelu, M., 2012, "Contour Crafting Simulation Plan for Lunar Settlement Infrastructure Buildup," Earth Sp. 2012, pp. 1458–1467.

[74] Leach, N., Carlson, A., Khoshnevis, B., and Thangavelu, M., 2012, "Robotic Construction by Contour Crafting: The Case of Lunar Construction," Int. J. Archit. Comput., 10(3), pp. 423–438.

[75] Khoshnevis, B., Thangavelu, M., Yuan, X., and Zhang, J., 2013, "Advances in Contour Crafting Technology for Extraterrestrial Settlement Infrastructure Buildup," *In AIAA SPACE 2013 Conference and Exposition,* p. 5438.

[76] Thangavelu, M., Khoshnevis, B., Carlson, A., and Leach, N., 2012, "Architectural Concepts Employing Co-Robot Strategy and Contour Crafting Technologies for Lunar Settlement Infrastructure Development," AIAA Sp. 2012 Conf. Expo., p. 5173.

[77] Khoshnevis, B., 2017, "Large Scale 3-D Printing: Past, Present and Future Project" [Online]. Available: https://static.tti.tamu.edu/conferences/tamu-engineering/nsf-3dp-workshop/day1/invited-talks-2/khoshnevis.pdf. [Accessed: 10-Oct-2017].

[78] Sanders, G. B., and Larson, W. E., 2011, "Integration of In-Situ Resource Utilization into Lunar/Mars Exploration through Field Analogs," Adv. Sp. Res.,

47(1), pp. 20–29.

[79] Mueller, R. P., Howe, S., Kochmann, D., Ali, H., Andersen, C., Burgoyne, H., Chambers, W., Clinton, R., De Kestellier, X., Ebelt, K., Gerner, S., Hofmann, D., Hogstrom, K., Ilves, E., and Jerves, A., 2016, "Automated Additive Construction (AAC) for Earth and Space Using In-Situ Resources," Proc. Fifteenth Bienn. ASCE Aerosp. Div. Int. Conf. Eng. Sci. Constr. Oper. Challenging Environ. (Earth Sp. 2016).

[80] Lim, S., Buswell, R. A., Le, T. T., Wackrow, R., Austin, S. A., Gibb, A. G. F., and Thorpe, T., 2011, "Development of a Viable Concrete Printing Process," *Proceedings of the 28th International Symposium on Automation and Robotics in Construction, (ISARC2011), Seoul, South Korea,* © International Association for Automation and Robotics in Construction (I.A.A.R.C.), pp. 665–670.

[81] Le, T. T., Austin, S. A., Lim, S., Buswell, R. A., Gibb, A. G. F., and Thorpe, T., 2012, "Mix Design and Fresh Properties for High-Performance Printing Concrete," Mater. Struct., 45(8), pp. 1221–1232.

[82] Buswell, R. A., Silva, W. R. L. De, Jones, S. Z., and Dirrenberger, J., 2018, "Cement and Concrete Research 3D Printing Using Concrete Extrusion : A Roadmap for Research," Cem. Concr. Res., 112, pp. 37–49.

[83] ASTM, 2018, "ASTM C125-18 Standard Terminology Relating to Concrete and Concrete Aggregates," pp. 1–4.

[84] Rushing, T. S., Al-Chaar, G., Eick, B. A., Burroughs, J., Shannon, J., Barna, L., and Case, M., 2017, "Investigation of Concrete Mixtures for Additive Construction,"

Rapid Prototyp. J., 23(1), pp. 74–80.

[85] Malaeb, Z., Hachem, H., Tourbah, A., Maalouf, T., El Zarwi, N., and Hamzeh, F., 2015, "3D Concrete Printing: Machine and Mix Design," Int. J. Civ. Eng. Technol., 6, pp. 14–22.

[86] Hambach, M., and Volkmer, D., 2017, "Properties of 3D-Printed Fiber-Reinforced Portland Cement Paste," Cem. Concr. Compos., 79, pp. 62–70.

[87] Panda, B., Paul, S. C., Mohamed, N. A. N., Tay, Y. W. D., and Tan, M. J., 2018, "Measurement of Tensile Bond Strength of 3D Printed Geopolymer Mortar," Meas. J. Int. Meas. Confed., 113, pp. 108–116.

[88] Panda, B., Paul, S. C., Hui, L. J., Tay, Y. W. D., and Tan, M. J., 2018, "Additive Manufacturing of Geopolymer for Sustainable Built Environment," J. Clean. Prod., 167, pp. 281–288.

[89] Salet, T. A. M., Bos, F. P., Wolfs, R. J. M., and Ahmed, Z. Y., 2017, "3D Concrete Printing - A Structural Engineering Perspective," *Proceedings of the 2017 Fib Symposium, High Tech Concrete: Where Technology and Engineering Meet*, pp. xliii–lvii.

[90] Panda, B., and Tan, M. J., 2018, "Experimental Study on Mix Proportion and Fresh Properties of Fly Ash Based Geopolymer for 3D Concrete Printing," Ceram. Int., 44(9), pp. 10258–10265.

[91] Paul, S. C., Tay, Y. W. D., Panda, B., and Tan, M. J., 2018, "Fresh and Hardened Properties of 3D Printable Cementitious Materials for Building and Construction," Arch. Civ. Mech. Eng., 18(1), pp. 311–319.

[92] Feng, L., and Yuhong, L., 2014, “Study on the Status Quo and Problems of 3D Printed Buildings in China,” Glob. J. Human-Social Sci. Res., 14(5).

[93] Nerella, V. N., Krause, M., Näther, M., and Mechtcherine, V., 2016, “Studying Printability of Fresh Concrete for Formwork Free Concrete On-Site 3D Printing Technology Technology (CONPrint3D),” Rheol. Messungen an Baustoffen, pp. 236–246.

[94] Gosselin, C., Duballet, R., Roux, P., Gaudillière, N., Dirrenberger, J., and Morel, P., 2016, “Large-Scale 3D Printing of Ultra-High Performance Concrete - a New Processing Route for Architects and Builders,” Mater. Des., 100, pp. 102–109.

[95] World’s Advanced Saving Project-WASP, 2018, “Delta WASP 2040,” 2018 [Online]. Available: https://www.personalfab.it/en/shop/clay-3d-printer-delta-wasp-2040-clay/.

[96] (WASP, W. A. S. P., 2016, “DeltaWASP 2040” [Online]. Available: https://www.personalfab.it/en/shop/delta-printer-deltawasp-20-40/.

[97] Xu, J., Ding, L., and Love, P. E. D., 2017, “Digital Reproduction of Historical Building Ornamental Components: From 3D Scanning to 3D Printing,” Autom. Constr., 76, pp. 85–96.

[98] Perrot, A., Rangeard, D., and Pierre, A., 2016, “Structural Built-up of Cement-Based Materials Used for 3D-Printing Extrusion Techniques,” Mater. Struct. Constr., 49(4), pp. 1213–1220.

[99] A.S.J. Suiker, 2018, “Mechanical Performance of Wall Structures in 3D Printing Processes : Theory , Design Tools and Experiments.”

[100] Wolfs, R. J. M., Bos, F. P., and Salet, T. A. M., 2018, “Early Age Mechanical Behaviour of 3D Printed Concrete: Numerical Modelling and Experimental Testing,” Cem. Concr. Res., 106, pp. 103–116.

[101] Roussel, N., 2018, “Rheological Requirements for Printable Concretes,” Cem. Concr. Res., 112, pp. 76–85.

[102] Reiter, L., Wangler, T., Roussel, N., and Flatt, R. J., 2018, “The Role of Early Age Structural Build-up in Digital Fabrication with Concrete,” Cem. Concr. Res., 112, pp. 86–95.

[103] Ramachandran, V. S., and Beaudoin, J. J., 2000, Handbook of Analytical Techniques in Concrete Science and Technology: Principles, Techniques and Applications, Elsevier.

[104] Marchon, D., Kawashima, S., Bessaies-bey, H., Mantellato, S., and Ng, S., 2018, “Hydration and Rheology Control of Concrete for Digital Fabrication : Potential Admixtures and Cement Chemistry,” Cem. Concr. Res., 112, pp. 96–110.

[105] Wijffels, M. J. H., Wolfs, R. J. M., Suiker, A. S. J., and Salet, T. A. M., 2017, “Magnetic Orientation of Steel Fibres in Self-Compacting Concrete Beams: Effect on Failure Behaviour,” Cem. Concr. Compos., 80, pp. 342–355.

[106] Bos, F. P., Ahmed, Z. Y., Jutinov, E. R., and Salet, T. A. M., 2017, “Experimental Exploration of Metal Cable as Reinforcement in 3D Printed Concrete,” Materials (Basel)., 10(11).

[107] Mechtcherine, V., Grafe, J., Nerella, V. N., Spaniol, E., Hertel, M., and Füssel, U., 2018, “3D-Printed Steel Reinforcement for Digital Concrete Construction –

Manufacture, Mechanical Properties and Bond Behaviour," Constr. Build. Mater., 179, pp. 125–137.

[108] Asprone, D., Menna, C., Bos, F. P., Salet, T. A. M., and Mata-falcón, J., 2018, "Rethinking Reinforcement for Digital Fabrication with Concrete," Cem. Concr. Res., 112, pp. 111–121.

[109] Asprone, D., Auricchio, F., Menna, C., and Mercuri, V., 2018, "3D Printing of Reinforced Concrete Elements: Technology and Design Approach," Constr. Build. Mater., 165, pp. 218–231.

[110] Mata-Falcón, J., Bischof, P., and Kaufmann, W., 2018, "Exploiting the Potential of Digital Fabrication for Sustainable and Economic Concrete Structures," *RILEM International Conference on Concrete and Digital Fabrication*, pp. 157–166.

[111] Lloret, E., Shahab, A. R., Linus, M., Flatt, R. J., Gramazio, F., Kohler, M., and Langenberg, S., 2015, "Complex Concrete Structures: Merging Existing Casting Techniques with Digital Fabrication," CAD Comput. Aided Des., 60, pp. 40–49.

[112] Lloret Fritschi, E., Reiter, L., Wangler, T., Gramazio, F., Kohler, M., and Flatt, R. J., 2017, "Smart Dynamic Casting Slipforming with Flexible Formwork - Inline Measurement and Control," *HPC/CIC Tromsø 2017*, Norwegian Concrete Association.

[113] Szabo, A., Reiter, L., Lloret-Fritschi, E., Gramazio, F., Kohler, M., and Flatt, R. J., 2018, "Adapting Smart Dynamic Casting to Thin Folded Geometries," *RILEM International Conference on Concrete and Digital Fabrication*, pp. 81–93.

[114] Lloret-Fritschi, E., Scotto, F., Gramazio, F., Kohler, M., Graser, K., Wangler, T.,

Reiter, L., Flatt, R. J., and Mata-Falcón, J., 2018, "Challenges of Real-Scale Production with Smart Dynamic Casting," *RILEM International Conference on Concrete and Digital Fabrication*, pp. 299–310.

[115] Zavattieri, P. D., 2017, "Material Architecture Inspired by Nature: Harnessing the Role of Interfaces and Uncovering Hidden Possibilities" [Online]. Available: https://static.tti.tamu.edu/conferences/tamu-engineering/nsf-3dp-workshop/day1/invited-talks-2/zavattieri.pdf. [Accessed: 10-Oct-2017].

[116] Gao, W., Zhang, Y., Ramanujan, D., Ramani, K., Chen, Y., Williams, C. B., Wang, C. C. L., Shin, Y. C., Zhang, S., and Zavattieri, P. D., 2015, "The Status, Challenges, and Future of Additive Manufacturing in Engineering," Comput. Des., 69, pp. 65–89.

[117] Moini, M., Olek, J., Magee, B., Zavattieri, P., and Youngblood, J., 2019, "Additive Manufacturing and Characterization of Architectured Cement-Based Materials via X-Ray Micro-Computed Tomography," RILEM Bookseries, 19, pp. 176–189.

[118] Moini, M., Olek, J., Youngblood, J. P., Magee, B., and Zavattieri, P. D., 2018, "Additive Manufacturing and Performance of Architectured Cement-Based Materials," Adv. Mater., 1802123, pp. 1–11.

[119] Salet, T. (Theo), 2017, "3D Concrete Printing – A Journey with Destination Unknown" [Online]. Available: https://static.tti.tamu.edu/conferences/tamu-engineering/nsf-3dp-workshop/day1/invited-talks-3/salet.pdf. [Accessed: 10-Oct-2017].

[120] Wangler, T., 2017, "Materials Challenges in Digital Fabrication with Concrete"

[Online]. Available: https://static.tti.tamu.edu/conferences/tamu-engineering/nsf-3dp-workshop/day2/invited-talks-1/wangler.pdf. [Accessed: 11-Oct-2017].

[121] Schutter, G. De, Lesage, K., Mechtcherine, V., Naidu, V., Habert, G., and Agusti-juan, I., 2018, "Vision of 3D Printing with Concrete — Technical , Economic and Environmental Potentials," Cem. Concr. Res., 112, pp. 25–36.

[122] Jones, S. Z., 2017, "NIST Perspectives on Additive Manufacturing for Civil Infrastructure Design and Construction" [Online]. Available: https://static.tti.tamu.edu/conferences/tamu-engineering/nsf-3dp-workshop/day2/invited-talks-2/jones.pdf. [Accessed: 11-Oct-2017].

[123] Sanchez, F., Biernacki, J. J., Olek, J., and Zavattieri, P. D., 2017, "3D Printing: A New Promising Avenue for Concrete and the Construction Industry."

[124] Keating, S. J., Leland, J. C., Cai, L., and Oxman, N., 2017, "Toward Site-Specific and Self-Sufficient Robotic Fabrication on Architectural Scales," Sci. Robot., 2(5), p. eaam8986.

[125] Reuters, 2018, "3D-Printed Public Housing Unveiled in France" [Online]. Available: https://www.reuters.com/article/us-france-robot-printer-house/3d-printed-public-housing-unveiled-in-france-idUSKBN1HH2HW.

[126] Miyamoto, Y., Kaysser, W. A., Rabin, B. H., Kawasaki, A., and Ford, R. G., eds., 2013, Functionally Graded Materials: Design, Processing and Applications Volume 5 of Materials Technology Series, Springer Science & Business Media.

[127] Duro-Royo, J., Mogas-Soldevila, L., and Oxman, N., 2015, "Flow-Based Fabrication: An Integrated Computational Workflow for Design and Digital

Additive Manufacturing of Multifunctional Heterogeneously Structured Objects," CAD Comput. Aided Des., 69, pp. 143–154.

[128] Mogas-Soldevila, L., Duro-Royo, J., and Oxman, N., 2014, "Water-Based Robotic Fabrication: Large-Scale Additive Manufacturing of Functionally Graded Hydrogel Composites via Multichamber Extrusion," 3D Print. Addit. Manuf., 1(3), pp. 141–151.

[129] Duty, C. E., Kunc, V., Compton, B., Post, B., Erdman, D., Smith, R., Lind, R., Lloyd, P., and Love, L., 2017, "Structure and Mechanical Behavior of Big Area Additive Manufacturing (BAAM) Materials," Rapid Prototyp. J., 23(1), pp. 181–189.

[130] Duty, C. E., Kunc, V., Compton, B., Post, B., Erdman, D., Smith, R., Lind, R., Lloyd, P., Duty, C. E., Kunc, V., Compton, B., Post, B., Erdman, D., Smith, R., Lind, R., Lloyd, P., Duty, C. E., Lind, R., Lloyd, P., and Love, L., 2017, "Structure and Mechanical Behavior of Big Area Additive Manufacturing (BAAM) Materials."

[131] Oak Ridge National Laboratory, 2016, "ORNL/Boeing Guinness World Record" [Online]. Available: https://www.ornl.gov/news/3d-printed-tool-building-aircraft-achieves-guinness-world-records-title.

[132] Biswas, K., Rose, J., Eikevik, L., Guerguis, M., Enquist, P., Lee, B., Love, L., Green, J., and Jackson, R., 2016, "Additive Manufacturing Integrated Energy—Enabling Innovative Solutions for Buildings of the Future," J. Sol. Energy Eng., 139(1), p. 015001.

[133] Love, L. J., Kunc, V., Rios, O., Duty, C. E., Elliott, A. M., Post, B. K., Smith, R. J., and Blue, C. A., 2014, "The Importance of Carbon Fiber to Polymer Additive Manufacturing," J. Mater. Res., 29(17), pp. 1893–1898.

[134] Giftthaler, M., Sandy, T., Dörfler, K., Brooks, I., Buckingham, M., Rey, G., Kohler, M., Gramazio, F., and Buchli, J., 2017, "Mobile Robotic Fabrication at 1:1 Scale: The In Situ Fabricator," pp. 1–11.

[135] Hack, N., and Lauer, W. V., 2014, "Mesh-Mould: Robotically Fabricated Spatial Meshes as Reinforced Concrete Formwork," Archit. Des., 84(3), pp. 44–53.

[136] Hack, N., Lauer, W. V., Gramazio, F., and Kohler, M., 2015, "Mesh Mould: Robotically Fabricated Metal Meshes as Concrete Formwork and Reinforcement," Proc. 11th Int. Symp. Ferrocem. 3rd ICTRC Int. Conf. Text. Reinf. Concr., pp. 347–359.

[137] Dini, E., 2009, "D-SHAPE - The 21st Century Revolution in Building Technology Has a Name.," pp. 1–16.

[138] Cesaretti, G., Dini, E., De Kestelier, X., Colla, V., and Pambaguian, L., 2014, "Building Components for an Outpost on the Lunar Soil by Means of a Novel 3D Printing Technology," Acta Astronaut., 93, pp. 430–450.

[139] Weger, D., Lowke, D., and Gehlen, C., 2016, "3D Printing of Concrete Structures Using the Selective Binding Method – Effect of Concrete Technology on Contour Precision and Compressive Strength 3D Printing of Concrete Structures Using the Selective Binding Method – Effect of Concrete Technology on Co," *In Proceedings of 11th Fib International PhD Symposium in Civil Engineering, The University of*

Tokyo, Tokyo, pp. 403–410.

[140] Weger, D., Lowke, D., Gehlen, C., and Talke, D., 2018, "Additive Manufacturing of Concrete Elements Using Selective Cement Paste Intrusion-Effect of Layer Orientation on Strength and Durability," *In Proceedings of RILEM 1st International Conference on Concrete and Digital Fabrication*.

[141] Zhang, J., and Khoshnevis, B., 2015, "Selective Separation Sintering (SSS) A New Layer Based Additive Manufacturing Approach for Metals and Ceramics," Proc. Solid Free. Fabr. Symp., pp. 71–79.

[142] Khoshnevis, B., and Zhang, J., 2015, "Selective Separation Sintering (SSS) - An Additive Manufacturing Approach for Fabrication of Ceramic and Metallic Parts with Application in Planetary Construction," AIAA Sp. 2015 Conf. Expo.

[143] Agustí-Juan, I., and Habert, G., 2017, "Environmental Design Guidelines for Digital Fabrication," J. Clean. Prod., 142, pp. 2780–2791.

[144] Buswell, R. A., Silva, W. R. L. De, Jones, S. Z., and Dirrenberger, J., 2018, "Cement and Concrete Research 3D Printing Using Concrete Extrusion : A Roadmap for Research," Cem. Concr. Res., 112(June), pp. 37–49.

[145] Cerovsek, T., 2011, "A Review and Outlook for a 'Building Information Model' (BIM): A Multi-Standpoint Framework for Technological Development," Adv. Eng. Informatics, 25(2), pp. 224–244.

[146] Duballet, R., Baverel, O., and Dirrenberger, J., 2017, "Classification of Building Systems for Concrete 3D Printing," Autom. Constr., 83, pp. 247–258.

[147] Goodings, D. J., 2017, "NSF Perspectives on Additive Manufacturing for Civil

Infrastructure Design and Construction" [Online]. Available: https://static.tti.tamu.edu/conferences/tamu-engineering/nsf-3dp-workshop/day2/invited-talks-2/goodings.pdf. [Accessed: 11-Oct-2017].

[148] Kalil Tom And Wadia, C., 2011, Materials Genome Initiative for Global Competitiveness.

3. EXTRUSION-BASED 3D PRINTING OF PORCELAIN: FEASIBLE REGIONS[3]

3.1. Introduction

The construction industry is of international significance. The global annual output of the construction industry is $8.5 trillion [3]. However, this vital industry also faces challenges in safety and productivity. This labor-intensive industry accounts for at least 60,000 fatal accidents every year [4]. Productivity growth rates in this industry have lagged since the 1960s [8]. Additive manufacturing (AM) could help address these challenges. With new AM processes, construction could be carried out for 24 hours of the day leading to improved productivity. Furthermore, automation in construction could reduce human involvement in risky tasks and therefore, improve safety.

In recent years, development of binder jetting and material extrusion processes has fueled applications of AM in the construction industry. In the binder jetting process, a liquid bonding agent is selectively deposited to join powder materials [1]. D-shape [137] is an example of binder jetting process for construction applications. In this process, inorganic binder is deposited in a sand substrate using multiple nozzles [137]. However, parts printed using this process exhibit a rough surface [53]. Material extrusion-based AM processes rely on selective deposition of material through a nozzle or orifice [1]. Examples of this process include concrete printing [42,80] and contour crafting [51]. While concrete

[3] Reprinted with permission from "Extrusion-Based 3D Printing of Porcelain: Feasible Regions" by Bhardwaj et al., 2019. Proceedings of the ASME 2019 14th International Manufacturing Science and Engineering Conference. Volume 1: Additive Manufacturing, V001T01A007, Copyright 2019 by ASME.

printing produces a ribbed finish [53], the use of trowels in contour crafting facilitates a smother surface.

Porcelain stoneware tiles are a common building material due to their good mechanical strength, and wear and chemical resistance [149]. Binder jetting based processes have been used for 3D printing of porcelain [150–152]. Studies were conducted to optimize process parameters such as spread speed and power level for binder jetting [151]. Mechanical properties and geometric accuracy of printed parts were studied. For porcelain tiles, a good surface quality can increase the visual appeal of an artefact through improved texture. Hence, surface quality is an important feature for aesthetic applications. Researchers have analyzed the effect of surface angle (i.e. angle between fabrication direction and tangent plane of a curved surface) on the surface roughness for binder jetting based processes [152]. However, effects of process parameters on surface quality are not clear for extrusion-based printing of porcelain.

The objective of this study is to identify regions of printing parameters (such as print speed, air pressure, extruder height, and layer thickness) that yield samples with good surface quality. The paper is structured as follows: experimental setup and procedure are presented in section 3.2. Measurement method for evaluating surface quality of samples is discussed in section 3.3. Section 3.4 provides experimental results and their discussion. Finally, conclusions and future work are presented in section 3.5.

3.2. Experimental Setup and procedure

3.2.1. Porcelain Preparation

The porcelain was procured from Spectrum Scientifics (Philadelphia, PA, USA). Its chemical composition is shown in Table 2.

Table 2: Chemical composition of porcelain (mass percent basis)

SiO_2	Al_2O_3	TiO_2	Fe_2O_3	MgO	CaO	Na_2O	K_2O	Other
67.1	26.55	0.06	0.53	0.45	0.52	0.96	3.77	-

The porcelain had a dough-like texture. To maintain a consistent moisture content for the experiments, the dough-like porcelain was manually pressed to one-inch thick sheets and dried at room temperature for a minimum of 72 hours. Thereafter, the hardened porcelain dough was manually pulverised. Water and ethyl alcohol were added to the crushed porcelain to prepare the mixture for extrusion. The material proportion of the mixture in Table 3 was based on preliminary experiments and was found to yield good extrudability. The mixture was kneaded until a consistent texture was achieved.

Table 3: Proportion of materials added for preparing the mixture

Material	Quantity added
Porcelain	1500 g
Water	300 ml
Ethyl alcohol	300 ml

3.2.2. 3D Printer

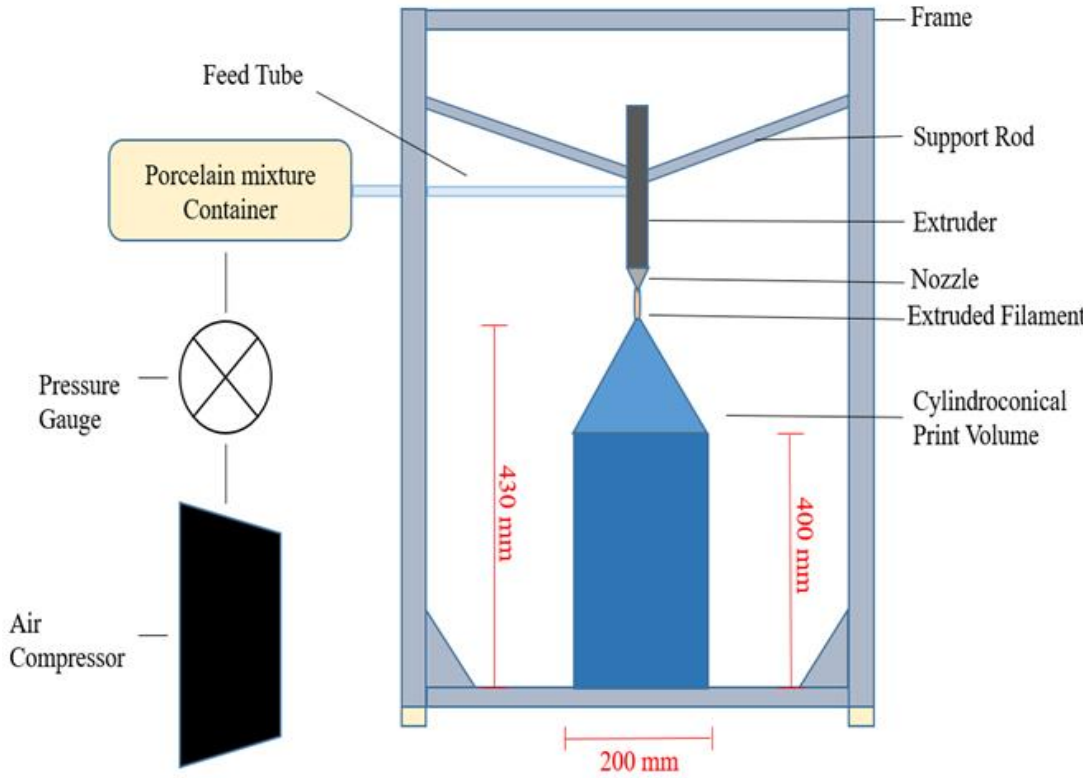

Figure 10: Illustration of the experimental set-up

The 3D printer used was a Delta WASP 2040 Clay 3D printer [95]. In Delta printers, the motion of the printer nozzle is controlled by three arms on rails. These arms move vertically along the rails to position the nozzle. The Delta printer had a cylindroconical build volume as shown in *Figure 10*. The cylinder measured 200 mm (diameter) X 400 mm (height), while the cone was approximately 30 mm tall. The extruder nozzle diameter was 1 mm. The mixture container consisted of a metallic body with an air-tight plastic piston to push the mixture to the extruder. Air pressure was used to push the piston. An air pressure of 0.4-0.6 MPa (4-6 bars) for extrusion was recommended by the Delta WASP

2040 printer manufacturer. Compressed air was provided by a Kobalt 4.3-gallon Electric Twin Stack Quiet Air Compressor (Mooresville, North Carolina, USA).

3.2.3. Sample Preparation

3D samples of dimensions 20 mm X 20 mm X 25 mm were sketched using AutoCAD. Thereafter, the prepared 3D sketches were sliced using an open-source application Cura (version 3.2.1). The samples had a 70% infill density (i.e., amount of material used on the inside of the sample) and were infilled using a concentric pattern (highlighted in yellow) as shown in Figure 11. As the name suggests, this infill pattern prints from the boundary of the design towards its centre [153].

Since porcelain samples were in a leathery/setting state after printing, the samples were printed on thin plastic sheets fixed to the printer bed. Printing on plastic sheets enabled easy removal of the samples from the print bed.

3.2.4. Experimental Conditions

Based on preliminary experiments, the following parameters were selected for the study:

- Print speed: The speed at which the nozzle moves while printing
- Extruder height: The distance from the top of the print volume to the print bed. Hence, the nozzle is closer to the print for an extruder height of 430.5 mm as compared to an extruder height of 428.5 mm.
- Layer thickness: Thickness of each extruded layer.
- Air pressure: The air pressure used to extrude the material.

Although reduced layer thickness is expected to yield a better surface finish, it would increase the number of layers required to print a sample and thereby increase the total printing time. While lower print speed could lead to improved surface quality, speeds greater than 150 mm/s led to jerky motion of the extruder. Hence, a wide range of print speed ranging from 10 mm/s to 150 mm/s was chosen to identify speeds that yield good surface finish. The extruder height was tested at three levels between 427.5 mm and 429.5 mm. Extruder height of less than 427.5 mm resulted in poor surface quality during preliminary testing and so lower settings of this parameter were excluded from the study. The maximum extruder height for the set up was 430.5 mm. Air pressure of 0.4 MPa and 0.6 MPa were tested.

Table 4: Process parameters and their values

Parameter	**Value**
Print speed (mm/s)	10, 50, 100, 150
Extruder Height (mm)	427.5, 428.5, 429.5
Layer thickness (mm)	0.7, 1
Air pressure (MPa)	0.4, 0.6

Parameter setting refers to each combination of parameter values. For example, one parameter setting would comprise print speed of 10 mm/s, extruder height of 427.5 mm, layer thickness of 0.7 mm and air pressure of 0.4 MPa. Hence, 48 parameter settings were tested, and 4 samples were printed for each parameter setting. In total, 192 samples were

printed in this study. Each print consisted of eight samples in which two parameter settings were tested.

The printer bed was levelled before the experiments as per the printer manufacturer's instructions. The extruder was cleaned before each experiment. Afterwards, the prepared porcelain mixture was added to the mixture container of the 3D printer. Since it was difficult to add all of the porcelain mixture in one step, the mixture was divided into nine batches. Ethyl alcohol was sprayed after the addition of each batch of porcelain mixture into the mixture container as per the printer manufacturer's instructions. The porcelain mixture in the container was replaced after every six prints.

By changing the print speed and layer thickness during experiments, the material flow could be altered. In the Cura application, material flow rate was defined as the volume of material that flows out of the extruder nozzle over a specific time. Mathematically, it was defined in Eq. (1) as:

$$Q = v \times h \times d \tag{1}$$

where, Q denotes material flow (mm^3/s). v, h and d represent print speed (mm/s), layer thickness (mm), and nozzle diameter (mm), respectively [154].

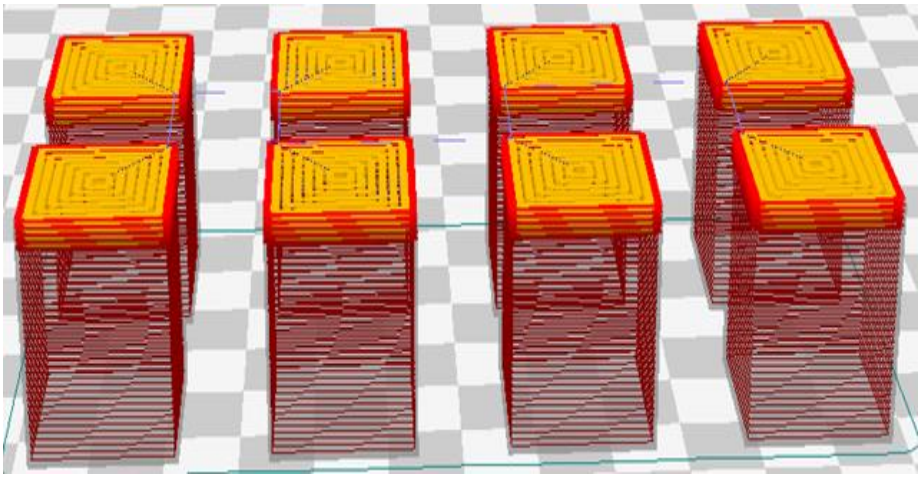

Figure 11: Designs prepared in cura with a concentric infill pattern (highlighted in yellow)

(a) *(b)* *(c)*

Figure 12: Examples of surface quality: (a) poor surface quality sample; (b) average surface quality sample; (c) good quality sample

3.3. Measurement Method for Evaluating Surface Quality

While some parameter settings resulted in good surface quality, others led to errors in extrusion thereby yielding a poor surface quality. Examples of these surface qualities are shown in Figure 11.

Certain parameter settings resulted in excess or reduced material deposition at the layer start/end point (these points are at the same location because each layer is a closed loop). This phenomenon led to edge defects as shown in Figure 12(a). Additionally, minor deviation/misalignment in the stacking of extruded filament could lead to stacking errors. These errors could result in reduced surface quality as shown in Figure 12(b). The porcelain could also get stuck to the nozzle and interfere with the printing as shown in Figure 13(a). Stacking defects produced at an early stage could lead to failed prints as shown in Figure 13(b).

(a) *(b)*

Figure 13: Example of a failed print (a) porcelain stuck on nozzle during a print; (b) a failed print

Since there were 48 parameter settings and 4 samples were printed for each setting, a total of 192 samples were printed for the study. The samples were dried at room temperature for a minimum of 24 hours before measurement. Based on surface quality, each side face (top and bottom surfaces were not evaluated) of the sample was categorized as poor, average, or good and assigned a rating of 0, 1 or 2, respectively. Hence, each sample was assigned a rating between 0 and 8 based on surface quality of all four faces. This evaluation was repeated for all four samples and an average was calculated as the final rating for the corresponding parameter setting. A final rating less than 4 was designated as poor surface quality, greater than 6 as high quality, and between 4 and 6 was categorized as average quality.

3.4. Results and Discussion

The final surface quality ratings for 48 parameter settings are shown in Figure 14. An air pressure of 0.4 MPa and a layer thickness of 0.7 mm yielded a poor surface quality (i.e., rating < 4) for majority of the samples as shown in Figure 14(a). Lower pressure coupled with reduced layer thickness resulted in irregular stacking of layers yielding a poor surface quality. The average quality occurred at 10 mm/s print speed and 427.5 mm extruder height. In addition, a set of samples failed to complete printing. Detachment of the sample from the plastic sheet placed on the print bed resulted in failure. During the course of printing, these detached samples moved or fell over on the print bed after coming in contact with the mixture built up on the nozzle. These errors resulted in a failed print. This observation has been shown in Figure 15.

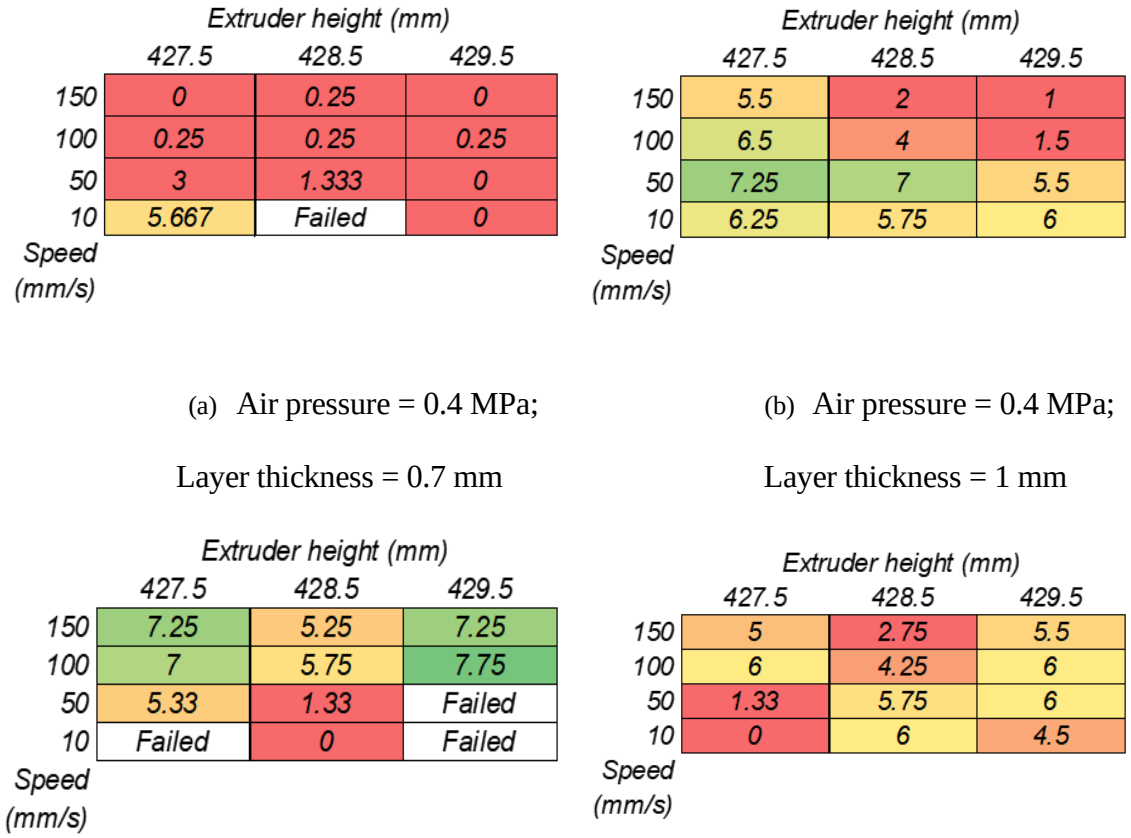

(a) Air pressure = 0.4 MPa; Layer thickness = 0.7 mm

(b) Air pressure = 0.4 MPa; Layer thickness = 1 mm

(c) Air pressure = 0.6 MPa; Layer thickness = 0.7 mm

(d) Air pressure = 0.6 MPa; Layer thickness = 1 mm

Figure 14: Surface quality and parameter settings

The surface qualities with larger layer thickness of 1 mm and an air pressure of 0.4 MPa are shown in Figure 14(b). This change in layer thickness from 0.7 mm to 1 mm resulted in a significant improvement in surface quality with the best surfaces observed for speed of 50 mm/s and an extruder height of 427.5 mm. However, faster speeds along

with high extruder heights resulted in edge defects as shown in Figure 3(a). Hence, using a pressure of 0.4 MPa, good results were obtained using an extruder height of 427.5 mm and print speeds of 10 and 50 mm/s.

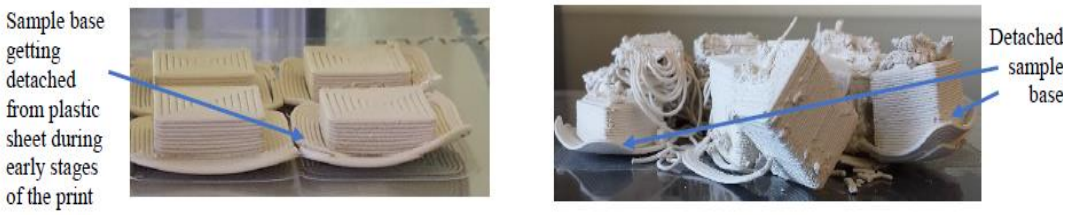

(a) *(b)*

Figure 15: Print failure resulting from sample detachment (a) detachment of the base of the sample from the plastic sheet; (b) failed print

Some of the best surface quality samples were obtained using a pressure of 0.6 MPa and a layer thickness of 0.7 mm as shown in Figure 14(c). High pressure of 0.6 MPa coupled with high print speeds of 100 mm/s and 150 mm/s produced samples with enhanced surface quality. This observation can be accounted to improved material flow. On the other hand, reduction in print speed resulted in over deposition of porcelain thereby yielding a reduced surface quality for all extruder heights.

Figure 14 (d) shows the surface quality of samples printed with a layer thickness of 1 mm. For extruder height of 427.5 mm, surface quality improved with print speed. High speed led to stacking defects for an extruder height of 428.5 mm. While reduced speed of 10 mm/s led to over deposition, faster print speeds led to improvement in surface quality for extruder height of 429.5 mm. Overall, better results for these parameter settings were obtained using a print speed of 100 mm/s and an extruder height of 429.5 mm.

Certain combinations of print speed, layer thickness and pressure generated improved surface quality. Since material flow is associated with print speed and layer thickness as shown in equation (1), it has an important effect on the surface quality of samples printed using this extrusion process. For a layer thickness of 0.7 mm, best surface quality samples were observed using a pressure of 0.6 MPa and higher print speeds of 100 to 150 mm/s. On the other hand, for samples printed with a layer thickness of 1 mm, best surface quality was observed using a pressure of 0.4 MPa and lower print speeds of 10 and 50 mm/s.

3.4.1. Conclusions

The paper presents an experimental study on the surface quality of porcelain samples printed using an extrusion-based 3D printing/AM process. A combination of parameters including print speed, layer thickness, and air pressure was found to have an effect on surface quality of samples. Best surface quality was obtained through optimum material flow achieved using a combination of high pressure, high speed, and reduced layer thickness. Alternately, this optimum flow could also be attained using low pressure, low speed, and increased layer thickness.

Future research would include a study using design of experiments to quantify the effects of various parameters and their interactions on mechanical properties. Additionally, the effects of printing parameters on geometric accuracy of printed samples will also be evaluated.

References

[1] Construction Intelligence Center, Global Construction Outlook 2020, 2015.

[2] International Labour Organization, Facts on safety at work, Int. Labor Off. Tech. Rep. (2005).

[3] H. Nasir, H. Ahmed, C. Haas, P.M. Goodrum, An analysis of construction productivity differences between Canada and the United States, Constr. Manag. Econ. 32 (2014) 595–607.

[4] A. ISO/ASTM52900-15, Standard Terminology for Additive Manufacturing – General Principles – Terminology, ASTM Int. (2015).

[5] E. Dini, D-SHAPE - The 21st century revolution in building technology has a name., (2009) 1–16. http://www.cadblog.pl/podcasty/luty_2012/d_shape_presentation.pdf.

[6] S. Lim, R.A. Buswell, T.T. Le, S.A. Austin, A.G.F. Gibb, T. Thorpe, Developments in construction-scale additive manufacturing processes, Autom. Constr. 21 (2012) 262–268. doi:10.1016/j.autcon.2011.06.010.

[7] S. Lim, R.A. Buswell, T.T. Le, R. Wackrow, S.A. Austin, A.G.F. Gibb, T. Thorpe, Development of a viable concrete printing process, in: Proc. 28th Int. Symp. Autom. Robot. Constr. (ISARC2011), Seoul, South Korea, © International Association for Automation and Robotics in Construction (I.A.A.R.C.), 2011: pp. 665–670.

[8] F. Bos, R. Wolfs, Z. Ahmed, T. Salet, Additive manufacturing of concrete in construction: potentials and challenges of 3D concrete printing, Virtual Phys. Prototyp. 11 (2016) 209–225.

[9] D. Hwang, B. Khoshnevis, Concrete Wall Fabrication by Contour Crafting, ISAR 2004 21st Int. Symp. Autom. Robot. Constr. (2004). http://www.irbnet.de/daten/iconda/CIB13583.pdf.

[10] L. Andre, J. Feltrin, M. Dal, A.M. Bernardin, D. Hotza, Effect of reduction of thickness on microstructure and properties of porcelain stoneware tiles, Ceram. Int. 40 (2014) 14693–14699. doi:10.1016/j.ceramint.2014.05.150.

[11] P. Lima, A. Zocca, W. Acchar, J. Günster, Journal of the European Ceramic Society 3D printing of porcelain by layerwise slurry deposition, J. Eur. Ceram. Soc. 38 (2018) 3395–3400. doi:10.1016/j.jeurceramsoc.2018.03.014.

[12] H. Miyanaji, S. Zhang, A. Lassell, A.A. Zandinejad, L. Yang, Optimal Process Parameters for 3D Printing of Porcelain Structures, Procedia Manuf. 5 (2016) 870–887. doi:10.1016/j.promfg.2016.08.074.

[13] X. Tian, D. Li, F.G. Heinrich, Rapid prototyping of porcelain products by layer-wise slurry deposition (LSD) and direct laser sintering, (2012). doi:10.1108/13552541211250364.

[14] World's Advanced Saving Project-WASP, Delta WASP 2040, 2018. (2018). https://www.personalfab.it/en/shop/clay-3d-printer-delta-wasp-2040-clay/.

[15] Ultimaker, Cura Infill, (2016). https://ultimaker.com/en/resources/20416-infill.

[16] Cura, Based on communication with Cura's technical support, (2018).

4. 3D PRINTING OF BIOMASS-FUNGI COMPOSITE MATERIAL: A PRELIMINARY STUDY[4]

4.1. Introduction

Environmental sustainability is a major challenge for the construction and packaging industries valued globally at $8.5 trillion and $1 trillion, respectively [1,2]. In the construction industry, the production of every ton of cement results in the release of 0.9 tons of CO_2 [3]. The packaging industry uses 38% of the petroleum-based plastics produced [4]. It is estimated that by the year 2050, 12,000 metric tons of plastic waste will end up in landfills or in the natural environment [5]. Hence, there is a need for sustainable materials for both construction and packaging industries.

Recently, there are reports on a new class of biomass-fungi composite material [6–8]. The biomass is derived from waste agricultural materials such as switch-grass, rice straw, sorghum stalks, and hemp [9]. Biologically, the biomass serves as a nutrition source for fungi, and the fungi grow through the biomass and bind the biomass together. This binding mechanism is facilitated by the growth of interconnecting fibrous filaments (up to 10 μm in diameter) of fungi [10,11].

This material has been used to manufacture sound absorption panels for automotive and construction installations [9], furniture, floor, and wall panels [12]. Additional applications of this material include packaging [13–16], textiles (as leather substitute)

---

[4] Reprinted with permission from "3D Printing of Biomass-Fungi Composite Material: A Preliminary Study" by Bhardwaj et al., 2020. Manufacturing Letters, Volume 24, Pages 96-99, Copyright 2020 by Society of Manufacturing Engineers (SME). Published by Elsevier Ltd.

[17], and food (as meat substitute) [18]. Advantages of this material include 100% biodegradability, low density, and low cost [19,20].

Reported studies on biomass-fungi composite materials are summarized in Table 5. These experimental and computational studies cover effects of parameters (such as biomass type, genetic modification, and environment condition) on chemical composition (such as polysaccharides, lipids, proteins, and chitin) [20,21], mechanical behavior and morphology of this material [10,22]. Recently, researchers also manufactured composite sandwich structures comprising this material and bioresin, with addition of natural fiber textiles (jute) [19]. A cost model for manufacturing of composite parts has also been reported [23].

Table 5: Summary of reported studies on biomass-fungi composite material

Study	***Research Contribution***
Haneef et al. [155]	Effect of fungal growth on mechanical properties of biomass-fungi composite material
Appels et al. [156]	Effect of genetic modification and environment conditions (light conditions and CO_2 concentration) on fungal density
Appels et al. [157]	Effect of factors such as biomass type, fungal species and processing technique (no pressing, cold pressing, or heat pressing) on

Study	*Research Contribution*
	morphology, density and mechanical properties of products using the molding-based process
Islam et al. [158,159]	Morphological and mechanical behavior of fungal mycelium (root structure of fungi)
Jiang et al. [160,161]	Manufacturing of biocomposite sandwich structures using biomass-fungi composite and a commercial bioresin, with addition of natural fiber textiles (jute and hemp)
Jiang et al. [26]	A cost model of a molding-based manufacturing method to produce biocomposite parts

A cost model of a molding-based manufacturing method to produce biocomposite parts

3D printing of this material has not been reported to the best knowledge of the authors. Currently, the molding process is used to manufacture parts using this material. 3D printing of biomass-fungi composite material would facilitate the manufacturing of complex shapes that cannot be easily produced using conventional molding-based methods. Furthermore, it would facilitate new applications of this material. This paper reports the first study on material extrusion-based 3D printing of biomass-fungi composite material. Material extrusion is defined as a “process in which material is selectively dispensed through a nozzle or orifice” [25].

4.2. 2. Experimental Procedure

Figure 16 shows the new method developed to 3D print this material. There are six stages.

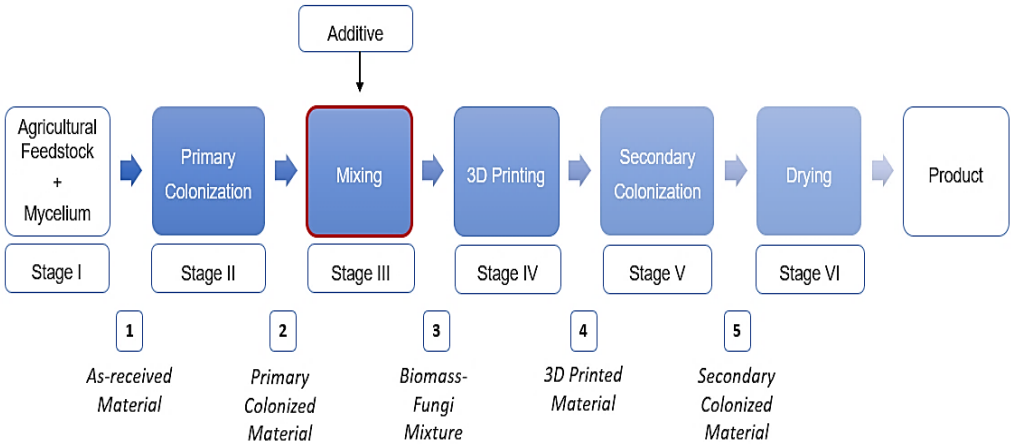

Figure 16: Six stages of the new method for 3D printing of biomass-fungi composite material

Stage I: Mycelium Inoculation of Agricultural Feedstock

First, the biomass material was pasteurized. Pasteurization refers to the exposure of material to elevated temperatures in order to kill harmful microorganisms that may be detrimental to fungal growth. After pasteurization, the biomass material was inoculated with mycelium (the root structure of the fungi) over a four-day period. Inoculation refers to the introduction of the fungi (inoculum) to the biomass material. This biomass material inoculated with fungi was packed in filter patch bags with each bag containing approximately 400 g of material. This stage of the method occurred at Ecovative Design

(New York, USA). The material after this stage is called ‘As-received material’. Based on the sieve analysis of the as-received material, more than 80% of the particles were greater than 1 mm in size. While 92% of the particles passed through a sieve with a mesh opening of 4.75 mm, only 4% of the particles passed through a sieve with the mesh opening of 600 µm.

Stage II: Primary Colonization

Fungi generally grow as colonies on host materials; hence this stage is referred to as primary colonization. To reduce any chances of microbial contamination of the material, the apparatus (such as beakers) were cleaned with a 70 percent ethyl alcohol solution before starting any experiments. During this stage, the as-received material was combined with water and additional nutrients (a solution containing 700 ml water and 32 g of wheat flour) to facilitate the growth of fungi. In this study, 400 g of as-received material contained in the filter patch bag was combined with the nutrient solution. Thereafter, this combination was manually shaken vigorously for one minute. Next, the combination was kept in the dark at 23℃ for 3-5 days. This stage created a foam-like, dense, biomass-fungi composite. The material is now referred to as primary colonized material.

Stage III: Mixing

The primary colonized material was too dense to be extruded through the printing nozzle. Therefore, a commercial benchtop mixer (NutriBullet PRO, Nutribullet) was used to transform the primary colonized material into a printable mixture. This stage comprised breaking up the primary colonized material (100 g) into smaller chunks by hand and then adding these chunks into the sanitized commercial mixer for mixing. Additional water

(400 g) was added to facilitate the mixing process. After 30 seconds of mixing, psyllium husk powder (20 g) was manually added into the mixture using a spoon. This powder prevented phase segregation in the biomass-fungi mixture during the printing process thereby improving print quality.

Stage IV: 3D Printing

A WASP 2040 material extrusion-based 3D printer (illustrated in Figure 17) was used [26]. The build volume of this printer was cylindroconical in shape. The cylindrical portion had a diameter of 200 mm and a height of 400 mm. The height between the bottom of the cylinder and the tip of the cone at the top of the build volume was 430 mm. The printer included a 3-liter material container equipped with a plastic piston that was operated by compressed air. The motion of the piston facilitated the material transfer from the material container to the deposition head. The deposition head comprised a screw extruder, a plastic casing (to hold the screw extruder), and a metallic nozzle with a diameter of 4 mm. The clearance between the screw extruder and the plastic casing was approximately 1-2 mm. Cura software was used to generate the G-code for printing.

To reduce any chances of microbial contamination of the prepared mixture, the components of the 3D printer such as the print bed, material container, screw extruder, plastic casing, and nozzle were all cleaned with a 70 percent ethyl alcohol solution before 3D printing. Thereafter, the prepared mixture was added to the sterilized material container and the biomass-fungi mixture was 3D printed using the sterilized 3D printer. The sample was printed using a print speed of 15 mm/s and an air pressure of 3.5 bar.

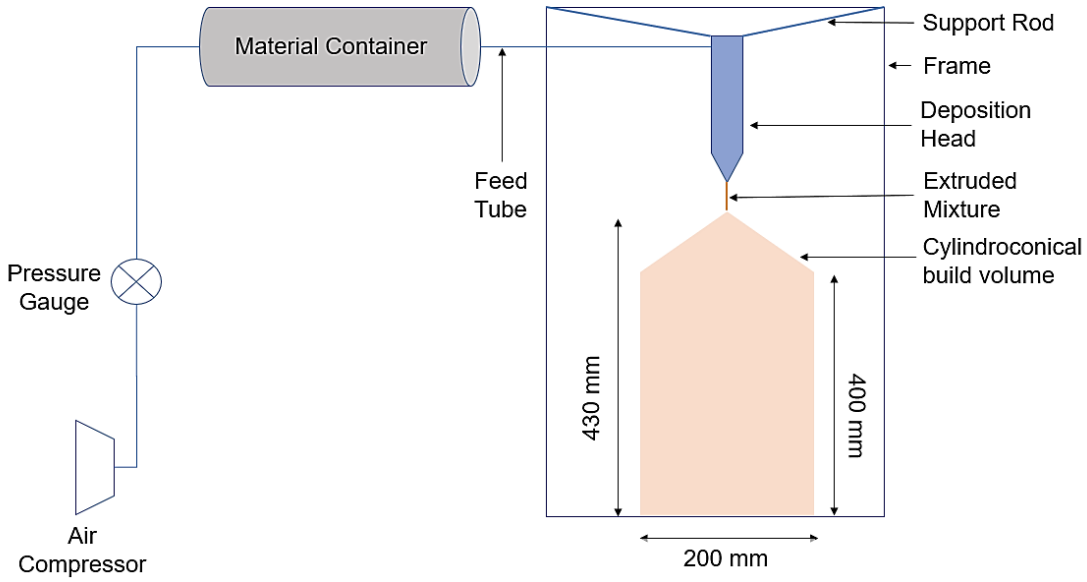

Figure 17: Schematic illustration of Delta WASP 2040 3D Printer

Stage V: Secondary Colonization

In this stage, the 3D printed samples were kept in perforated ziplock plastic bags. These plastic bags were stored in plastic containers away from direct sunlight to facilitate the fungal growth. These plastic bags and containers were sterilized using a 70 percent ethyl alcohol solution before use. This is the second stage in the method where the fungi grow, hence, it is referred to as secondary colonization. This stage lasted for 3-5 days.

Stage VI: Drying

In this stage, the fungi were deactivated by heating the printed sample in a countertop convection oven for approximately 4 hours at 95°C [27].

4.3. 3. Results and Discussion

Using the prepared mixture, a test sample was printed with the following dimensions: 100 mm X 100 mm X 20 mm. Figure 18(a) shows a 3D printed sample. Figure 18(b) shows the 3D printed sample after secondary colonization. The white fungal growth on the sample can be observed. The results show that the fungi did not lose their ability to grow throughout mixing and 3D printing.

(a) *(b)*

Figure 18: 3D printed sample using biomass-fungi mixture (a) After 3D printing; (b) After secondary colonization

Prior to being able to print the above samples, many technical barriers were encountered. Overcoming each of these barriers can probably constitute a separate paper. It is the authors' intention to publish separate papers on some of these barriers. The first technical barrier was encountered when preparing a printable biomass-fungi mixture. Initially, the mixture consisted of porcelain clay and biomass-fungi material. This mixture had three problems: (1) clogging of the material container and the deposition head; (2) poor print quality; and (3) hindering of fungi growth. Subsequently, a new mixing process was incorporated in the method to prepare a printable mixture. Water and psyllium husk

powder contents in this mixture had to be optimized to avoid phase segregation and nozzle clogging. The second barrier was encountered when determining the duration of mixing because it had a significant effect on fungal growth. The third barrier was microbial contamination (growth of undesirable microbes on the printed biomass-fungi sample). Growth of these microbes deters the fungal growth in the printed sample.

4.4. Conclusions and Future Research Directions

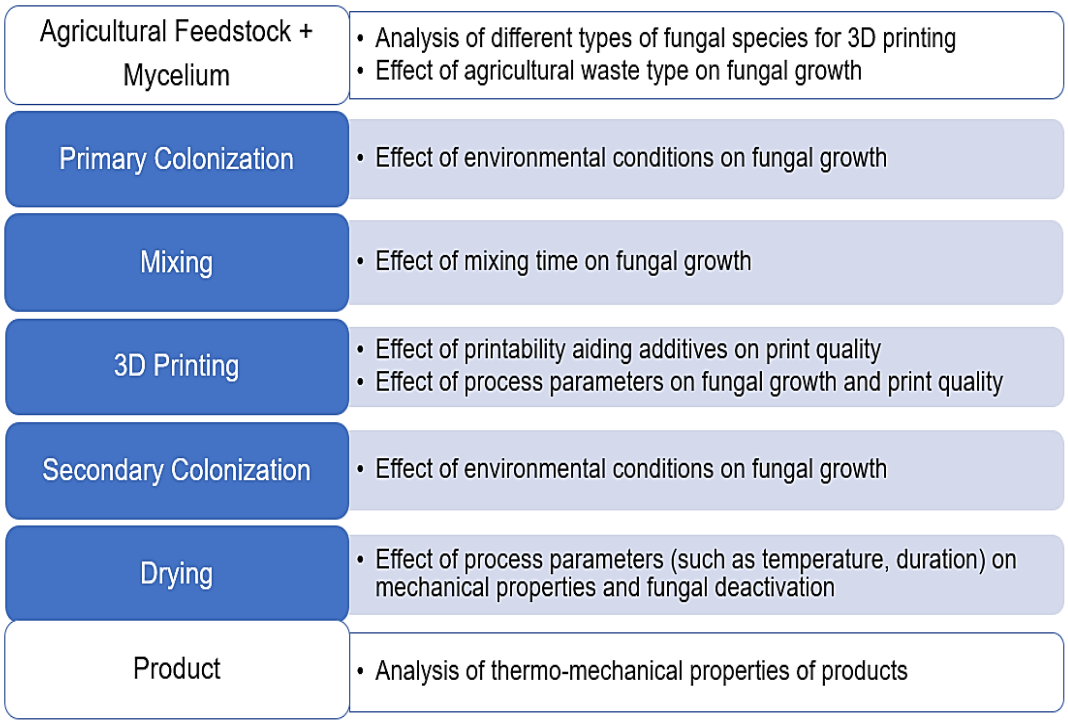

Figure 19: Knowledge gaps in 3D printing of biomass-fungi composite material

A new method for 3D printing with biomass-fungi material has been demonstrated. This novel method used a mixing stage to produce a printable mixture for material extrusion-based 3D printing. More research is needed to fill several knowledge gaps

(Figure 19) for this new method. This new method could have a major impact in the construction and packaging industries.

References

[1] Construction Intelligence Center, Global Construction Outlook 2020, 2015.

[2] J. Poole, Packaging education: Specialized degrees can help solve sustainability challenges and more, experts say, Packag. Insights. (2019). https://www.packaginginsights.com/news/packaging-education-specialized-degrees-can-help-solve-sustainability-challenges-and-more-experts-say.html.

[3] G. Habert, Environmental impact of Portland cement production, Eco-Efficient Concr. (2013) 3–25. doi:10.1533/9780857098993.1.3.

[4] M. Rabnawaz, I. Wyman, R. Auras, S. Cheng, A roadmap towards green packaging: the current status and future outlook for polyesters in the packaging industry, Green Chem. (2017) 4737–4753. doi:10.1039/c7gc02521a.

[5] R. Geyer, J.R. Jambeck, K.L. Law, Production, use, and fate of all plastics ever made, Sci. Adv. 3 (2017) 25–29. doi:10.1126/sciadv.1700782.

[6] Skanda Kadirgamar (JSTOR), Company Uses Mushrooms to Grow Plastic Alternatives, (2017). https://daily.jstor.org/company-uses-mushrooms-grows-plastic-alternatives/ (accessed September 12, 2019).

[7] Erin Demuth Judd (Phys.Org), Can fungi replace plastics?, (2013). https://phys.org/news/2013-03-fungi-plastics.html (accessed December 9, 2019).

[8] Fiona Graham (BBC), “Air” plastic and mushroom cushions - Dell packages the future, (2014). https://www.bbc.com/news/business-29543834 (accessed December 9, 2019).

[9] M.G. Pelletier, G.A. Holt, J.D. Wanjura, E. Bayer, G. Mcintyre, An evaluation study of mycelium based acoustic absorbers grown on agricultural by-product substrates, Ind. Crop. Prod. 51 (2013) 480–485. doi:10.1016/j.indcrop.2013.09.008.

[10] M.R. Islam, G. Tudryn, R. Bucinell, L. Schadler, R.C. Picu, Stochastic continuum model for mycelium-based bio-foam, 160 (2018) 549–556. doi:10.1016/j.matdes.2018.09.046.

[11] F.V.W. Appels, S. Camere, M. Montalti, E. Karana, K.M.B. Jansen, J. Dijksterhuis, P. Krijgsheld, H.A.B. Wösten, Fabrication factors influencing mechanical , moisture- and water-related properties of mycelium-based composites, 161 (2019) 64–71. doi:10.1016/j.matdes.2018.11.027.

[12] M.G. Pelletier, G.A. Holt, J.D. Wanjura, A.J. Lara, A. Tapia-carillo, G. Mcintyre, E. Bayer, An evaluation study of pressure-compressed acoustic absorbers grown on agricultural by-products, 95 (2017) 342–347.

[13] NSF, Latest “Green” Packing Material? Mushrooms!, (2010). https://www.nsf.gov/news/news_summ.jsp?cntn_id=117385 (accessed April 2, 2019).

[14] Ecovative Design, Ecoative Design-Packaging, (2020). https://ecovativedesign.com/packaging (accessed September 12, 2019).

[15] G. Holt, G. McIntyre, D. Flagg, E. Bayer, J. Wanjura, M. Pelletier, Fungal mycelium and cotton plant materials in the manufacture of biodegradable molded

packaging material: Evaluation study of select blends of cotton byproducts, J. Biobased Mater. Bioenergy. 6 (2012) 431–439.

[16] R. Abhijith, A. Ashok, C.R. Rejeesh, ScienceDirect Sustainable packaging applications from mycelium to substitute polystyrene : a review, 5 (2018) 2139–2145. doi:10.1016/j.matpr.2017.09.211.

[17] Ecovative Design, Ecovative Design-Textiles, (2020). https://ecovativedesign.com/textiles (accessed September 13, 2019).

[18] Ecovative Design-Meat substitute, Ecovative Des. (2020). https://ecovativedesign.com/food (accessed September 13, 2019).

[19] L. Jiang, D. Walczyk, G. Mcintyre, R. Bucinell, G. Tudryn, Manufacturing of biocomposite sandwich structures using mycelium-bound cores and preforms, 28 (2017) 50–59.

[20] M. Haneef, L. Ceseracciu, C. Canale, I.S. Bayer, J.A. Heredia-, Advanced Materials From Fungal Mycelium : Fabrication and Tuning of Physical Properties, Nat. Publ. Gr. (2017) 1–11. doi:10.1038/srep41292.

[21] F.V.W. Appels, J. Dijksterhuis, C.E. Lukasiewicz, K.M.B. Jansen, H.A.B. Wösten, P. Krijgsheld, Hydrophobin gene deletion and environmental growth conditions impact mechanical properties of mycelium by affecting the density of the material, (2018) 1–7. doi:10.1038/s41598-018-23171-2.

[22] M.R. Islam, G. Tudryn, R. Bucinell, L. Schadler, R.C. Picu, Morphology and mechanics of fungal mycelium, Sci. Rep. (2017) 1–12. doi:10.1038/s41598-017-13295-2.

[23] L. Jiang, D. Walczyk, G. Mcintyre, W. Kin, Cost modeling and optimization of a manufacturing system for mycelium-based biocomposite parts, 41 (2016) 8–20.

[24] L. Jiang, D. Walczyk, G. Mcintyre, R. Bucinell, B. Li, Bioresin infused then cured mycelium-based sandwich-structure biocomposites : Resin transfer molding (RTM) process, flexural properties, and simulation, 207 (2019). doi:10.1016/j.jclepro.2018.09.255.

[25] A. ISO/ASTM52900-15, Standard Terminology for Additive Manufacturing – General Principles – Terminology, 2015.

[26] World's Advanced Saving Project-WASP, Delta WASP 2040, 2018. (2018). https://www.personalfab.it/en/shop/clay-3d-printer-delta-wasp-2040-clay/.

[27] Ecovative Design, Grow.bio, (2020). https://grow.bio/collections/shop/products/grow-it-yourself-material.

5. 3D PRINTING OF BIOMASS-FUNGI COMPOSITE MATERIAL: EFFECTS OF MIXTURE COMPOSITION ON PRINT QUALITY[5]

5.1. Introduction

Environmental sustainability is a major concern for the construction and packaging industries. Production of 1 ton of cement generates an average of 0.9 tons of CO_2, resulting in approximately 5-7% of the global CO_2 emissions [1]. Additionally, the packaging industry consumes 38% of petroleum-based plastics produced globally [2]. It is estimated that, with current production and waste-management trends, 12 billion metric tons of plastic waste will be in landfills by 2050 [3].

Sustainable materials such as biomass-fungi composite materials can help reduce the negative impacts of construction and packaging industries [4–7]. In biomass-fungi composite materials, biomass derived from agricultural waste (such as rice straw and corn stover) acts as the substrate and a nutrition source for the fungi. The fungi grow as a network of fine white filaments (hyphae), also known as mycelium. This mycelium binds the biomass together. The mechanical properties of the mycelium are similar to materials such as wood and cork [8]. This is understandable since fungi are a natural source of structural polymers such as chitin that are present in the mycelium [9,10].

Advantages of biomass-fungi composite materials include low cost (estimated cost for raw materials: 0.07-0.17 kg/m^3 [9]), biodegradability and low environmental impact [11–13]. These materials have found applications in the automotive and construction industries

[5] Reprinted from "3D Printing of Biomass–Fungi Composite Material: Effects of Mixture Composition on Print Quality" by Bhardwaj et al., 2021. Journal of Manufacturing and Materials Processing, Volume 5, Issue 4, Copyright 2021 by the authors. Published by MDPI Ltd.

(e.g., as sound absorption panels, and wall panels [14]), the furniture industry, and the packaging industry [5,15]. Production of these parts uses molding-based manufacturing methods [5] that are expensive at low-production scales. 3D printing is more economical for producing parts with customized and complex shapes in small quantity than molding-based manufacturing methods.

There are many reported studies on biomass-fungi composite materials. Jones et al. [9] presented a critical review of biomass-fungi composite materials as construction materials. Haneef et al. [13] showed that the mechanical properties of mycelia were associated with the nutrition source for the fungi. Appels et al. [16] reported that fac-tors such as type of nutrition source, fungal species, and processing (no pressing, cold pressing, heat pressing) affected the physical properties (such as morphology, density, tensile strength) of the composite. Environmental factors such as light conditions and CO_2 concentration also impact fungal density [8]. Attias et al. [7] highlighted the need to develop sustainable production methods for these materials that avoid using plastic molds [7]. Soh et al. [17] developed an extrudable composition for mycelium compo-sites that was tested using a syringe.

Recently, the authors reported their first study on 3D printing of biomass-fungi composites in a journal publication [18]. The study demonstrated the feasibility of the 3D printing-based method by showing that a printable mixture could be prepared from biomass-fungi material and that fungi could survive the printing process and grow in the printed sample [18]. This paper reports a follow-up study to determine the effects of

mixture composition, specifically, psyllium husk powder on printing quality, as well as rheological properties of the prepared mixtures. Psyllium husk powder, derived from the seed husk or leaves of the plants of the Plantago genus [19], is a source of psyllium polysaccharide that exhibits gelation properties in aqueous solutions [19,20]. It possesses many advantages such as favorable viscoelastic properties, low cost, bio-degradability, and availability [19–21]. While researchers have studied psyllium husk/gelatin blends for bioprinting [19], its role in 3D printing of biomass-fungi composites remains a knowledge gap.

The structure of the paper is as follows. Section 5.2. describes materials and methods used in the study. Section 5.3. presents and discusses experimental results. Finally, in Section 5.4, conclusions and future research directions are discussed.

5.2. Materials and Methods

5.2.1. Biomass-Fungi Material

The biomass-fungi material (its commercial name is "Grow-It-Yourself") was procured from Ecovative Design, NY. The as-received material was in polypropylene filter patch bags that have a filter (1.5 inch square filter with a pore size of 0.2 μm) as part of the bag to facilitate fungi growth. Each bag contained 400 g of the material, as shown in Figure 20. This as-received material was converted into a biomass-fungi mixture that can be 3D printed by using the material extrusion process.

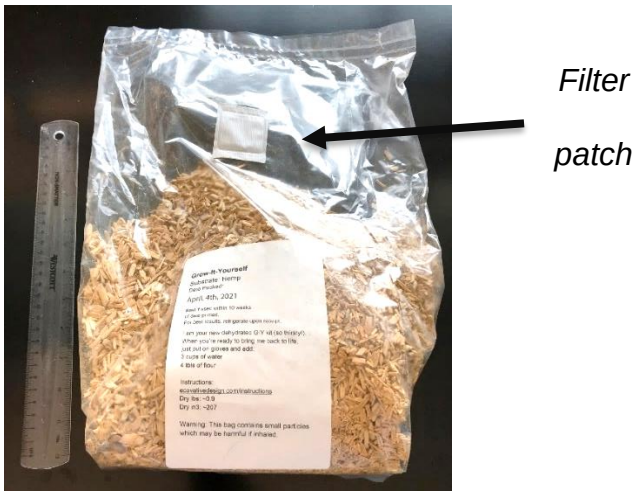

Figure 20. As-received biomass-fungi material in a filter patch bag

5.2.2. Experimental Procedure

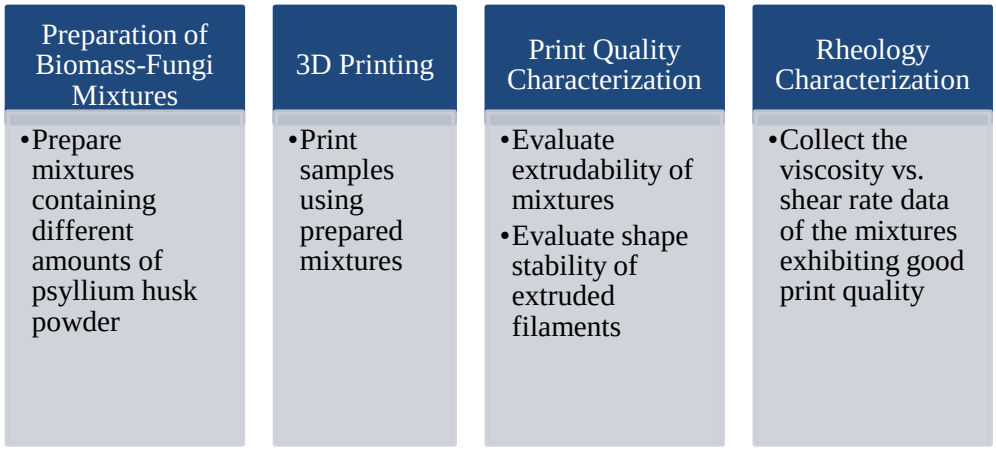

Figure 21. Experimental Procedure

The experimental procedure is shown in Figure 21. First, the biomass-fungi mixtures were prepared. Thereafter, samples were 3D printed using these mixtures. Next, print quality was evaluated using extrudability and shape stability. Finally, rheological properties of the biomass-fungi mixtures were characterized.

5.2.3. Preparation of Biomass-Fungi Mixtures

Preparation of the biomass-fungi mixtures comprised two stages.

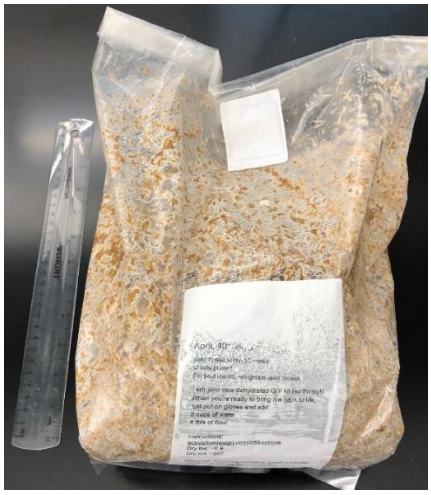

(a)

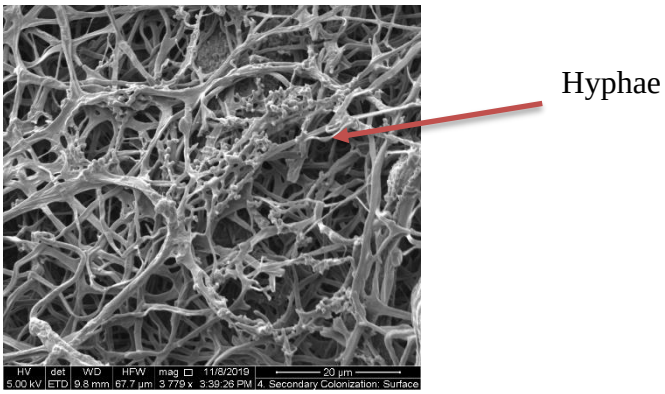

(b)

Figure 22. Biomass-fungi material after primary colonization: (a) Primary colonized material in filter-patch bag; (b) Scanning Electron Microscopy (SEM) image of surface of samples after colonization, scale bar is 20 µm

1. In Stage 1, the as-received biomass-fungi material underwent primary colonization. A wheat flour solution was prepared in a beaker by mixing 32 g of wheat flour and 700 mL of water. The mixing was performed manually using a spoon. Thereafter, this solution was poured into the filter-patch bag containing the biomass-fungi material. The filter-patch bag containing the com-bination was shaken vigorously by hand for one minute. After that, the filter-patch bag was kept in a bucket away from sunlight at a temperature of 23 ℃ for 3-5 days. This stage created a foam-like, dense, primary colonized, biomass-fungi composite material (see Figure 22(a)).

2. In Stage 2, the primary colonized biomass-fungi material was mixed by using a commercial benchtop mixer (NutriBullet PRO, Nutribullet). The mixing process was performed in two batches. For each batch, 50 g of the primary colonized material (as shown in Figure 22(a)) was broken off by hands into small chunks. These chunks along with 200 mL of water (at room temperature) and 20 g of wheat flour were then mixed in the mixer for 15 seconds. The mixture container was manually shaken after every 5 seconds to ensure uniform con-tact of the mixer blade with the material during the mixing process. Psyllium husk powder (procured from NOW Supplements, USA) was used as an additive to aid printability. After mixing the primary colonized material, psyllium husk powder was added into the mixture and mixed manually using a spoon. This mixing process transformed the dense, foam-like primary colonized material into a printable paste-like mixture. Biomass-fungi mixtures with four different compositions were prepared as shown in Table 6.

Table 6: Mixture composition

	Amount of Psyllium Husk Powder (w_p)	**Volume of Water (v_w)**	**Ratio of Psyllium Husk Powder Weight over Volume of Water (w_p:v_w)**
Mixture A	0 g	400 mL	0
Mixture B	10 g		1:40
Mixture C	20 g		2:40
Mixture D	30 g		3:40

To avoid any microbial contamination, the apparatus (such as 3D printer, beakers) was regularly cleaned with 70 percent ethyl alcohol solution.

5.2.4. 3D Printing

The printer used in this study was a Delta WASP 2040 (Figure 23 (a)) material-extrusion 3D printer, purchased from Spectrum Scientific (Philadelphia, PA). Material extrusion is defined as a ‘‘process in which material is selectively dispensed through a nozzle or orifice” [1]. This printer had a cylindroconical build volume whose cylindrical section had a diameter of 20 cm and a height of 40 cm. The conical section was situated on top of the cylindrical section with a base diameter of 20 cm and a height of 30 cm. The printer had a material storage container and an extruder assembly. The mixture for printing was stored in the material storage container before extrusion and pushed to the extruder assembly using a pneumatically operated piston. The extruder assembly comprised a screw extruder and a casing (Figure 23(b)). The casing surrounded the screw extruder had

a 6 mm nozzle with a square cross-section. Ultimaker Cura software (15.04.2) was used to generate the G-code file for printing the samples.

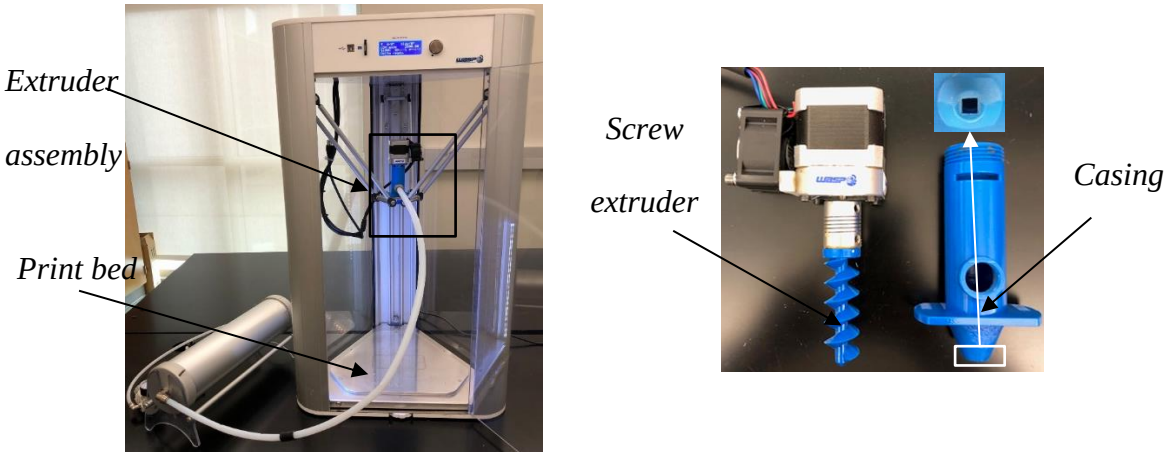

Figure 23. Material-extrusion3D Printer: (a) Delta WASP 2040 Printer; (b) extruder assembly including screw extruder and casing with a square cross-section 6 mm x 6 mm

The print speed was kept constant at 30 mm/s for all the experiments. Print speed refers to the speed at which the extruder moves across the print bed (in the X-Y plane) while depositing the material during 3D printing.

5.2.5. Print Quality Characterization

In this study, the print quality was assessed using two parameters: extrudability and shape stability. Extrudability is defined as the capacity of the mixture to pass through the nozzle of the 3D printer [23] and is characterized using two criteria. First, whether the

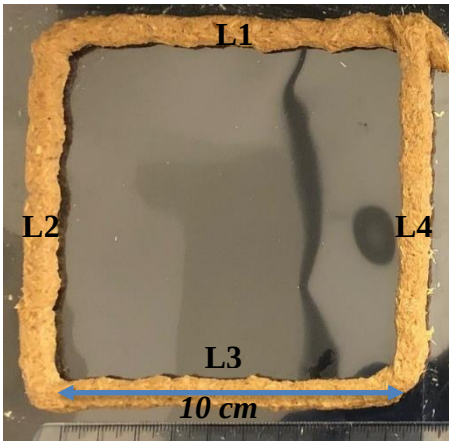

(a)

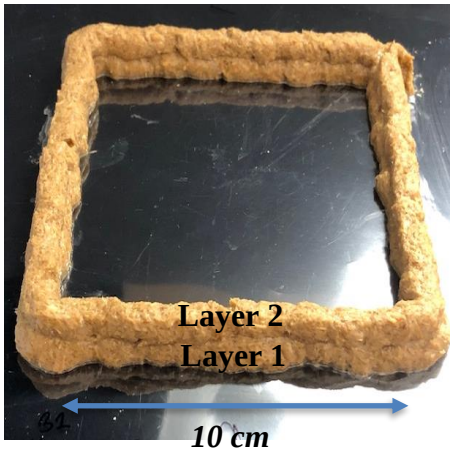

(b)

Figure 24. Printed samples for assessing print quality: (a) extrudability sample; (b) shape stability sample

material can be extruded without visible tearing in the extruded filament. Second, whether the extruded filament exhibits dimensional consistency. Dimensional consistency was measured by the variation of filament width in the printed sample. A sample was designated to have good dimensional consistency if no more than ±5% variation (from the

mean) was observed through the length of the filament [24]. To measure extrudability, two square samples (S1 and S2) were printed. Each sample consisted of four filaments (L1 through L4) having a length of 10 cm each (see Figure 24). Five measurements (width and height) were taken uniformly over the length of each filament.

In addition to extrudability, the deposited filaments must also possess sufficient strength to support the successive layers during the printing process. The deposited layer is subjected to deformation from three sources: (i) self-weight; (ii) weight of subsequent layers deposited on top of it; and (iii) extrusion pressure [24]. In this study, shape stability refers to the ability of the extruded filaments to resist deformations. (This concept was used by other researchers. For example, Kazemian et al. [24] used shape stability to refer the ability of the concrete material to resist deformations during layer-wise construction [24]). To quantify shape stability, two square samples (S3 and S4) having two layers (10 cm long) were printed. The initial height of Layer 1 right after deposition was recorded from samples S1 and S2. For samples S3 and S4, the height of Layer 1 was recorded 20 minutes after the deposition of Layer 2 (see Figure 24). The mixture was characterized to have good shape stability if the average height of Layer 1 after deposition of Layer 2 was within ±5% of the initial height.

5.2.6. Rheological Characterization

The rheological characterization of the biomass-fungi mixtures was conducted using a TA Instruments DHR-2 Rheometer. The gap between the base Peltier plate and the Flat plate (8 mm in diameter) was 500 μm (see Figure 25). Shear rate was changed from 0.01

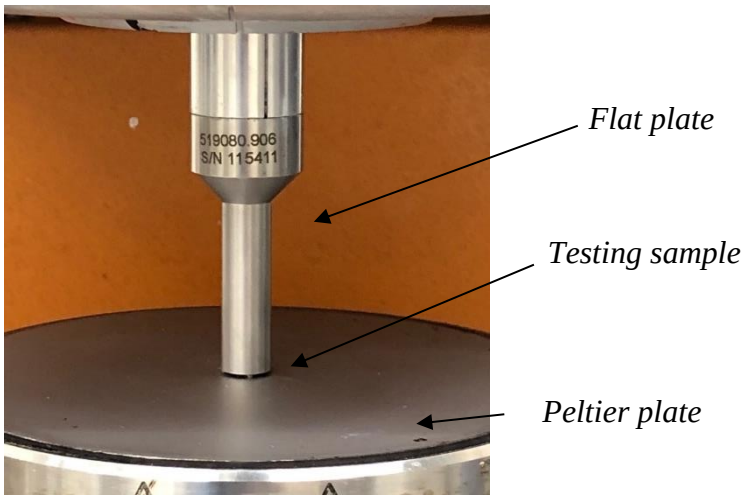

Figure 25. Apparatus for rheological characterization

to 2000 s-1. Shear thinning behavior of the mixtures was characterized by plotting a viscosity vs. shear rate curve. Shear elastic modulus (G'), shear loss modulus (G''), loss tangent, i.e., tan(δ), were also measured, where δ is the phase angle of the material. Loss tangent (tanδ) is the ratio of shear loss modulus (G'') to shear elastic modulus (G') as shown in equation (1). This ratio determines the liquid-like or solid-like nature of a mixture [19,25]. Mixtures behaving like solids would fail to extrude through the printer nozzle. Alternately, mixtures exhibiting dominant liquid characteristics would not be printable for multiple layers as the extruded layers would collapse as soon as the second layer is printed on top of them.

$$\tan(\delta) = \frac{Shear\ Loss\ Modulus,\ \ G''}{Shear\ Elastic\ Modulus,\ \ G'} \quad (1)$$

Frequency sweep testing ranging from 0.1 to 100 rad/s was used for the measurement of these moduli and loss tangent parameters. All measurements were conducted at 25 ℃. At least five test runs were performed to characterize the rheological properties of each mixture (for each composition). In this paper, average of the five test runs is reported for each mixture.

5.3. Results and Discussion

5.3.1. Effect of Psyllium Husk Powder Content on Extrudability

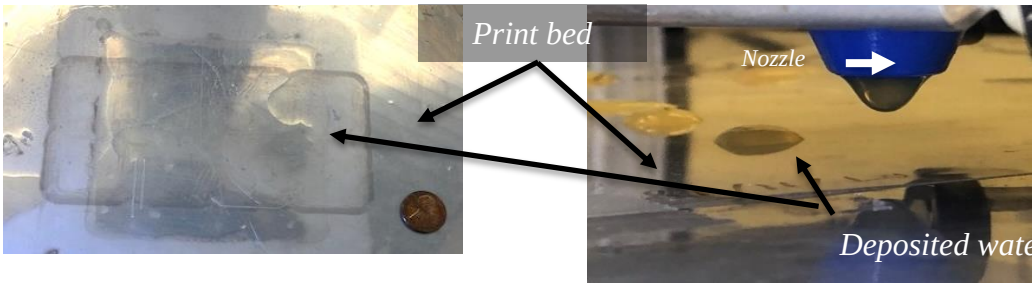

(a)

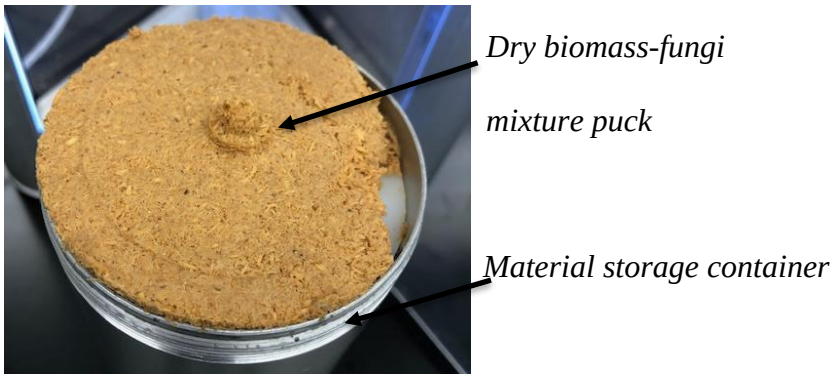

(b)

Figure 26. Printing results of Mixture A (a) only water from the biomass-fungi mixture was deposited during the printing process; (b) non-extrudable, dry biomass-fungi mixture puck left behind

Mixture A (without any psyllium husk powder) was not extrudable. As shown in Figure 26(a), the piston in the material container pushed the water out of the biomass-fungi mixture. This water was deposited on the print bed. The non-printable biomass-fungi mixture was left as a dry puck in the material storage container as shown in Figure 26(b).

Figure 27 shows the printed samples using Mixture B (wp:vw = 1:40), Mixture C (wp:vw = 2:40), and Mixture D (wp:vw = 3:40). Extruded filaments of mixtures B and C, as shown in Figure 27 (a) and (b), did not have tearing. The average filament width was 9.57 mm for Mixture B, and 8.68 mm for Mixture C. Filaments from both mixtures exhibited good dimensional consistency as well. The average variation in filament width was 1.87% for Mixture B and 2.5% for Mixture C.

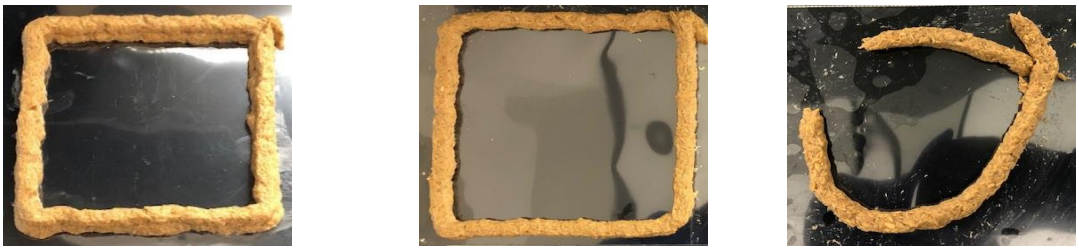

(**a**) (**b**) (**c**)

Figure 27: Printed samples using three mixtures with different levels of psyllium husk powder: (a) mixture B (wp/vw = 1:40); (b) mixture C (wp/vw = 2:40); (c) mixture D (wp/vw = 3:40).

This variation was within the ±5% variation defined for good extrudability. The detailed data for the width measurements of samples S1 and S2 are shown in **Error! Not a valid bookmark self-reference.**.

Table 7. Filament width data for samples S1 and S2 printed using Mixtures B and C

MIXTURE B (W_P:V_W = 1:40)

Test run	***S1***				***S2***				***Average***
	Filament Width (mm)				***Filament Width (mm)***				
	L1	***L2***	***L3***	***L4***	***L1***	***L2***	***L3***	***L4***	
1	*8.30*	*10.44*	*9.15*	*9.77*	*10.69*	*10.12*	*9.19*	*9.96*	
2	*9.56*	*9.50*	*9.18*	*9.78*	*10.04*	*9.10*	*9.24*	*9.72*	
3	*9.82*	*10.50*	*8.91*	*9.65*	*9.93*	*10.6*	*8.81*	*9.13*	
4	*9.94*	*9.45*	*9.16*	*9.26*	*9.89*	*8.95*	*9.68*	*9.16*	
5	*10.66*	*9.41*	*9.95*	*9.61*	*8.78*	*8.71*	*9.38*	*9.72*	
Average width (mm)	*9.66*	*9.86*	*9.27*	*9.61*	*9.87*	*9.50*	*9.26*	*9.54*	*9.57*
Variation from average width (%)	*0.90*	*3.03*	*3.13*	*0.46*	*3.09*	*0.77*	*3.24*	*0.33*	*1.87*

MIXTURE C (W_P:V_W = 2:40)

Test run	***S1***				***S2***				***Average***
	Filament Width (mm)				***Filament Width (mm)***				
	L1	***L2***	***L3***	***L4***	***L1***	***L2***	***L3***	***L4***	
1	*8.60*	*9.13*	*8.97*	*9.41*	*8.31*	*8.00*	*8.13*	*8.20*	
2	*8.56*	*8.66*	*8.21*	*9.80*	*9.04*	*8.49*	*8.71*	*8.54*	
3	*9.19*	*8.88*	*8.61*	*8.84*	*9.55*	*8.36*	*8.01*	*8.59*	
4	*8.56*	*8.46*	*8.87*	*9.10*	*8.01*	*8.47*	*8.31*	*8.84*	
5	*9.20*	*9.09*	*8.64*	*8.98*	*8.32*	*8.72*	*7.80*	*8.88*	
Average width (mm)	*8.82*	*8.84*	*8.66*	*9.23*	*8.65*	*8.41*	*8.19*	*8.61*	*8.68*
Variation from average Width (%)	*1.64*	*1.89*	*0.23*	*6.29*	*0.39*	*3.13*	*5.62*	*0.81*	*2.50*

5.3.2. Effect of Psyllium Husk Powder Content on Shape Stability

Figure 28 shows height data of Layer 1 after depositing Layer 2 for samples printed using Mixtures B and C. The reduction in the height of Layer 1 was 11% for the samples printed using Mixture B, and 5% for the samples printed using Mixture C. Samples printed using Mixture C showed much better shape stability than samples printed using Mixture B.

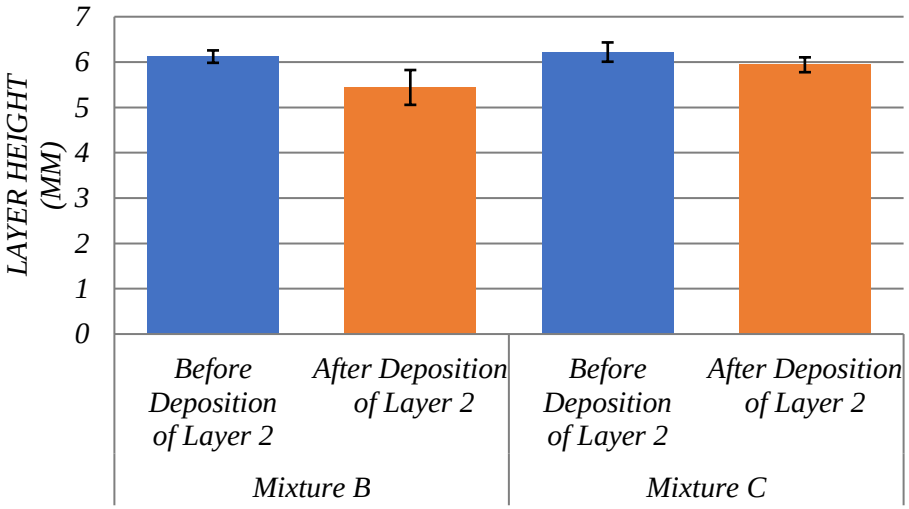

Figure 28. Height change of Layer 1 after depositing Layer 2

To summarize, Mixtures A and D performed poorly in the extrudability test, and, therefore, did not have shape stability data. Mixture C exhibited the best print quality in terms of both extrudability and shape stability. Mixture B displayed good extrudability, but its shape stability was not as good as Mixture C.

5.3.3. Effect of Psyllium Husk Powder Content on Rheological Properties

Figure 29 shows viscosity versus shear rate plots for all the mixtures. These plots show that the mixtures had shear-thinning behavior. Shear thinning refers to the behavior of non-Newtonian fluids whose viscosity decreases with increasing shear rate. For mixtures A, B and C, increasing their psyllium husk powder content led to a reduction in the viscosity of the mixtures. Not much difference was observed in the viscosity of Mixtures C and D.

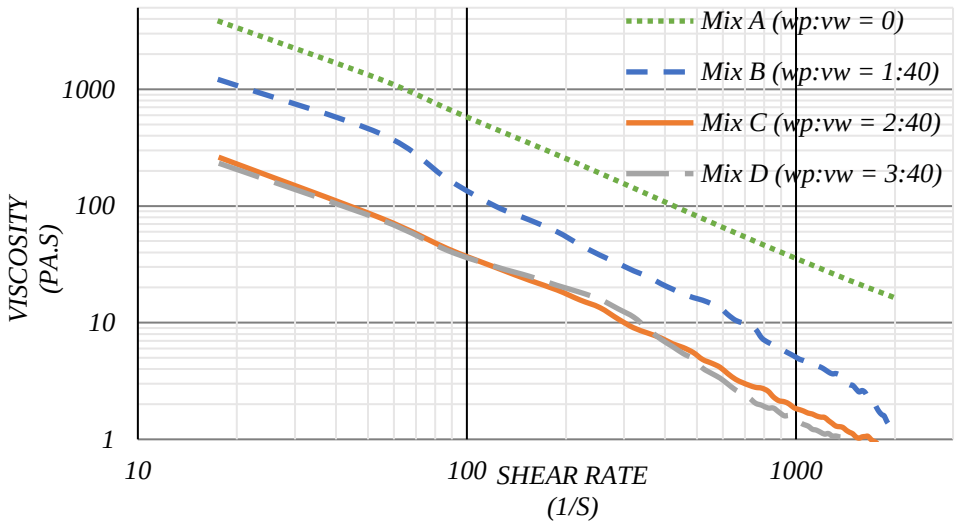

Figure 29. Effect of psyllium husk powder content on biomass-fungi mixture rheological behavior

As the psyllium husk powder content was increased, the elastic modulus of the biomass-fungi mixtures reduced for Mixtures A, B, and C (see *Figure 30*). Further

addition of psyllium husk powder resulted in a 37% average increase of G' for Mixture D compared to Mixture C.

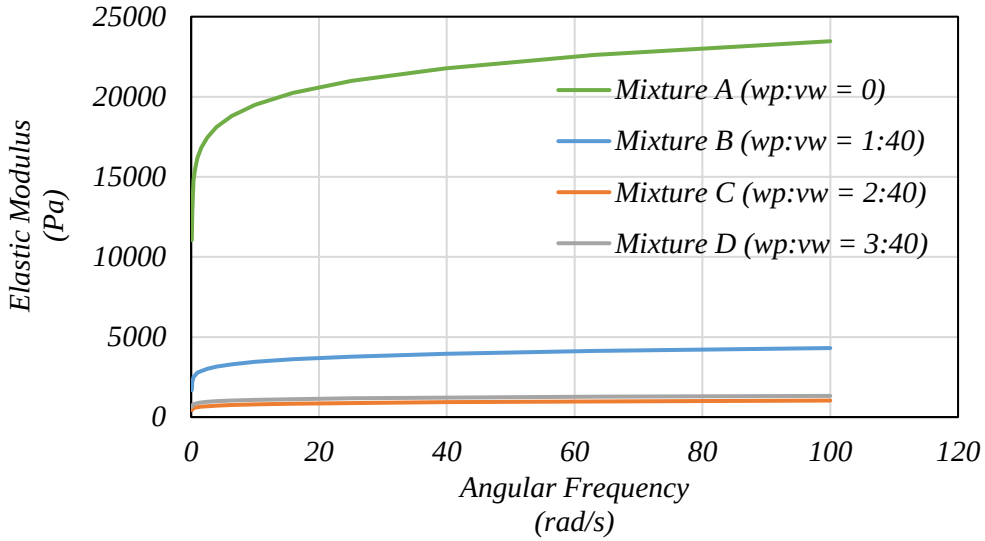

Figure 30. Relationships between elastic modulus (G') and angular frequency for four biomass-fungi mixtures

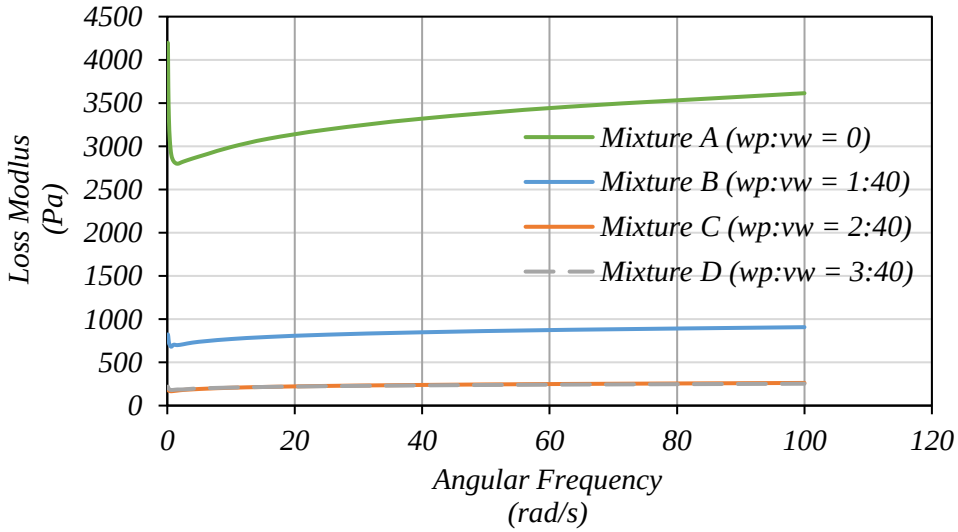

Figure 31. Relationships between loss modulus (G") and angular frequency for four biomass-fungi mixtures

Shear loss modulus (G'') represents the viscous nature of the mixture. An increase in the psyllium husk powder content in the mixtures resulted in a decrease in G'' for mixtures A, B, and C (see *Figure 31*). Mixture D had a loss modulus similar to that of Mixture C This was expected since Mixtures C and D had similar viscosity characteristics as shown in *Figure 29*.

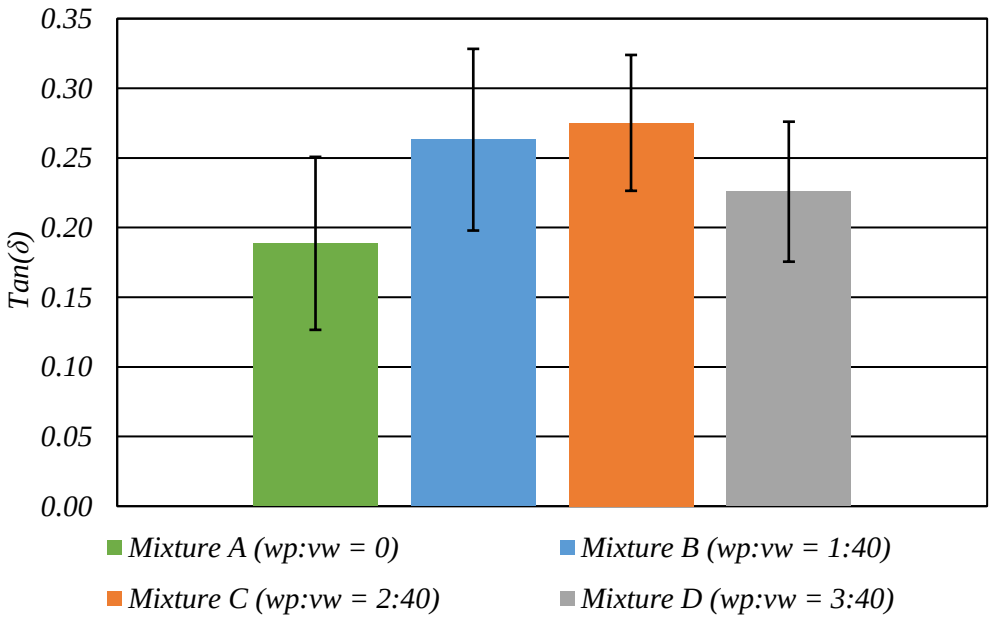

Figure 32. Loss tangent values of mixtures

Loss tangent tan(δ) values less than 1 are related to solid-like properties and values greater than unity are associated with liquid-like properties. Increasing the psyllium husk powder content increased the loss tangent tan(δ) i.e., 0.19, 0.26, and 0.28 for Mixtures A, B and C, respectively (see *Figure 32*). Therefore, as more psyllium husk powder was

added, the mixture went from being non-extrudable (Mixture A) to printable (Mixture C). Further addition of psyllium husk powder resulted in a reduction of tan(δ) value to 0.23 which represented the increased solid-like behavior of Mixture D compared with Mixtures B and C. This led to the observation of tearing in the extruded filament for Mixture D. While Mixture D was extrudable, Mixture A was not. This could be attributed to the fact that Mixture D had a higher tan(δ) value (0.23) than Mixture A (0.19).

5.4. Concluding Remarks

This paper reports an experimental study on 3D printing of a new class of sustainable materials for applications in the construction and packaging industries. Specifically, the study was focused on the effects of mixture composition (the content of psyllium husk powder) on print quality and rheological behavior. Main conclusions are:

- The mixture having no psyllium husk powder could not be extruded.
- Mixtures containing wp:vw ratios of 1:40 and 2:40 exhibited good extrudability (i.e., deposited filaments had no tearing).
- The mixture containing wp:vw = 2:40 was the only mixture that met the shape stability criteria for print quality.
- When wp:vw ratio was increased to 3:40, the mixture did not have good extrudability (printed filaments were not continuous). This performance was reflected in the increase in solid-like behavior of the mixture as observed in the loss tangent i.e., tan(δ) data.

- Mixture B (wp:vw = 1:40) had higher viscosity than Mixture C (wp:vw = 2:40). Both mixtures showed shear-thinning behavior.

Future studies will include SEM characterization of the bio-mass-fungi mixture and printed samples. Furthermore, effects of elapsed time after mixture preparation on mixture rheology and printability will also be analyzed.

References

[1] Cornell University Media Relations Office, 2021, "Bill Gates Shines Spotlight on Carbon-Emitting Cement and Need for Something New" [Online]. Available: https://news.cornell.edu/media-relations/tip-sheets/bill-gates-shines-spotlight-carbon-emitting-cement-and-need-something#:~:text="In 2020%2C 4.37 billion tons, of the global CO2 emissions.

[2] Rabnawaz, M., Wyman, I., Auras, R., and Cheng, S., 2017, "A Roadmap towards Green Packaging: The Current Status and Future Outlook for Polyesters in the Packaging Industry," Green Chem., pp. 4737–4753.

[3] Geyer, R., Jambeck, J. R., and Law, K. L., 2017, "Production, Use, and Fate of All Plastics Ever Made," Sci. Adv., 3(July), pp. 25–29.

[4] Grimm, D., and Wösten, H. A. B., 2018, "Mushroom Cultivation in the Circular Economy," Appl. Microbiol. Biotechnol., 102(18), pp. 7795–7803.

[5] Holt, G., McIntyre, G., Flagg, D., Bayer, E., Wanjura, J., and Pelletier, M., 2012, "Fungal Mycelium and Cotton Plant Materials in the Manufacture of Biodegradable Molded Packaging Material: Evaluation Study of Select Blends of Cotton Byproducts," J. Biobased Mater. Bioenergy, 6(4), pp. 431–439.

[6] Hook, S. Van, 2010, "SBIR Phase I: Using Mycelium as A Matrix For Binding Natural Fibers And Core Filler Materials In Sustainable Composites," Award Abstr. Number1045849 [Online]. Available: https://www.nsf.gov/awardsearch/showAward?AWD_ID=1045849.

[7] Attias, N., Danai, O., Abitbol, T., Tarazi, E., Ezov, N., Pereman, I., and Grobman, Y. J., 2020, "Mycelium Bio-Composites in Industrial Design and Architecture: Comparative Review and Experimental Analysis," J. Clean. Prod., 246, p. 119037.

[8] Appels, F. V. W., Dijksterhuis, J., Lukasiewicz, C. E., Jansen, K. M. B., Wösten, H. A. B., and Krijgsheld, P., 2018, "Hydrophobin Gene Deletion and Environmental Growth Conditions Impact Mechanical Properties of Mycelium by Affecting the Density of the Material," Sci. Rep., 8(1), p. 4703.

[9] Jones, M., Mautner, A., Luenco, S., Bismarck, A., and John, S., 2020, "Engineered Mycelium Composite Construction Materials from Fungal Biorefineries: A Critical Review," Mater. Des., 187, p. 108397.

[10] Wessels, J. G. H., Mol, P. C., Sietsma, J. H., and Vermeulen, C. A., 1990, "Wall Structure, Wall Growth, and Fungal Cell Morphogenesis BT - Biochemistry of Cell Walls

and Membranes in Fungi," P.J. Kuhn, A.P.J. Trinci, M.J. Jung, M.W. Goosey, and L.G. Copping, eds., Springer Berlin Heidelberg, Berlin, Heidelberg, pp. 81–95.

[11] Abhijith, R., Ashok, A., and Rejeesh, C. R., 2018, "Sustainable Packaging Applications from Mycelium to Substitute Polystyrene: A Review," Mater. Today Proc., 5(1), pp. 2139–2145.

[12] Arifin, Y. H., and Yusuf, Y., 2013, "Mycelium Fibers as New Resource For Environmental Sustainability," Procedia Eng., 53, pp. 504–508.

[13] Haneef, M., Ceseracciu, L., Canale, C., Bayer, I. S., and Heredia-, J. A., 2017, "Advanced Materials from Fungal Mycelium : Fabrication and Tuning of Physical Properties," Nat. Publ. Gr., (January), pp. 1–11.

[14] Pelletier, M. G., Holt, G. A., Wanjura, J. D., Bayer, E., and Mcintyre, G., 2013, "An Evaluation Study of Mycelium Based Acoustic Absorbers Grown on Agricultural By-Product Substrates," Ind. Crop. Prod., 51, pp. 480–485.

[15] NSF News Release 10-126, 2010, "Latest 'Green' Packing Material? Mushrooms!" [Online]. Available: https://www.nsf.gov/news/news_summ.jsp?cntn_id=117385. [Accessed: 01-Apr-2021].

[16] Appels, F. V. W., Camere, S., Montalti, M., Karana, E., Jansen, K. M. B., Dijksterhuis, J., Krijgsheld, P., and Wösten, H. A. B., 2019, "Fabrication Factors Influencing Mechanical, Moisture- and Water-Related Properties of Mycelium-Based Composites," Mater. Des., 161, pp. 64–71.

[17] Soh, E., Yong, Z., Saeidi, N., Javadian, A., Hebel, D., and Le, H., 2020, "Development of an Extrudable Paste to Build Mycelium-Bound Composites," Mater. Des., 195, p. 109058.

[18] Bhardwaj, A., Joseph Vasselli, Matt Lucht, Z.J. Pei, Shaw, B., Grasley, Z., Wei, X., and Zou, N., 2020, "3d Printing of Biomass-Fungi Composite Material: A Preliminary Study," Manuf. Lett., 24, pp. 96–99.

[19] Agarwal, P. S., Poddar, S., Varshney, N., Sahi, A. K., Vajanthri, K. Y., Yadav, K., Parmar, A. S., and Mahto, S. K., 2020, "Printability Assessment of Psyllium Husk (Isabgol)/ Gelatin Blends Using Rheological and Mechanical Properties," J. Biomater. Appl., 35(9), pp. 1132–1142.

[20] Farahnaky, A., Askari, H., Majzoobi, M., and Mesbahi, G., 2010, "The Impact of Concentration, Temperature and PH on Dynamic Rheology of Psyllium Gels," J. Food Eng., 100(2), pp. 294–301.

[21] Hussain, M. A., Muhammad, G., Jantan, I., and Bukhari, S. N. A., 2016, "Psyllium Arabinoxylan: A Versatile Biomaterial for Potential Medicinal and Pharmaceutical Applications," Polym. Rev., 56(1), pp. 1–30.

6. 3D PRINTING OF BIOMASS-FUNGI COMPOSITE MATERIAL: EFFECTS OF PROCESS PARAMETERS ON FUNGAL GROWTH

6.1. Introduction

Biomass-fungi composites represent an emerging class of sustainable materials for packaging [1–3] and construction applications [4]. In these composites, biomass (for example, agricultural waste such as corn stover) is bound together by fungal mycelium (vegetative part of fungi) through the growth of a network of tubular filaments also known as hyphae.

Low cost and biodegradability are key advantages of biomass-fungi composites. They also demonstrate good thermal and acoustic insulation properties [5–7]. Jones et al. [6] estimated raw material costs of these composites in the range of 0.07-0.17 $US/kg. In contrast, plastic materials such as polystyrene and polyurethane cost approximately 2 $US/kg and 9 $US/kg, respectively. These composites can be composted at end of life. In contrast, plastic materials are not environmentally sustainable. As of 2015, only 9% of plastic materials has been recycled whereas 91% of plastic waste ends up in incineration and landfills [8] where it takes years and decades to degrade.

Research interest in biomass-fungi composites is increasing with multiple review papers published in recent years [2,6,9]. Jones et al. [6] reviewed the engineering of the material properties of these composites and their applications. Attias et al. [9] provided a review of literature on the use of biomass-fungi composites in design and architecture.

Furthermore, the authors also conducted an experimental analysis on the effect of different fungal species, substrate mixtures and fabrication methods on material characteristics [9]. Elsacker et al. [10] presented a comprehensive framework for production of these composites. Haneef et al. [11] reported the effects of nutrient substrates on material properties of composites derived from two fungi Ganoderma lucidum and Pleurotus ostreatus. Appels et al. [12] studied the effects of deletion of the gene sc3 and environmental growth conditions (light or dark, CO_2 concentration) on material properties of the fungus Schizophyllum commune. The morphology, density, mechanical strength (tensile and flexural) and water-uptake properties can be tuned by changing the nutrient substrates, fungal species, and mechanical processing technique (no pressing, hot pressing, cold pressing) [13]. Islam et al. [14] provided a stochastic continuum model for mycelium-based bio-foam characterized under axial loading. The morphological and mechanical characterization of mycelium has also been reported using an integrated computational and experimental approach [15]. Researchers have developed a cost-model for molding-based manufacturing of biomass-fungi composites [16]. Furthermore, researchers have incorporated natural fiber derived from materials such as jute and hemp in the manufacturing of biomass-fungi composites [17]. Recently, the authors of this paper reported the preliminary results of 3D printing of biomass-fungi mixture using the material-extrusion process [18]. In that study, a biomass-fungi mixture comprising living fungal cells and biomass material was prepared and 3D printed. After 3D printing, the fungi grew on the printed sample.

Health of living cells during printing is critical to the success of 3D bioprinting. 3D bioprinting refers to the layer-by-layer, spatially controlled deposition of biological material, biochemicals and living cells to fabricate a 3D structure [19]. Process parameters can impact the health of living cells during 3D printing. Blaeser et al. [20] reported that printing related shear stress could affect the viability of cells (mouse fibroblasts). Cell viability refers to "the ratio of living and dead cells" [20]. At low shear stress (<5 kPa), cell viability and hence, membrane integrity were unaffected. However, increasing the shear stress (>10 kPa) resulted in a 20% drop in cell viability.

In contrast to mammalian cells, fungal cells have cell walls composed of chitin, glucans mannans and glycoproteins [21]. While the consequences of 3D printing induced effects on cell viability have been reported for mammalian cells [20], these effects remain a knowledge gap for 3D printing of biomass-fungi mixtures. This study addresses these gaps regarding the effects of the mixing process parameters on fungal growth. Furthermore, it also analyzes the impact of printing parameters such as print speed and extrusion pressure on fungal growth. Lastly, the tensile and compression strength of the biomass-fungi composites are presented.

6.2. Materials and Methods

6.2.1. Biomass-Fungi Material

The biomass-fungi material as shown in Figure 33(a) (commercial name: Grow-It-Yourself Material) was procured from GROW.bio (NY, USA). The biomass material comprises agricultural waste matter (such as corn stover). On receiving hydration and

nutrition, the fungi undergo primary colonization to bind the biomass material together as shown in Figure 33(b).

This binding mechanism is favored through the growth of thread-like cells called hyphae. Collectively, these structures are referred to as mycelium (see Figure 36). Typical hyphae diameters range from 1-30 µm depending on various factors such as fungi species and growth environment [15].

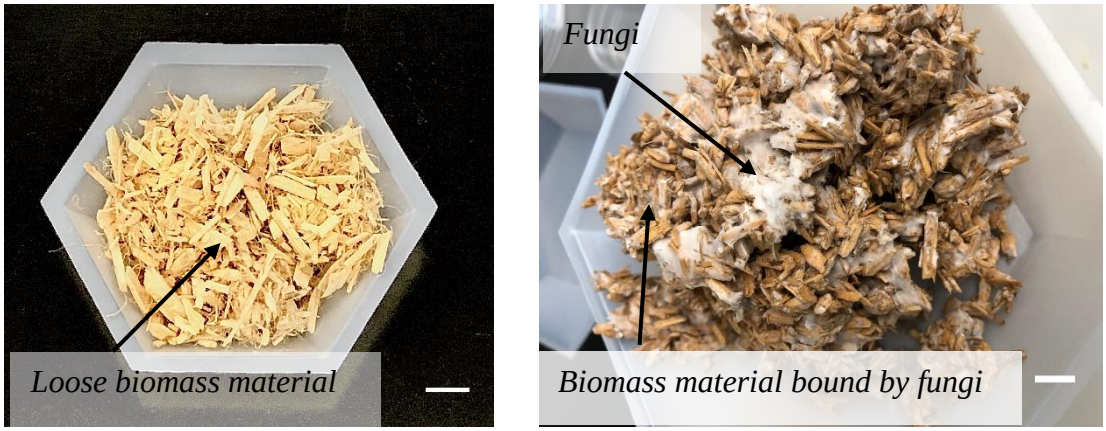

(a) *(b)*

Figure 33: Biomass-Fungi material: (a) as obtained from supplier, scale bar is 1 cm; (b) after primary colonization, biomass material is bound by fungi, scale bar is 1 cm

6.2.2. Preparation of Biomass-Fungi Mixtures and 3D Printing

Figure 34 shows the six stages of the preparation and 3D printing of biomass-fungi mixtures.

In stage I, the biomass material is pasteurized and then, inoculated with the fungi. The pasteurization process exposes the biomass material to elevated temperatures to kill microorganisms that might compete for nutrition with the fungi. Inoculation involves the

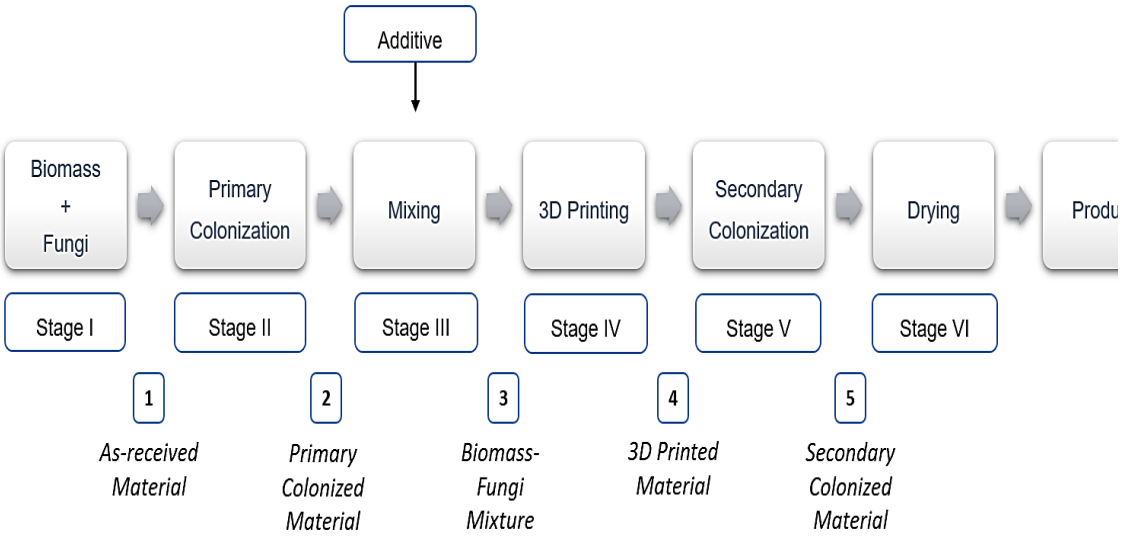

Figure 34: Six stages of the 3D printing manufacturing process of biomass-fungi mixtures [18]

addition of the fungi to the biomass material. During this process, the fungi fully colonize the biomass material to create a biomass-fungi composite that is dehydrated prior to packaging and shipping. These steps occur at the vendor site after which the material is packed in filter patch bags and shipped to the lab. This as-received biomass-fungi material is then made to undergo primary colonization during Stage II. During this stage, a solution of 700 mL water and 32 g of wheat flour is added to the filter patch bag and shaken vigorously by hand for sixty seconds. This bag is then stored in a closet at 23°C for five

(a) *(b)*

Figure 35: Images of samples: (a) After 3D printing, scale bar is 1 cm; (b) 3D printed after undergoing secondary colonization, scale bar is 1 cm

days. During this time the fungi grow as colonies on the biomass material to create a foam-like, dense, primary colonized material as shown in *Figure 33*(b). In stage III, this primary colonized material is processed to create a printable biomass-fungi mixture. During this process, 100 g of primary colonized material is broken off into smaller pieces by hand and then mixed with 400 g of water and 20 g of wheat flour using a commercial mixer (Nutribullet Pro, USA). A mixing time of 30 seconds was used. The mixing was performed in a pulsed manner i.e., the mixing was stopped after every 5 seconds and manually shaken to ensure even distribution of the material around the mixer blades. Thereafter, 20 g of psyllium husk powder was mixed into this mixture using a spoon. This powder prevented phase segregation during the 3D printing process. This mixture is printed in Stage IV using a Delta WASP 2040 3D printer as shown in Figure 35(a). In stage V, the 3D printed parts are stored in filter patch bags and stored in a closet at 23°C for five days. This stage is referred to as the Secondary colonization. As the name suggests, the fungal colonies grow

on the 3D printed part during this stage. The 3D printed part now shows a layer of white mycelium on the exterior surface as shown in Figure 35(b). Finally, the 3D printed part is dried in a conventional oven at 95℃ for four hours.

Figure 36 shows SEM images of mycelium growth on samples prepared using extrusion after secondary colonization.

Further details of the preparation of the biomass-fungi mixtures is presented in a prior publication [18]. In this study, autoclaved wheat solution was used for the Primary Colonization and Mixing stages. 70% ethyl alcohol solution was used to clean the apparatus to remove any microbial contamination.

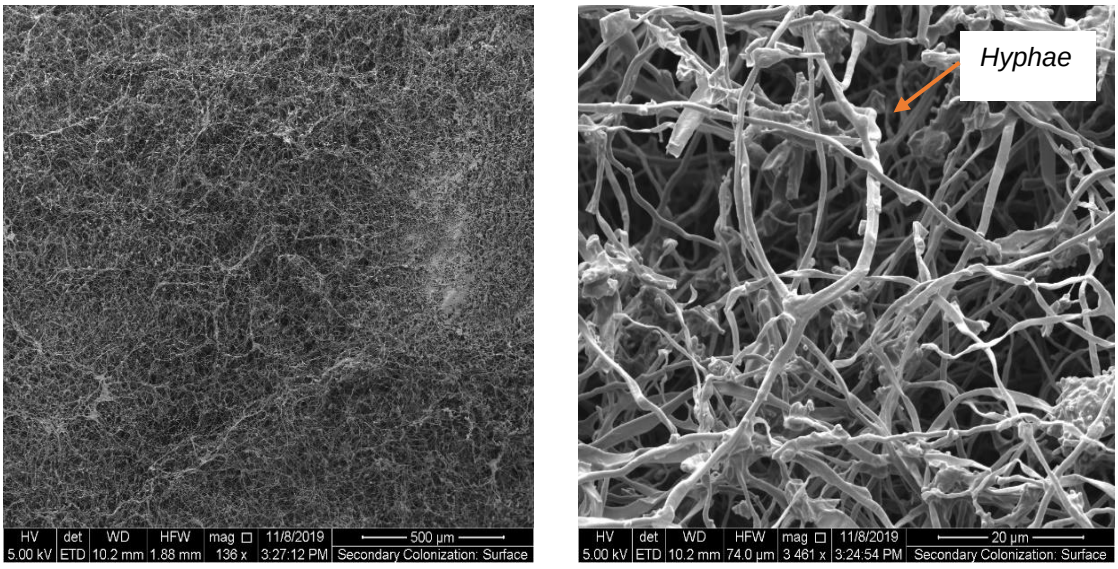

(a) *(b)*

Figure 36: SEM images of surfaces of samples after secondary colonization by the mycelium: (a) scale bar is 500 µm; (b) scale bar is 20 µm

6.2.3. 3D Printer

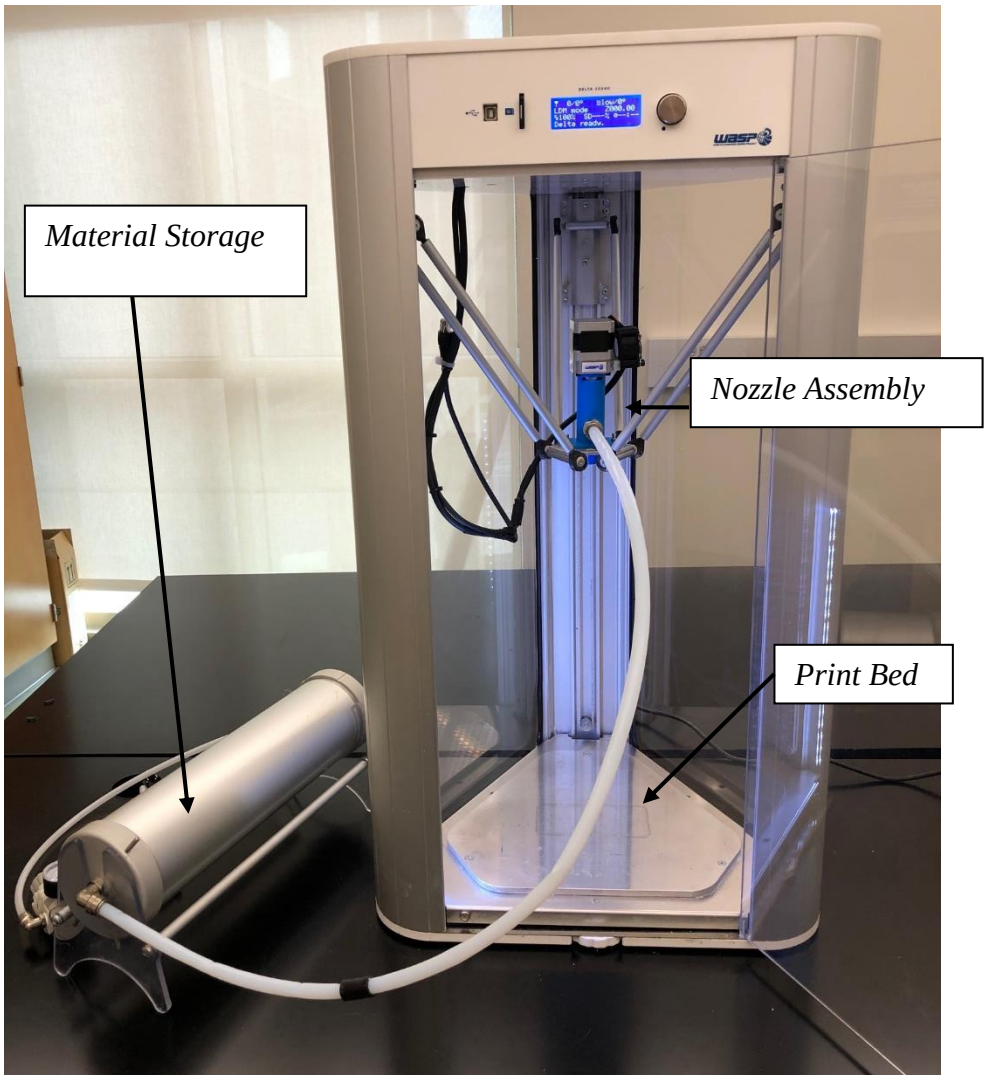

Figure 37: Delta WASP 2040 3D Printer

The WASP 2040 3D printer shown in Figure 37 was used for the experiments. This printer was purchased from Spectrum Scientific (Philadelphia, PA), with an LDM (Liquid deposit modeling) WASP extruder kit [22] to print fluid, paste-like materials. This printer came equipped with a material storage container (storage volume: 3L) that used a

pneumatically operated plastic piston to push the mixture through the printer nozzle assembly. The nozzle assembly comprised a screw extruder and a casing with a 6-mm opening. The nozzle assembly was custom built to eliminate nozzle blocking problems faced when using the vendor-provided nozzle assembly having a 2 mm opening.

6.2.4. Experimental Procedure

Mechanical processing of biomass-fungi materials to facilitate their 3D printing could expose them to high shear stress during two stages: Mixing Stage and 3D Printing Stage. During the mixing stage, the primary colonized biomass-fungi material is broken down into a liquid slurry by using a commercial mixer. The mixing process could subject the material to high shear stress. Moreover, the duration of mixing could also increase the temperature of the material due to the friction from the blades. The high shear stress generated during the mixing process along with elevated temperatures could affect fungal growth in later stages. The effect of the mixing process parameters on fungal growth remains a knowledge gap. To address this knowledge gap, Phase I of the study focused on analyzing the impact of the mixing process on fungal growth in the biomass-fungi mixture. Towards this end, samples were prepared by varying the mixing process parameters shown in Table 8. Mixing time refers to the duration of mixing employed for preparing the biomass-fungi mixture. Mixing type describes the type of mixing process used: continuous or pulsed. During continuous mixing, the biomass-fungi mixture was mixed continuously. For pulsed mixing, the mixture was mixed for a period of five seconds. Afterwards, the mixing container was manually shaken twice to ensure good contact of the mixture with

the blades before restarting the mixing process. This procedure was followed for the 15 seconds and 120 seconds. It was assumed that pulsed mixing could help keep the temperature low in the mixture during the mixing process. Five runs were performed for each parameter setting per day. This experiment was replicated over three days. Hence, sixty runs were performed in total. Fungal colonies were counted in the prepared samples after 48 hours. The procedure for fungal colony quantification is discussed in section 6.2.5.

Table 8: Input variables for Phase I

Variable	**Value**
Mixing Time (seconds)	*15, 120*
Mixing Type	*Pulsed, Continuous*

Shear stress generated during the 3D printing process can affect the health of mammalian cells [20]. However, the effects of printing process parameters such as extrusion pressure and print speed on fungal heath remains a knowledge gap. During isothermal flow through a circular tube, the maximum shear stress is generated at the wall of the tube. This shear stress at the wall is directly proportional to the volumetric flow rate of the material [23]. During 3D printing of biomass-fungi mixtures, this volumetric flow rate is controlled by two printing parameters: extrusion pressure and print speed. Phase II of the study analyzed the effect of these printing parameters on fungal growth. Extrusion pressure refers to the compressed air pressure used to push the material through the printer

nozzle. Print speed refers to the speed at which the nozzle moves on the print bed during the printing process. Samples exposed to high shear stress were prepared by extruding the biomass-fungi mixture at a pressure of 6 bars and print speed of 120 mm/s. The pressure of 6 bars was selected for the high setting since the safety valve on the material storage container was rated at 7 bars. The low shear samples were extruded at a pressure of 2 bars and print sped of 30 mm/s. Results from Phase I of the study were used to select a mixing time and mixing type for the preparation of these mixtures (see Table 9). Therefore, both samples were prepared by mixing the biomass-fungi mixtures for 120 seconds using the pulsed-type mixing process. Five samples were collected from each extruded mixture to quantify fungal growth. Fungal growth data was also collected from mixtures that were not used for printing. This data helped establish a baseline for the experiment.

Table 9: Input variables for Phase II

Variable	Value
Shear stress	*Low: Print speed: 30 mm/s, Pressure: 2 bars* *High: Print speed: 120 mm/s, Pressure: 6 bars*

Thereafter, the tensile and compressive strength of the high shear and low shear samples was analyzed. Extruded mixtures from Phase II were packed in molds and prepared for tensile and compressive testing. Details of the sample preparation are presented in section 6.2.6.

6.2.5. Measurement of Fungal Growth

Colony forming units per milliliter (CFUs/mL) was used as a metric to quantify the fungal growth in mixtures. After the mixtures were prepared, one gram of mixture was suspended in 10 mL of sterile water. This solution was serially diluted to a concentration of 10^{-2} to facilitate the counting of colonies and 100 µL of the solution was spread onto ½ PDA plates (19.5 g/L Difco PDA, adjusted to 1.5% agar). To calculate colony forming units, the resulting number of colonies counted after 48 hours incubation at 22**°C** was multiplied by 10,000 to calculate the number of viable fungal colonies in the mixture, reported here in CFUs/mL. An example of this plate is shown in Figure 38(a) The fungal colonies observed on these plates were counted after 48 hours using an optical microscope as shown in Figure 38(b).

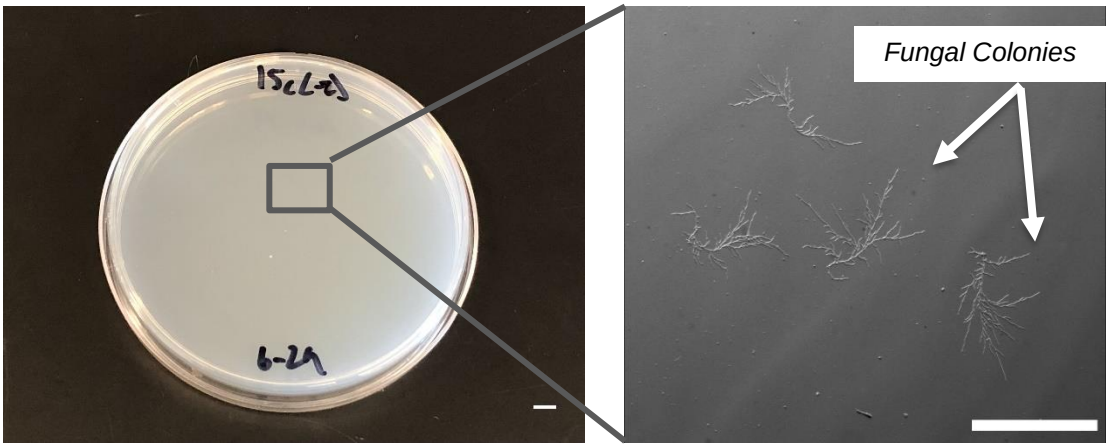

(a) *(b)*

Figure 38: Measurement of fungal growth (a) Plated test samples, scale bar is 1 cm; (b) Fungal colonies observed on plated samples, scale bar is 0.25 cm

6.2.6. Mechanical Characterization

Mixtures extruded from the printer at low and high shear stress were used to prepare molded samples for mechanical testing. These samples were shaped using rectangular molds. Thereafter, these samples were kept on plates having slotted bases where they underwent secondary colonization over the course of five days (Figure 39). The samples were flipped after 2.5 days to facilitate fungal growth on the base sides of the samples. After another 2.5 days, these samples were dried in countertop convection oven (Black+Decker TO3250XSB) at a temperature of 95℃ for 6 hours.

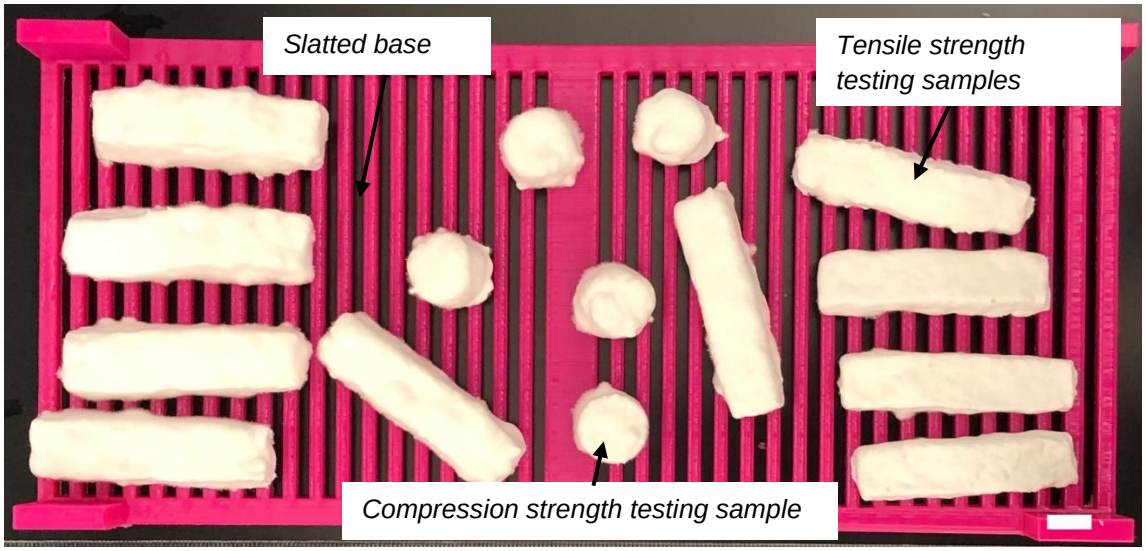

Figure 39: Samples prepared for tensile and compression strength testing after secondary colonization, scale bar is 1 cm

6.2.6.1. Tensile Strength

The tensile strength of the samples was measured using the Instron 68TM-5 Universal Testing Machine. A load cell of 500 N and a loading rate of 10 mm/min. was used. Resin

(UV curable) was applied on the ends of the sample to facilitate good grip with the clamp during testing. This resin was cured using a UV flashlight (395-405 nm). Five samples were tested for each mixture (low shear and high shear). These samples had dimensions of 48 mm X 11 mm X 13 mm (see Figure 39).

6.2.6.2. Compressive Strength

To study compressive strength of the material, cylindrical samples were prepared using molds 1.5 cm in diameter and 1 cm tall (see Figure 39). Testing was performed using Instron 5943 Universal Testing System with a 1kN load cell and a strain rate of 50% strain per minute. Three samples were prepared for compressive testing.

6.2.7. Microscopy

Fungal colonies were observed using an Olympus SZX9 dissecting microscope using a Hamamatsu ORCA-ER digital camera connected to Slidebook 5.0 software. Fluorescently-labeled samples were observed using an Olympus FV3000 laser scanning confocal system mounted to an Olympus IX83 inverted microscope with a Galvonometer scanner and High Sensitivity GaAsP PMT detectors (Olympus America, Center Valley, PA, USA). The objective used to image fluorescently-labeled hyphae was the UPlanSAPO 10x (NA = 0.4), which utilized the 405nm laser line to excite hyphal cell walls labeled with 10µg/mL Calcoflour-white. Fluorescence images were generated via optical sectioning of multiple planes in the z-axis and combining them into a single max-projected image. These images were then exported via Olympus Cellsens software and figures were created using GIMP software (2.10.20).

6.3. Results and Discussion

6.3.1. Effect of Mixing Time on Fungal Growth

As shown in Figure 40, samples mixed for 15 seconds had an average fungal growth of 6.9 X 10^5 CFUs/mL. In contrast, samples mixed for 120 seconds had an average fungal

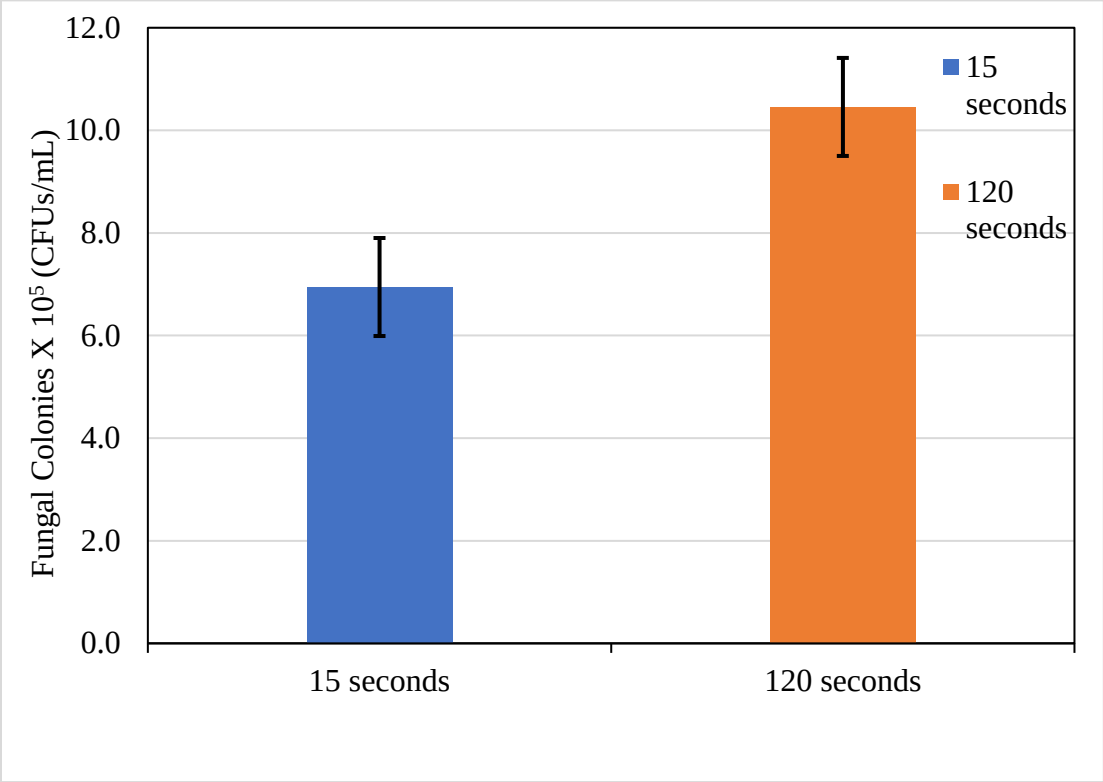

Figure 40: Effect of mixing time on fungal growth

growth of 10.5 X 10^5 CFUs/mL. In Figure 40, the error bars indicate a 95% confidence interval of the mean. Therefore, mixing time had a significant effect on fungal growth. A possible explanation for this observation could be as follows: a mixing time of 120 seconds would facilitate a better breakdown of the biomass material and the fungal inoculum as compared to the 15 second samples. More surface area available for the fungi to derive

nutrition. Additionally, longer mixing times could potentially enhance the distribution of the number of viable hyphal fragments dispersed throughout the mixture. The temperature recorded after mixing continuously for 120 seconds was 37.3 ℃. This temperature was significantly lower than the temperature used to deactivate the fungi during the drying stage (93℃). Hence, more fungal growth in these samples is expected as mixing times are increased.

6.3.2. Effect of Mixing Type on Fungal Growth

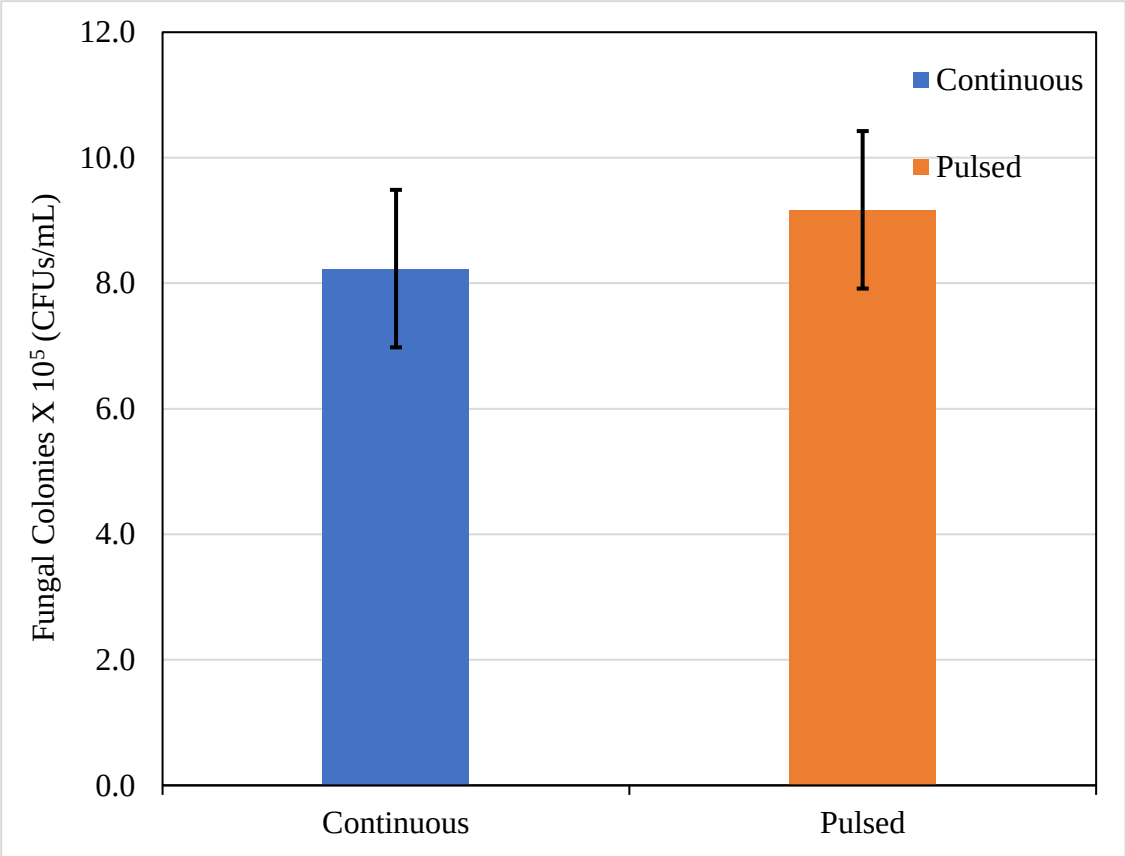

Figure 41: Effect of mixing type on fungal growth

As shown in Figure 41, effect of mixing type on fungal growth is not statistically significant. Samples prepared by continuous mixing had a mean value of 8.2 X 10^5 CFUs/mL. This value was close to the mean of pulsed samples (9.17 X 10^5 CFUs/mL). The error bars in Figure 41 indicate a 95% confidence interval of the mean. Maximum temperatures recorded during the mixing process for continuous and pulsed mixing were 37.7 ℃ and 36.3 ℃, respectively, when mixed for a duration of 120 seconds. The results suggest that the heat generated during continuous mixing did not have any significant detrimental impact on fungal growth.

6.3.3. Effect of Shear Stress on Fungal Growth

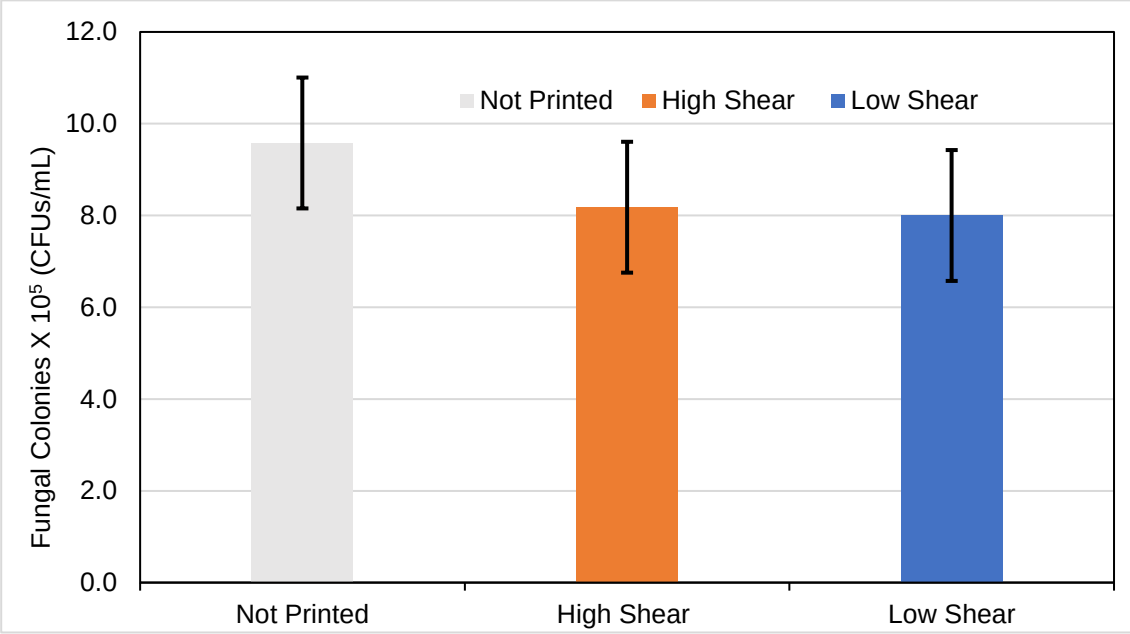

Figure 42: Effect of shear stress on fungal growth

Shear stress did not have any statistically significant effect on fungal growth. Biomass-fungi mixtures that were not subjected to 3D printing had an average fungal growth of

9.58 X 10^5 CFUs/mL. Mixture exposed to 3D printing and high shear stress exhibited a 14.6% reduction in fungal growth. In contrast, mixtures extruded at low shear stress had an average reduction of 16.5% in fungal growth. Therefore, the low shear and high shear samples had less than 2% difference in the number of colonies forming units per milliliter. The results of the effect of shear stress on fungal growth is shown in Figure 42 where the error bars represent a 95% confidence interval of the mean. Unlike mammalian cells, fungal cells have a cell wall made of glucans, chitin and glycoproteins [21]. A possible reason for this observation could be that the presence of this cell wall would make the fungal cells more resilient to damage. Therefore, even in the high shear extrusion, the fungal cells may not have been subjected to adverse conditions to impact their growth significantly.

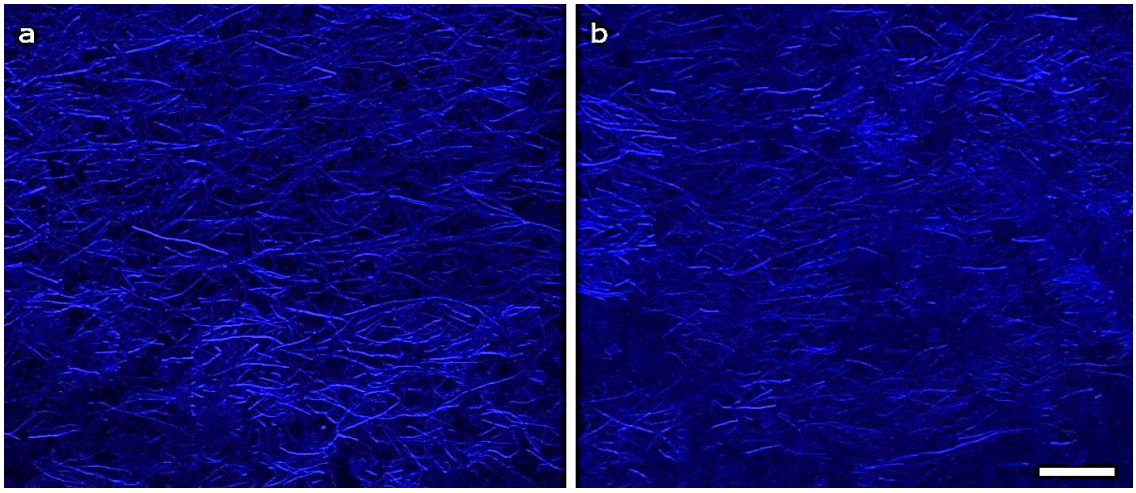

(a) *(b)*

Figure 43:Confocal microscope generated optical images of fungal mycelium colonizing the surface of samples. Fungal cells are labeled with CFW dye: (a) Low shear sample; (b) High shear sample, scale bar is 50 µm

Figure 43 shows the optical images of the low shear and high shear samples using Calcofluor-white (CFW). CFW is a chitin-binding fluorescent dye that has been shown to effectively label fungal cell walls [24]. As shown in Figure 43, no visible difference was observed in the amount of colonization detected in the samples.

6.3.4. Mechanical Characterization

6.3.4.1. Tensile Strength of Samples

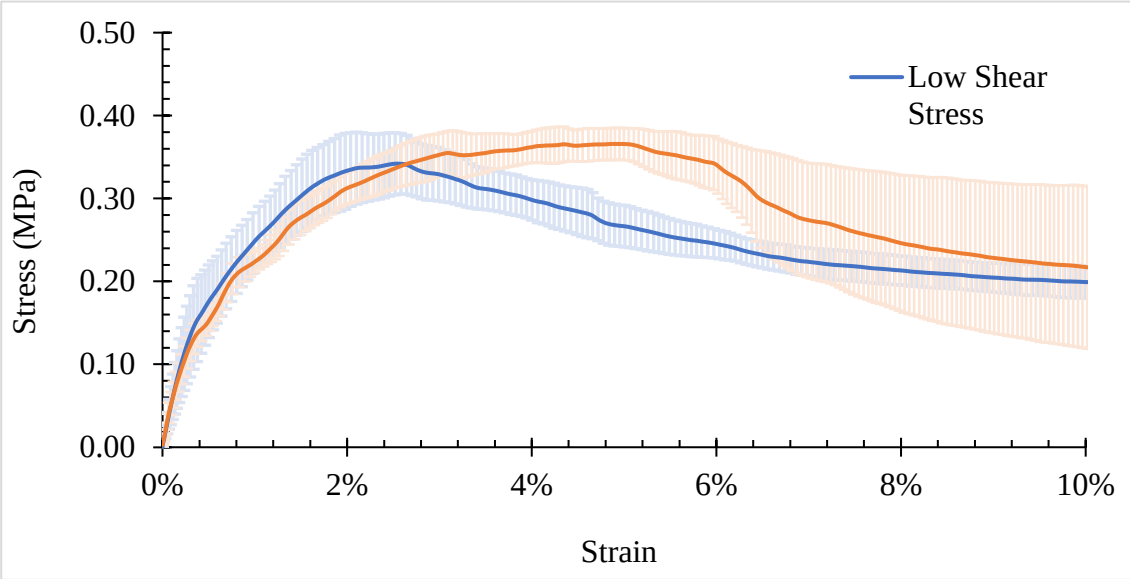

- *Figure 44: Effect of shear stress on tensile strength of biomass-fungi composites*

Figure *44* shows the stress-strain curves for the tensile testing of the low shear stress and the high-shear stress samples. The shaded region denotes the standard deviation in the data. The samples displayed no significant difference in their tensile strengths. The Young's modulus of the low shear stress samples was 55.51 MPa whereas that for high

shear stress samples was 55.67 MPa. The ultimate tensile strength of the high shear stress and the low shear stress samples was 0.37 MPa and 0.34 MPa, respectively. This result was expected since the biomass-fungi mixtures did not show significant difference in fungal growth as discussed in section 6.3.3.

6.3.4.2. Compression Strength of Samples

As shown in Figure 45, low shear and high shear samples did not differ significantly in their compressive strength. The shaded regions indicate the standard deviation for the respective sample. While the compressive strength of low shear samples was 0.72 MPa, that of high shear samples possessed compressive strength of 0.90 MPa. The compressive modulus for the low shear and the high shear samples was 1.96 MPa and 0.59 MPa, respectively.

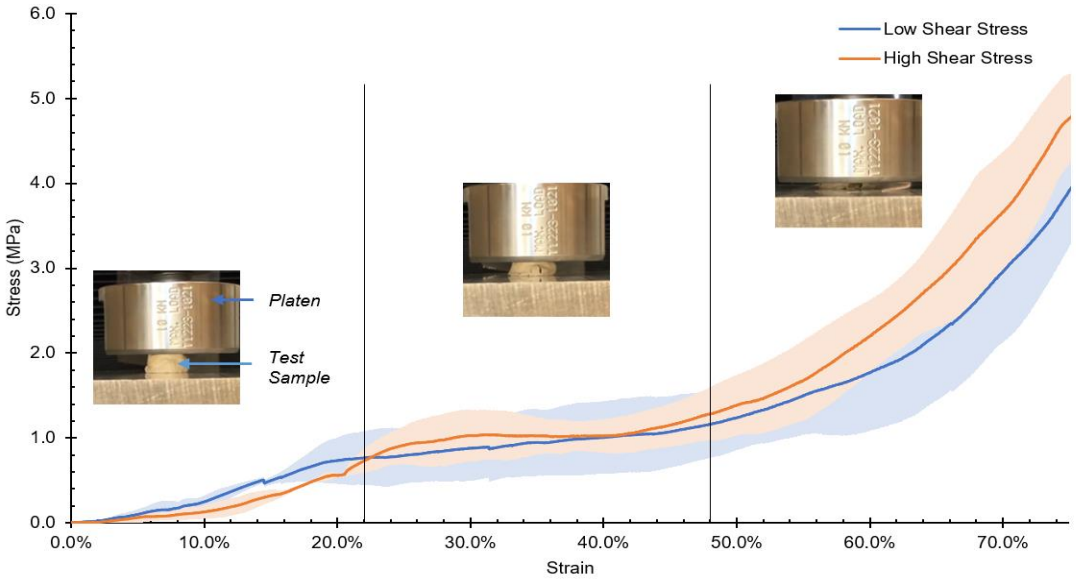

Figure 45: Effect of shear stress on compressive strength of biomass-fungi composites

-

6.4. Concluding Remarks

This paper reports on the effects of mixing process parameters (mixing time and mixing type) and printing process parameters (print speed and extrusion pressure) on fungal growth in biomass-fungi mixtures. Fungal growth in samples was quantified using the metric of colony forming units per milliliter (CFUs/mL). Furthermore, the tensile and compressive strength of the materials has been reported. Main conclusions are:

Increasing mixing time from 15 seconds to 120 seconds led to a 52% increase in fungal growth. A possible explanation for this observation could be that the increased mixing time led to a better breakdown of the biomass material and the fungal inoculum. While this process would have improved the spread of the viable hyphal fragments, it would also have made more surface area of biomass available for the fungi to derive nutrition.

Mixing type did not have a statistically significant effect on fungal growth. A potential justification for this result could be that mixing the biomass-fungi material for 120 seconds continuously did not have a substantial detrimental impact on the fungal growth.

The difference in fungal growth observed in the high shear stress and low shear stress samples was not statistically significant. A probable cause for this observation could be that even at high print speed and extrusion pressure, the shear stress generated may not be substantial to damage the fungal cell wall.

Future studies would evaluate the effect of increasing durations of mixing times on fungal growth. Moreover, the impact of environmental factors such as temperature and humidity on fungal growth during the primary and secondary colonization stages would be analyzed.

References

[1] Ecovative Design, 2020, "Ecoative Design-Packaging" [Online]. Available: https://mushroompackaging.com/. [Accessed: 12-Sep-2019].

[2] Abhijith, R., Ashok, A., and Rejeesh, C. R., 2018, "Sustainable Packaging Applications from Mycelium to Substitute Polystyrene: A Review," Mater. Today Proc., 5(1), pp. 2139–2145.

[3] Holt, G., McIntyre, G., Flagg, D., Bayer, E., Wanjura, J., and Pelletier, M., 2012, "Fungal Mycelium and Cotton Plant Materials in the Manufacture of Biodegradable Molded Packaging Material: Evaluation Study of Select Blends of Cotton Byproducts," J. Biobased Mater. Bioenergy, 6(4), pp. 431–439.

[4] Buckminster Fuller Institute, 2014, "ECOVATIVE AT MOMA PS1" [Online]. Available: https://www.bfi.org/dymaxion-forum/2014/07/ecovative-moma-ps1.

[5] Pelletier, M. G., Holt, G. A., Wanjura, J. D., Lara, A. J., Tapia-carillo, A., Mcintyre, G., and Bayer, E., 2017, “An Evaluation Study of Pressure-Compressed Acoustic Absorbers Grown on Agricultural by-Products,” 95, pp. 342–347.

[6] Jones, M., Mautner, A., Luenco, S., Bismarck, A., and John, S., 2020, “Engineered Mycelium Composite Construction Materials from Fungal Biore Fi Neries : A Critical Review,” 187.

[7] Gandia, A., van den Brandhof, J. G., Appels, F. V. W., and Jones, M. P., 2021, “Flexible Fungal Materials: Shaping the Future,” Trends Biotechnol.

[8] Geyer, R., Jambeck, J. R., and Law, K. L., 2017, “Production, Use, and Fate of All Plastics Ever Made,” Sci. Adv., 3(July), pp. 25–29.

[9] Attias, N., Danai, O., Abitbol, T., Tarazi, E., Ezov, N., Pereman, I., and Grobman, Y. J., 2020, “Mycelium Bio-Composites in Industrial Design and Architecture: Comparative Review and Experimental Analysis,” J. Clean. Prod., 246, p. 119037.

[10] Elsacker, E., Vandelook, S., Van Wylick, A., Ruytinx, J., De Laet, L., and Peeters, E., 2020, “A Comprehensive Framework for the Production of Mycelium-Based Lignocellulosic Composites,” Sci. Total Environ., 725, p. 138431.

[11] Haneef, M., Ceseracciu, L., Canale, C., Bayer, I. S., and Heredia-, J. A., 2017, “Advanced Materials From Fungal Mycelium : Fabrication and Tuning of Physical Properties,” Nat. Publ. Gr., (January), pp. 1–11.

[12] Appels, F. V. W., Dijksterhuis, J., Lukasiewicz, C. E., Jansen, K. M. B., Wösten, H. A. B., and Krijgsheld, P., 2018, "Hydrophobin Gene Deletion and Environmental Growth Conditions Impact Mechanical Properties of Mycelium by Affecting the Density of the Material," Sci. Rep., 8(1), p. 4703.

[13] Appels, F. V. W., Camere, S., Montalti, M., Karana, E., Jansen, K. M. B., Dijksterhuis, J., Krijgsheld, P., and Wösten, H. A. B., 2019, "Fabrication Factors Influencing Mechanical, Moisture- and Water-Related Properties of Mycelium-Based Composites," Mater. Des., 161, pp. 64–71.

[14] Islam, M. R., Tudryn, G., Bucinell, R., Schadler, L., and Picu, R. C., 2018, "Stochastic Continuum Model for Mycelium-Based Bio-Foam," Mater. Des., 160, pp. 549–556.

[15] Islam, M. R., Tudryn, G., Bucinell, R., Schadler, L., and Picu, R. C., 2017, "Morphology and Mechanics of Fungal Mycelium," Sci. Rep., pp. 1–12.

[16] Jiang, L., Walczyk, D., Mcintyre, G., and Kin, W., 2016, "Cost Modeling and Optimization of a Manufacturing System for Mycelium-Based Biocomposite Parts," 41, pp. 8–20.

[17] Jiang, L., Walczyk, D., Mcintyre, G., Bucinell, R., and Li, B., 2019, "Bioresin Infused Then Cured Mycelium-Based Sandwich-Structure Biocomposites : Resin Transfer Molding (RTM) Process, Flexural Properties, and Simulation," 207.

[18] Bhardwaj, A., Joseph Vasselli, Matt Lucht, Z.J. Pei, Shaw, B., Grasley, Z., Wei, X., and Zou, N., 2020, "3d Printing of Biomass-Fungi Composite Material: A Preliminary Study," Manuf. Lett., 24, pp. 96–99.

[19] Murphy, S. V, and Atala, A., 2014, "3D Bioprinting of Tissues and Organs," Nat. Biotechnol., 32(8), pp. 773–785.

[20] Blaeser, A., Duarte Campos, D. F., Puster, U., Richtering, W., Stevens, M. M., and Fischer, H., 2016, "Controlling Shear Stress in 3D Bioprinting Is a Key Factor to Balance Printing Resolution and Stem Cell Integrity," Adv. Healthc. Mater., 5(3), pp. 326–333.

[21] Boynton, T. T., and Ferneini, E. M., 2016, "9 - Antimicrobial Pharmacology for Head, Neck, and Orofacial Nonbacterial Infections," J.R. Hupp, and E.M.B.T.-H. Ferneini Neck, and Orofacial Infections, eds., Elsevier, St. Louis, pp. 164–173.

[22] World's Advanced Saving Project-WASP, 2018, "Delta WASP 2040," 2018 [Online]. Available: https://www.personalfab.it/en/shop/clay-3d-printer-delta-wasp-2040-clay/.

[23] Chung, C. I., 2019, Extrusion of Polymers - Theory and Practice (3rd Edition), Hanser Publishers.

[24] Lichius, A., and Zeilinger, S., 2019, "Application of Membrane and Cell Wall Selective Fluorescent Dyes for Live-Cell Imaging of Filamentous Fungi.," J. Vis. Exp., (153).

7. SUMMARY

7.1. Contributions of the Dissertation

In this chapter, I summarize the contributions of each part of the Dissertation.

7.1.1. Identification of Feasible Parameter Regions for Material Extrusion-based 3D Printing of Porcelain

In Chapter 3, I presented experimental results to identify feasible parameter regions that yielded the best surface quality for parts manufactured using the material-extrusion 3D printer. The study analyzed the effect of process parameters (such as print speed, extruder height, layer thickness, and air pressure) on the surface quality of printed parts.

The results of the study reported that a combination of parameters comprising print speed, layer thickness, and air pressure affected the print quality of parts. This was plausible since the surface quality was improved by optimizing the material flow through the printer nozzle. Therefore, best surface quality was observed in samples printed using a combination of high air pressure, high print speed, and reduced layer thickness. Alternately, this print quality was also obtained by using low air pressure, low print speed, and increased layer thickness.

This work demonstrated the importance of material flow on the surface quality of samples manufactured using the material extrusion-based 3D printing process. This information was not previously available for this Delta WASP 3D printer using the porcelain clay material.

7.1.2. 3D Printing of Biomass-Fungi Composites

In Chapter 4, I presented a new 3D printing (using material extrusion) process for biomass-fungi composites. This innovative process included a mixing step to facilitate the conversion of the biomass-fungi material into a liquid slurry. Furthermore, psyllium husk powder was used as an additive to facilitate material extrusion during the printing process. Importantly, the fungi survived the mixing and printing processes and colonized the 3D printed parts. I demonstrated that biomass-fungi composites could be successfully 3D printed using this material-extrusion process.

In addition, I also identified the optimal content of printability aiding additive required to facilitate good quality prints. Furthermore, the effect of the additive on rheological properties was also studied. Chapter 5 analyzed the effects of psyllium husk powder content on print quality for 3D printing of biomass-fungi composites. Print quality was characterized using the criteria of extrudability and shape stability. The use of these criteria to assess print quality was extended from the field of 3D printing of concrete mixtures since that application also employs the material extrusion process. Mixtures prepared without psyllium husk powder were not extrudable due to phase segregation in the biomass-fungi mixture. Best print quality was observed using mixtures having psyllium husk to water ratio of 2:40 (g:mL). Further increase in psyllium husk content resulted in reduction in print quality as extruded filaments were not continuous. This observation was attributed to the increase in solid-like behavior of the mixture as observed in the loss-tangent data. All mixtures displayed shear thinning behavior.

For successfully 3D printing biomass-fungi composites, ensuring fungal growth during the process is a critical requirement. However, there was no information available regarding the effects of process parameters on fungal growth. This information represented a key gap in the body of knowledge in this field. Chapter 6 presented the effects of mixing process parameters (such as mixing time and mixing type) and printing process parameters (print speed and air pressure) on fungal growth in biomass-fungi mixtures prepared for 3D printing. Fungal growth was quantified using the metric of colony forming units per millilitre (CFUs/mL). Mixing times of 120 seconds were found to be favourable to the fungal growth. This observation could be attributed to a better distribution of viable fungi hyphal fragments in the mixture. Moreover, mixing for longer times would have resulted in increasing the surface area of biomass material available for fungal colonization. Mixing type did not have a statistically significant effect on fungal growth. The disparity in fungal growth observed in the mixtures subjected to high and low shear stress during 3D printing was also not statistically significant. This study also presented the tensile and compression strength of the samples.

The combined result of these studies enhances the body of knowledge for 3D printing of biomass-fungi composites and this approach can be extended to the development of new materials and processes.

7.2. Future work

There are various directions for future research in 3D printing of biomass-fungi composites. First, this process has been demonstrated for one type of fungal species and this novel methodology could be extended to 3D print millions of other species of fungi. Furthermore, the effects of various types of nutrition sources on fungi growth also needs evaluation.

The effects of environmental factors (such as lighting conditions, humidity) on fungal growth need to be evaluated for the primary and secondary colonization stages. These environmental factors could affect the growth of hyphae and impact the mechanical properties of the composites. Moreover, the impact of the time allowed for the fungi to grow and its impact on thermo-mechanical properties also need to be studied.

While psyllium husk powder was found to be a printability aiding additive, further exploration of additives needs to be conducted that would improve the printability of the biomass-fungi mixtures without having any detrimental effects on fungal growth in the 3D printed samples. Supplementary additives could also be explored to develop application-specific functionality for these sustainable materials.

Lastly, printing with biomaterials brings with it the challenges of eliminating contamination. While I identified certain procedures for dealing with contaminants in our process, more steps need to be evaluated to make this process more robust to contamination. Additionally, economic analysis of the 3D printing processes also needs to

be evaluated. Addressing these challenges would facilitate the development of a scalable, robust manufacturing process.